

**University of Alberta**

**FROST HEAVE: NEW ICE LENS INITIATION CONDITION  
AND HYDRAULIC CONDUCTIVITY PREDICTION**

by

**Tezera Firew Azmatch**

A thesis submitted to the Faculty of Graduate Studies and Research

in partial fulfillment of the requirements for the degree of

Doctor of Philosophy

in

Geotechnical Engineering

Department of Civil and Environmental Engineering

©Tezera Firew Azmatch

Spring 2013

Edmonton, Alberta

Permission is hereby granted to the University of Alberta Libraries to reproduce single copies of this thesis and to lend or sell such copies for private, scholarly or scientific research purposes only. Where the thesis is converted to, or otherwise made available in digital form, the University of Alberta will advise potential users of the thesis of these terms.

The author reserves all other publication and other rights in association with the copyright in the thesis and, except as herein before provided, neither the thesis nor any substantial portion thereof may be printed or otherwise reproduced in any material form whatsoever without the author's prior written permission.

*Dedicated to my loving father,*

*Firew Azmatch Bekele*

*Dearest Father,*

*This is for you, as promised!*

## **ABSTRACT**

Studies on frost heave indicate that significant frost heave observed in the field or laboratory is attributed to ice lens formation associated with water migration to the freezing front and the segregational ice that develops. Hence frost heave prediction models require ice lens initiation criteria and hydraulic conductivity estimation method for the frozen fringe. Existing frost heave prediction methods do involve complex procedures of estimating the hydraulic conductivity. Ice lens initiation conditions by existing methods are not also easy to implement. In fact, some of the exiting frost heave prediction methods lack ice lens initiation condition.

The objective of this thesis is to investigate and develop ice lens initiation criteria and hydraulic conductivity estimation methods that are simple to implement in frost heave prediction. Simple methods, involving the use of SFCC, for predicting ice lens initiation condition and hydraulic conductivity of the frozen fringe have been proposed and verified in this study.

A new fundamental approach is proposed to determine the ice lens initiation condition using the soil freezing characteristics curve (SFCC). It is demonstrated that an ice lens initiates close to the so-called ice-entry value defined using the SFCC. Ice lens initiation conditions for different boundary conditions were determined in a laboratory using the SFCC and were then compared with the ice lens initiation conditions from a one-dimensional open

system frost heave tests. The results using the SFCC showed good agreement with the values determined experimentally.

A new approach, using the soil freezing characteristic curve (SFCC), is proposed to estimate the hydraulic conductivity of partially frozen soils. The hydraulic conductivity function for partially frozen Devon Silt is derived using the SFCC and the empirical relationships for hydraulic conductivity estimation method developed by Fredlund et al (1994). The SFCC for Devon Silt is determined from unfrozen water content measurement using time domain reflectometry and temperature measurements inside the soil sample. The results using this novel approach compare well with results presented by others that use different methods to determine the hydraulic conductivity function of partially frozen soils.

Results from previous studies on frost heave indicate the presence of freezing-induced cracks in the frozen fringe (e.g., Arenson et al., 2008). These cracks affect the hydraulic conductivity of the frozen fringe and hence the moisture transfer process during frost heave. The presence of the cracks necessitates the use of a dual porosity model for estimating the hydraulic conductivity function of the frozen fringe. This study proposed a dual porosity model for estimating the hydraulic conductivity of the frozen fringe. Hence, the hydraulic conductivity of the frozen fringe will have two components: hydraulic conductivity of the soil matrix and hydraulic conductivity of the cracks. Methods are discussed to estimate the two hydraulic conductivity components.

The hydraulic conductivity of the cracked frozen fringe is estimated as the weighted average of the two components based on the respective porosity ratio. The proposed dual porosity hydraulic conductivity model is then used to carry out parametric study of the influence of the cracks on the hydraulic conductivity of the frozen fringe. The results indicated that the cracks have considerable influence on the hydraulic conductivity of the frozen fringe while taking only a few percent of the pore space.

## **ACKNOWLEDGEMENT**

The author would like to sincerely thank Dr. Dave Sego, Dr. Lukas Arenson and Dr. Kevin Biggar for their commitment to the research undertaken and for providing valuable technical guidance. Dr. Dave Sego's patience, generosity, and understanding is greatly appreciated.

Financial support provided by the National Science and Engineering Research Council (NSERC) is greatly appreciated.

I would also like to thank the technical support staffs in the Geotechnical Engineering section, Mrs Christine Hereygers and Mr Steve Gamble, for the technical support they provided me in the laboratory. You guys are wonderful and your contribution to this research is very valuable.

My sincere thanks are also for all my friends and all the people I came across throughout my lifetime. Thanks for the encouragement and for all the smiles you put on my face.

Finally, and most importantly, are my special thanks to my family; my mother Hiwot Kifetew, my brother Eskinder Firew, and my sisters Tigist Firew and Netsanet Firew. Their support, encouragement and love helped me overcome the most difficult obstacles.

Let all the glory be to God the Almighty. Thank you Jesus!

## **TABLE OF CONTENTS**

<b>ABSTRACT</b>	<b>III</b>
<b>ACKNOWLEDGEMENT</b>	<b>VI</b>
<b>LIST OF TABLES</b>	<b>XX</b>
<b>CHAPTER 1 INTRODUCTION</b>	<b>1</b>
<b>FROST HEAVE MODELS</b>	<b>2</b>
<b>ICE LENS INITIATION CONDITION</b>	<b>4</b>
<b>HYDRAULIC CONDUCTIVITY OF FROZEN FRINGE</b>	<b>5</b>
<b>RESEARCH OBJECTIVES</b>	<b>9</b>
<b>SCOPE OF THESIS</b>	<b>9</b>
<b>ORGANIZATION OF THESIS</b>	<b>10</b>
<b>PUBLICATIONS RELATED TO THIS RESEARCH</b>	<b>12</b>
<b>Journal Papers</b>	<b>12</b>
<b>Conference and Symposium Publications</b>	<b>12</b>
<b>REFERENCES</b>	<b>13</b>
<b>CHAPTER 2. TENSILE STRENGTH OF FROZEN SOILS USING FOUR-POINT BENDING TEST</b>	<b>20</b>
<b>ABSTRACT</b>	<b>20</b>
<b>INTRODUCTION</b>	<b>20</b>
<b>EXPERIMENTAL PROGRAM AND MATERIAL STUDIED</b>	<b>23</b>

<b>Soil Properties and Sample Preparation</b>	<b>23</b>
<b>Soil Freezing</b>	<b>23</b>
<b>Tensile Strength Test using Four-Point Bending Test</b>	<b>23</b>
<b>Unfrozen Water Content</b>	<b>24</b>
<b>EXPERIMENTAL RESULTS AND DISCUSSION</b>	<b>25</b>
<b>Effect of Subzero Temperatures on Tensile Strength</b>	<b>26</b>
<b>Effect of Loading Rate on Tensile Strength</b>	<b>28</b>
<b>Relationship between Unfrozen Water Content and Tensile Strength</b>	<b>29</b>
<b>Stress-Strain Relationship and Modulus of Elasticity</b>	<b>31</b>
<b>Modulus of Elasticity</b>	<b>32</b>
<b>Strain at Failure</b>	<b>32</b>
<b>CONCLUSION</b>	<b>34</b>
<b>REFERENCES</b>	<b>36</b>
<b>CHAPTER 3. TENSILE STRENGTH AND STRESS-STRAIN BEHAVIOUR OF DEVON SILT UNDER FROZEN FRINGE CONDITIONS</b>	<b>40</b>
<b>ABSTRACT</b>	<b>40</b>
<b>INTRODUCTION</b>	<b>40</b>
<b>SOIL PROPERTIES AND SAMPLE PREPARATION</b>	<b>45</b>

Soil Sample Freezing and Freezing Temperatures	45
Temperature range of the frozen fringe	46
Tensile Strength Test using Four-Point Bending Test	46
Unfrozen Water Content	47
<b>EXPERIMENTAL RESULTS AND DISCUSSION</b>	<b>49</b>
Effect of Subzero Temperatures on Tensile Strength	49
Effect of Deformation Rate on Tensile Strength of the Frozen Fringe	51
Relationship between Unfrozen Water Content and Tensile Strength	54
Relationship between Volumetric Ice Content and Tensile Strength	54
Stress-Strain Relationship and Modulus of Elasticity	55
Modulus of Elasticity	56
<b>CONCLUSION</b>	<b>57</b>
<b>REFERENCES</b>	<b>59</b>
<b>ADDENDUM TO CHAPTER 3</b>	<b>63</b>
Ice Lens Initiation condition based on the tensile strength of frozen fringe	63
<b>REFERENCE</b>	<b>65</b>
<b>CHAPTER 4. SOIL FREEZING CHARACTERISTIC CURVE OF DEVON SILT</b>	<b>67</b>
<b>ABSTRACT</b>	<b>67</b>
<b>INTRODUCTION</b>	<b>67</b>

<b>EXPERIMENTAL PROGRAM</b>	<b>70</b>
<b>Soil Properties and Sample Preparation</b>	<b>70</b>
<b>Test for Soil Freezing Characteristics Curve</b>	<b>70</b>
<b>EXPERIMENTAL RESULTS AND DISCUSSION</b>	<b>71</b>
<b>Influence of Initial Void Ratio</b>	<b>71</b>
<b>Influence of Freezing Temperature and Cooling Rate</b>	<b>73</b>
<b>Influence of Freeze-Thaw Cycles</b>	<b>74</b>
<b>CONCLUSION</b>	<b>77</b>
<b>REFERENCES</b>	<b>77</b>
<b>CHAPTER 5. NEW ICE LENS INITIATION CONDITION FOR FROST HEAVE IN FINE-GRAINED SOILS</b>	<b>81</b>
<b>ABSTRACT</b>	<b>81</b>
<b>INTRODUCTION</b>	<b>81</b>
<b>ICE LENS INITIATION CONDITION IN FROZEN SOILS</b>	<b>83</b>
<b>CRACK INITIATION CONDITION IN NONFROZEN SOILS</b>	<b>85</b>
<b>EXPERIMENTAL PROGRAM</b>	<b>86</b>
<b>Soil Properties and Sample Preparation</b>	<b>86</b>
<b>Soil Freezing Characteristics Curve</b>	<b>86</b>
<b>One-dimensional Frost Heave Tests</b>	<b>87</b>
<b>EXPERIMENTAL RESULTS AND DISCUSSION</b>	<b>89</b>

<b>Influence of External Pressure</b>	<b>93</b>
<b>Comparison of results from Current Study with results from Previous Studies</b>	<b>95</b>
<b>CONCLUSIONS</b>	<b>97</b>
<b>REFERENCES</b>	<b>98</b>
<b>CHAPTER 6. USING SOIL FREEZING CHARACTERISTIC CURVE TO ESTIMATE THE HYDRAULIC CONDUCTIVITY FUNCTION OF PARTIALLY FROZEN SOILS</b>	<b>104</b>
<b>ABSTRACT</b>	<b>104</b>
<b>INTRODUCTION</b>	<b>104</b>
<b>INDIRECT METHODS TO ESTIMATE THE HYDRAULIC CONDUCTIVITY OF PARTIALLY FROZEN SOILS</b>	<b>106</b>
<b>EXPERIMENTAL PROGRAM</b>	<b>110</b>
<b>Soil Properties and Sample Preparation</b>	<b>110</b>
<b>Test for Soil Freezing Characteristics Curve</b>	<b>110</b>
<b>Test for Soil Water Characteristics Curve</b>	<b>111</b>
<b>EXPERIMENTAL RESULTS AND DISCUSSION</b>	<b>111</b>

<b>Influence of Solutes</b>	<b>113</b>
<b>Hydraulic Conductivity of Partially Frozen Soils</b>	<b>114</b>
<b>Comparison of Hydraulic Conductivity Estimation using SFCC with Hydraulic Conductivity Estimation using SWCC for Devon Silt</b>	<b>119</b>
<b>Comparison of predicted hydraulic conductivity with direct measurements</b>	<b>121</b>
<b>Comparison of results from this study with results from other indirect methods</b>	<b>123</b>
<b>CONCLUSIONS</b>	<b>125</b>
<b>REFERENCES</b>	<b>125</b>
<b>CHAPTER 7. HYDRAULIC CONDUCTIVITY ESTIMATION OF THE FROZEN FRINGE TAKING INTO ACCOUNT THE PRESENCE OF CRACKS IN THE FROZEN FRINGE</b>	<b>131</b>
<b>ABSTRACT</b>	<b>131</b>
<b>INTRODUCTION</b>	<b>131</b>
<b>DUAL POROSITY MODEL FOR THE HYDRAULIC CONDUCTIVITY OF THE FROZEN FRINGE</b>	<b>134</b>
<b>Hydraulic conductivity estimation of the frozen soil matrix</b>	<b>135</b>
<b>Hydraulic Conductivity of the Cracks /Secondary Pore System in the frozen Fringe</b>	<b>137</b>
<b>Flow through Cracks</b>	<b>138</b>
<b>Unfrozen water film thickness in the cracks of the frozen fringe</b>	<b>139</b>

<b>INFLUENCE OF THE FREEZING-INDUCED CRACKS ON THE HYDRAULIC CONDUCTIVITY OF THE FROZEN FRINGE</b>	<b>141</b>
<b>Matrix Component of the Hydraulic Conductivity of the Frozen     Fringe</b>	<b>143</b>
<b>Hydraulic conductivity of the cracks</b>	<b>143</b>
<b>Hydraulic conductivity of the frozen fringe with the influence of     the Cracks</b>	<b>146</b>
<b>DISCUSSION</b>	<b>150</b>
<b>CONCLUSION</b>	<b>152</b>
<b>REFERENCES</b>	<b>153</b>
<b>CHAPTER 8. SUMMARY, CONCLUSIONS AND RECOMMENDATIONS</b>	<b>158</b>
<b>NEW ICE LENS INITIATION CONDITION</b>	<b>159</b>
<b>ESTIMATION OF THE HYDRAULIC CONDUCTIVITY     WITHIN THE FROZEN FRINGE AND IN PARTIALLY FROZEN     SOILS</b>	<b>160</b>
<b>CONCLUSIONS</b>	<b>163</b>
<b>RECOMMENDATIONS</b>	<b>164</b>
<b>REFERENCES</b>	<b>166</b>
<b>APPENDIX</b>	<b>168</b>

## LIST OF FIGURES

	<b>Page</b>
<b>Chapter 1</b>	
Figure 1. Frost heave features: (a) Reticulate ice structure viewed in vertical sample section and, (b) freezing-induced cracks within the frozen fringe viewed on a horizontal sample cross section at the base of the final ice lens (Xia, 2006). Sample diameter = 10.0 cm.	2
<b>Chapter 2</b>	
Figure 1. Sample dimensions, $h = 76.2$ mm.	24
Figure 2. Schematics of (FPBT) tension test set-up.	24
Figure 3. Soil sample after loading.	25
Figure 4. Tensile strength as a function of temperature.	27
Figure 5. Tensile strength as a function of loading rate.	28
Figure 6. Tensile strength as a function of strain rate.	29
Figure 7. Freezing characteristics (unfrozen water content) curve for Devon Silt.	30
Figure 8. Effect of unfrozen water content on tensile strength.	31
Figure 9. Stress-strain plot for the tension tests at different temperatures for a loading rate of 0.8 mm/min.	33
Figure 10. Stress-strain plot for the tension tests at different loading rates at a temperature of $-5.45$ °C.	33
Figure 11. Variation of modulus of elasticity with temperature.	34
Figure 12. Variation of failure strain with temperature.	34

### Chapter 3

Figure 1: Frost heave features: (a) Reticulate Ice lens structure and, (b) freezing-induced cracks in the frozen fringe (Xia, 2006)	41
Figure 2. Sample dimensions, $h = 76.2$ mm.	45
Figure 3. Schematics of Four-Point Bending Test tension test set-up.	47
Figure 4. Freezing characteristics (unfrozen water content) curve for Devon Silt ( $\theta$ is the temperature at which the sample is frozen and $\theta_0$ is a reference temperature taken as $-1.0^\circ\text{C}$ ).	48
Figure 5. Soil sample after loading.	49
Figure 6. Tensile strength as a function of temperature ( $\theta$ is the temperature at which the sample is frozen and $\theta_0$ is a reference temperature taken as $-1.0^\circ\text{C}$ ).	50
Figure 7. Influence of deformation rate on the tensile strength of the frozen fringe. The deformation rate is the rate of displacement of compression test machine.	51
Figure 8. Temperature dependence of the influence of deformation rate on the tensile strength of the frozen fringe.	52
Figure 9. Tensile strength as a function of strain rate at a temperature of $-0.70^\circ\text{C}$ .	53
Figure 10. Effect of unfrozen water content on tensile strength of the frozen fringe.	54
Figure 11. Relationship between volumetric ice content and tensile strength.	55
Figure 12. Stress-strain plot for the tension tests at different temperatures for a deformation rate of $0.8$ mm/min.	55
Figure 13. Stress-strain plot for the tension tests at different deformation rates at a temperature of $-0.70^\circ\text{C}$ .	56

Figure 14. Variation of modulus of elasticity with temperature for a deformation rate of 0.8 mm/min. 56

Figure 15. Variation of modulus of elasticity with deformation rate for samples frozen at  $-0.70^{\circ}\text{C}$ . 57

Figure 3A.1. Tensile strength (at 2% tensile strain value) variation with temperature ( $\theta$  is the temperature at which the sample is frozen and  $\theta_0$  is a reference temperature taken as  $-1.0^{\circ}\text{C}$ ). 64

## Chapter 4

Figure 1. Typical SFCC (sample consolidated to 100 kPa) and procedure to determine the IEV. 69

Figure 2. SFCC (volumetric water content,  $\theta$ , versus temperature) for samples consolidated at different pressures. 72

Figure 3. SFCC curve (volumetric water content,  $\theta$ , versus temperature) for samples consolidated at different pressures. 72

Figure 4. Variation in the IEV with initial void ratio. 73

Figure 5. SFCC under different freezing temperatures. 75

Figure 6. SFCC of Devon Silt during first freezing and first thawing stages. 75

Figure 7. SFCC of Devon Silt during cycles of freezing. 76

Figure 8. SFCC of Devon Silt during cycles of thawing. 76

## Chapter 5

Figure 1: Frost heave features: (a) Reticulate ice structure viewed in vertical sample section and, (b) freezing-induced cracks within the frozen fringe viewed on a horizontal sample cross section at the base of the final ice lens (Xia, 2006). Sample diameter = 10.0 cm. 82

- Figure 2. Sketch showing the one-dimensional frost heave test set-up, modified from Xia, (2006). DC = Digital Camera, LP = displacement transducer, PC = Personal Computer. Sketch not drawn to scale. 89
- Figure 3. SFCC, unfrozen water content versus temperature, for Devon Silt consolidated to different consolidation pressures. 90
- Figure 4. SFCC, unfrozen water content versus suction, for Devon Silt consolidated to different consolidation pressures. 91
- Figure 5: Procedure to determine the IEV. The solid lines are linear extensions of the initial linear portion and the middle zone. 91
- Figure 6: Ice Lens initiation temperature as a function of consolidation pressure at 0 kPa external pressure. 92
- Figure 7. Final ice lenses in a soil consolidated at 100 kPa and frozen under different external pressures: (a) 0 kPa, (b) 50 kPa, (c) 100 kPa. 94
- Figure 8. Ice lens initiation temperature as a function of external pressure for a sample consolidated to 100 kPa. The solid line represents the trend of the segregation temperatures determined using the SFCC. 94
- Figure 9. Ice lens initiation temperature as a function of external pressure for a sample consolidated to 200 kPa. The solid line represents the trend of the segregation temperatures determined using the SFCC. 95
- Figure 10. Ice lens initiation temperature as a function of external pressure. 96
- Figure 11. Influence of cooling rate on ice lens initiation temperature versus applied external pressure 96

## **Chapter 6**

- Figure 1. SFCC of Devon Silt samples consolidated to different pressure, plotted as Volumetric water content versus –Temperature. 112

Figure 2. Experimental results of the SFCC plotted as volumetric water content versus Suction.	113
Figure 3. Comparison of SWCC and SFCC for Devon silt with salinity. Curves with broken lines show the SWCC and curves with solid lines show the SFCC.	114
Figure 4. Comparison of the SFCC from laboratory experiments with the SFCC fit using the Fredlund and Xing (1994) method.	116
Figure 5. Fredlund and Xing (1994) fit for the SFCC of Devon Silt consolidated to different pressures	116
Figure 6. Hydraulic conductivity functions of partially frozen Devon Silt estimated using the SFCC and Fredlund et al (1994) method. The hydraulic conductivity functions shown are for samples consolidated to different pressures.	117
Figure 7. Hydraulic conductivity functions of partially frozen Devon Silt estimated using the SFCC and Fredlund et al (1994) method. The hydraulic conductivity functions shown are for samples consolidated to different pressures and below the ice-entry values for each sample. The solid lines indicate trendlines fitted to the data.	119
Figure 8. Comparison of the SWCC and SFCC of Devon Silt consolidated to 100 kPa pressure.	120
Figure 9. Comparison of hydraulic conductivity functions of partially frozen Devon Silt estimated using the SFCC and the SWCC. Fredlund et al. (1994) method is used in both cases. The hydraulic conductivity functions shown are for a sample consolidated to 100 kPa pressure.	121
Figure 10. Comparison of hydraulic conductivity function from this study with hydraulic conductivity function reported by Horiguchi and Miller (1983) from direct laboratory test on Chena Silt.	122
Figure 11. Comparison of hydraulic conductivity functions from this study with other indirect methods of hydraulic conductivity function estimation.	124

## Chapter 7

Figure 1: Frost heave features: (a) Reticulate ice structure viewed in vertical sample section and, (b) freezing-induced cracks within the frozen fringe viewed on a horizontal sample cross section at the base of the final ice lens (Xia, 2006). Sample diameter = 10.0 cm. 132

Figure 2. Frozen fringe model for hydraulic conductivity estimation. 135

Figure 3. Soil freezing characteristic curve of Devon silt consolidated at 100 kPa 142

Figure 4: Scanning Electron Microscope (SEM) measurement of the width of the cracks in Devon silt. 142

Figure 5: Hydraulic conductivity function,  $k_m$ , of the soil matrix of Devon silt. 143

Figure 6. The assumed unfrozen water film thickness variation with temperature. 145

Figure 7. Hydraulic conductivity function,  $k_{cr}$ , of the cracks in the frozen fringe. 146

Figure 8. Hydraulic conductivity of the frozen fringe,  $k_{ff}$ . Unfrozen water film thickness variation from 125 $\mu\text{m}$  (at 0 $^\circ\text{C}$ ) to 10nm (at -1.0 $^\circ\text{C}$ ) in the cracks. 148

Figure 9. Hydraulic conductivity of the frozen fringe,  $k_{ff}$ . Unfrozen water film thickness variation from 125 $\mu\text{m}$  (at 0 $^\circ\text{C}$ ) to 50nm (at -1.0 $^\circ\text{C}$ ) in the cracks. 148

Figure 10. Hydraulic conductivity of the frozen fringe,  $k_{ff}$ . Unfrozen water film thickness variation from 125 $\mu\text{m}$  (at 0 $^\circ\text{C}$ ) to 100nm (at -1.0 $^\circ\text{C}$ ) in the cracks. 149

Figure 11. Hydraulic conductivity of the frozen fringe,  $k_{ff}$ . Unfrozen water film thickness variation from 125 $\mu\text{m}$  (at 0 $^\circ\text{C}$ ) to 1000nm (at -1.0 $^\circ\text{C}$ ) in the cracks. 149

Figure 12. Modified matrix hydraulic conductivity function taking into account the influence of the consolidation process that precedes freezing. 152

## **LIST OF TABLES**

### **Chapter 2**

Table 1: Tensile strength test results. 26

Table 2: Modulus of elasticity values. 32

### **Chapter 4**

Table 1. IEVs determined from the SFCCs. 71

### **Chapter 5**

Table 1: Ice entry values and Ice lens initiation temperatures of Devon Silt from SFCC. 92

### **Chapter 6**

Table 1: Fredlund and Xing (1994) curve fit parameters for the SFCCs 117

## CHAPTER 1 INTRODUCTION

Each year 10's of millions of dollars of damage occurs to Canada's civil infrastructure due to freezing and thawing. This damage, which is caused by frost heave and thawing, is illustrated through distortion of exposed walls, telephone poles and the famous spring "pothole" season that wrecks havoc on our vehicles each spring. Mitigation of this damage can only be achieved by improved understanding of the fundamental processes that occur during frost heave as soil freezes.

There are three necessary conditions for frost heave to occur: (1) frost susceptible soil, (2) availability of water, and (3) freezing temperatures, or more specifically, thermal conditions that will cause a freezing front propagation that allows water to be transported to internal ice lenses that form within the soil.

The phenomenon of frost heave has been studied both experimentally and theoretically for decades. Experimental observations suggest that frost heave is caused by horizontal ice lens formation associated with thermally-induced water migration. Water migration can take place at temperatures below the freezing point, by flowing via the unfrozen water film adsorbed around soil particles. Overburden pressure, temperature gradient, rate of cooling and depth to groundwater table are the most important factors that influence frost heave in a particular soil.

There are many features of frost heave that need to be understood and explained to develop a detailed frost heave theory. One dimensional frost heave tests using Devon silt and carried out by Xia (2006) show the different features associated with frost heave (Figure 1(a)). Horizontal ice lenses and vertical ice veins are formed during freezing giving the reticulate ice lens structure observed in Figure 1. Freezing-induced cracks are also formed during freezing (Figure 1 (b)).

Three distinct zones exist in a frost-susceptible soil subjected to one-dimensional freezing from the top down (Figure 1(a)): Frozen zone, frozen-fringe and unfrozen zone. The zone between the top of the soil sample and the final ice lens (the warmest ice lens) is called the frozen zone. The frozen zone contains pore and/or ice lenses. Negligible water redistribution or migration occurs in the frozen zone. The zone between the final ice lens and the freezing front ( $0^{\circ}\text{C}$  isotherm) is called the frozen fringe. The frozen fringe plays an important role in the frost heave process. The zone below the freezing front consists of unfrozen soil. Water moves from the unfrozen zone through the frozen fringe to facilitate the growth of the final (warmer) ice lens.

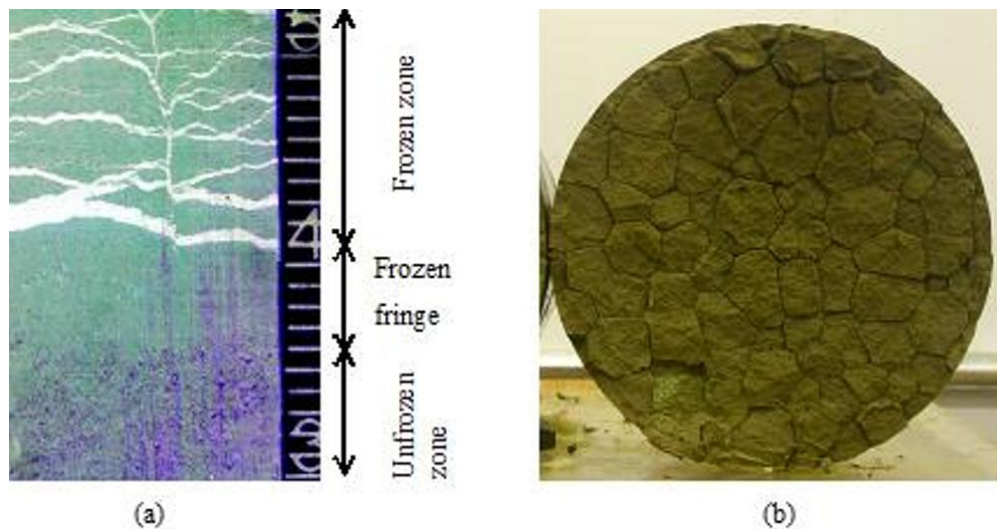


Figure 1: Frost heave features: (a) Reticulate ice structure viewed in vertical sample section and, (b) freezing-induced cracks within the frozen fringe viewed on a horizontal sample cross section at the base of the final ice lens (Xia, 2006). Sample diameter = 10.0 cm.

## FROST HEAVE MODELS

The scientific study of frost heave goes back to the 1920s. Early contributions to the study of frost heave include the works of Taber (1929) and Beskow (1935). Taber (1929) conducted open system freezing tests which showed that the increase in volume is not only due to the different densities of water and

ice (in-situ freezing), but mainly due to a water migration from the unfrozen part of the soil towards the freezing front. He found that if water was replaced with a liquid that solidifies with a decrease in volume, frost heave will still occur. Beskow (1935) noted similarity between unfrozen water content during soil freezing and residual water content during drying, which suggested that water transport during frost heave is similar to the capillary rise of water in a porous medium, driven by surface tension at the interfaces between ice and pore-water. This led to the development of the capillary theory of frost heave (Penner, 1959; Everett, 1961). However, experimental tests did not confirm its validity. Heaving pressures predicted by the theory were significantly smaller than measured experimentally. The theory also failed to explain formation of ice lenses behind the freezing front.

Following the works of Taber (1929) and Beskow (1935), a number of frost heave models have been proposed, e.g. Harlan (1973), Konrad and Morgenstem (1980, 1981, 1982), Gilpin (1980), Hopke (1980), Guymon et al. (1980, 1984), O'Neill and Miller (1980, 1985), Shen and Ladanyi (1987), Nixon (1991), Padilla and Villeneuve (1992), and Sheng et al (1995). These models are in general based upon the fundamental principles of thermodynamics and on experimental observations, and are useful in understanding the phenomenon of frost heave.

Each of the existing models has advantages and disadvantages. One of the major shortcomings of the models by O'Neill and Miller (1985), Harlan (1973), Guymon et al. (1980, 1984) and Konrad and Morgenstem (1980, 1981, 1982) is that an important feature of frost heave, i.e. the formation of discrete ice lenses, is not predicted by these models. All existing models do not take into account the influence of the freezing-induced cracks during the frost heave process.

In order to predict frost heave in soils, prediction of the following parameters is required: (1) Hydraulic conductivity within the frozen fringe, (2) Ice lens initiation criterion and/or prediction of the ice segregation temperature.

The approaches used by existing methods to determine the ice lens initiation condition and the hydraulic conductivity of the frozen fringe are not simple. They involve complex numerical analysis or complex laboratory testing. A review of existing approaches for the prediction of hydraulic conductivity of the frozen fringe and a review of existing ice lens initiation condition is presented in the following sections.

### **ICE LENS INITIATION CONDITION**

The criteria governing ice lens initiation has been studied by different researchers. Miller (1972, 1978) pointed out that ice lenses do not form until the pore water pressure is sufficient to separate soil particles. Gilpin (1980) suggested that a new ice lens appears when and where the maximum ice pressure reaches this separation pressure. O'Neill and Miller (1980) used a neutral stress defined as the difference between the overburden pressure and the effective stress instead of the ice pressure to define this initiation condition. A new ice lens appears when and where the maximum neutral stress reaches the overburden pressure, i.e., the effective stress approaches zero.

According to Akagawa et al. (2007) a new ice lens initiates when the ice pressure exceeds both the sum of the overburden pressure and the tensile strength of the freezing soil.

Konrad and Duquenois (1993) stated that a new ice lens is initiated when the strain exceeds the instantaneous tensile failure strain of the frozen soil. Konrad and Morgenstem (1980) stated that the starting position of a new ice lens is governed by the local permeability within the current frozen fringe, which is associated with the segregation temperature. As the temperature at the base of

the warmest ice lens reaches a critical value, the permeability is so low that no water is able to flow to the warm side of the previously growing ice lens. Thus a new ice lens forms at the location with a temperature identical to the segregation temperature.

All the ice lens initiation criteria discussed above have in common that they require the determination of the segregation temperature (i.e., ice lens initiation temperature). However, presently, there is no specified method, other than direct determination from one dimensional frost heave test (Akagawa, 1988; Konrad, 1980), for determining the segregation temperature. However, direct determination of the segregation temperature using frost heave test is very complex and a simplified approach is presented in this study.

The original intention of this study was to propose ice lens initiation condition as a function of the tensile strength of the frozen fringe as indicated in Azmatch et al (2011), Arenson et al. (2008) and Azmatch et al (2008). However, later on it was discovered that the criterion using the soil freezing characteristics curve is a much simpler and more straightforward approach to determine the ice lens initiation condition. Hence, the research was redirected to evaluation of this important ice lens initiation condition.

However, the importance of the tensile strength criterion as another option to define ice lens initiation condition is also discussed in this thesis.

## **HYDRAULIC CONDUCTIVITY OF FROZEN FRINGE**

Frost heave is due to ice lens formation associated with thermally-induced moisture migration. Proper evaluation of the moisture migration in partially frozen soils requires determining the hydraulic conductivity of these soils. Liquid water and pore ice coexist in a partially frozen soil. The pore ice reduces the hydraulic conductivity of partially frozen soil compared to the unfrozen soil. Since the pore ice content and the unfrozen water content

change with temperature, the hydraulic conductivity of the partially frozen soil also varies with temperature. A major challenge in characterizing flow through partially frozen soils is how to formulate changes in soil hydraulic conductivity as a function of temperature and water content under freezing, frozen and thawing conditions.

Two approaches have been proposed in literature to determine the hydraulic conductivity of partially frozen soils. The first one involves direct measurement of the hydraulic conductivity (Burt and Williams, 1974; Horiguchi and Miller, 1983) and the second approach is based on indirect measurements, assuming that the transport of water in partially frozen soils is controlled by the same process as in unsaturated unfrozen soils (Harlan, 1973).

Due to major challenges of measuring the hydraulic conductivity of partially frozen soils, only a limited number of papers report results from direct measurement of hydraulic conductivity of partially frozen soils. The difficulties faced in making direct measurement limit the credibility of the direct measurement values. Therefore, indirect methods to determine the hydraulic conductivity of partially frozen soils has become the generally accepted approach.

### **Indirect Methods to Estimate the Hydraulic Conductivity of Partially Frozen Soils**

Indirect measurement methods assume that the transport of water within partially frozen soils is controlled by the same process as in unsaturated unfrozen soils. This is based on the similarity between the drying and wetting phenomena in unfrozen soil to the freezing and thawing phenomena in frozen soil (e.g., Spaans and Baker, 1996). The relation between freezing soil temperatures (or suction) and unfrozen water content, referred to as the soil

freezing characteristic curve (SFCC) of partially frozen soil, is assumed to be similar to the soil water characteristic curve (SWCC), which is a relation between suction and water content, for unfrozen soil. This assumption has been used by different authors such as Williams (1964), Koopmans and Miller(1966), Black and Tice (1989), and Spaans and Baker (1996). It is also assumed that the hydraulic conductivity of frozen soils is a function of the unfrozen water content and equals the hydraulic conductivity of unfrozen soils at the same water content. Hence, the SWCC of the soil together with hydraulic conductivity estimation methods based on the use of the SWCC is used to get the hydraulic conductivity of partially frozen soils. This approach has been presented by many researchers (e.g., Cary and Maryland, 1972; Harlan, 1973; Tao and Gray, 1994; Tarnawski and Wagner, 1996; Newman and Wilson, 1997).

Of the different methods discussed above, the most commonly used approach to determine the hydraulic conductivity of partially frozen soils is the indirect method that makes use of SWCC in combination with different hydraulic conductivity estimation methods (e.g., van Genuchten, 1980; Fredlund et al., 1994). This approach was mainly used due to (1) The development of unsaturated soil mechanics theories and the subsequent availability of different methods to estimate the hydraulic conductivity functions from the SWCCs (Fredlund et al., 1994; Mualem, 1976; Van Genuchten, 1980); and (2) lack of a well established laboratory method to directly determine the SFCC in combination with the availability of the Tempe cell for measuring the SWCC.

However, recent studies show that the SWCC is difficult and time consuming to measure and it is actually easier in the laboratory to measure the SFCC than the SWCC (Flerchinger et al, 2006). With the widespread use of the time-domain reflectometry (TDR) and with it being accepted as a well established method for measuring unfrozen water content in partially frozen soils, it is now more straightforward to measure the SFCC than the SWCC. Authors are

even advocating the use of SFCC to get the SWCC especially for fine grained soils, which can be time consuming (Liu et al 2012).

The use of SWCC to model flow through partially frozen soils also has other challenges. One of its shortcomings is that the use of SWCC to estimate the hydraulic conductivity of partially frozen soils is based on an analogy between SWCC and SFCC and this requires a soil-dependent constant for which there is no established method available to determine this constant. This constant is supposed to account for the surface energy difference between the ice-water and air-water interface (i.e.,  $\sigma_{iw}$ ,  $\sigma_{aw}$ ). Another shortcoming of using the SWCC as an analogue to the SFCC for modeling the hydraulic conductivity of partially frozen soils is that the SWCC does not take into account the influence of solutes on the unfrozen water content. Most soils have dissolved solutes or impurities and these solutes are known to decrease the freezing point of water in the soils and hence to increase the unfrozen water content at a particular below zero temperature (Watanabe and Mizoguchi, 2002).

Assuming analogy between SWCC and SFCC also does not address the influence of the freezing rate and freezing temperature applied to a sample. Azmatch et al. (2012), for example, showed that the subzero temperature to which the sample is subjected to during freezing and hence the rate of freezing affects the SFCC of Devon Silt. However, the test method using a Tempe Cell for SWCC does not provide a means to simulate influence of rate of freezing.

Considering all the limitations discussed above of using the SWCC to estimate the hydraulic conductivity function of partially frozen soils, it is proposed in this research program to use the SFCC to determine the hydraulic conductivity function of partially frozen soils.

## **RESEARCH OBJECTIVES**

The objective of this research is to present simple methods that would enable frost heave prediction. This would include

- Presenting a simple ice lens initiation criterion
- Presenting a simple method to determine the segregation temperature.
- Presenting a simple method to estimate the hydraulic conductivity within the frozen fringe

In order to achieve the objectives of this research the following will be investigated:

- Mechanism of Ice Lens formation
- Hydraulic Conductivity of the frozen fringe

## **SCOPE OF THESIS**

To achieve the objectives of the thesis the following laboratory program would be conducted:

1. One-dimensional frost heave test: The results from the one-dimensional frost heave test provide experimental values for the ice lens initiation temperature and for the hydraulic conductivity of the frozen fringe and/or the rate of growth of ice lenses.
2. Soil freezing characteristic curve tests: the results from the soil freezing characteristic curve tests will be used for establishing the ice lens initiation condition using the new the ice lens initiation criterion presented in this thesis. The results will also be used as input parameter to estimate the hydraulic conductivity of the frozen fringe.

3. Tensile strength and stress-strain behavior tests: the results from these tests will be used to investigate the tensile strength and stress-strain behavior of the frozen fringe and to investigate the possibility of using ice lens initiation criterion based on crack initiation that is a function of the tensile strength of the frozen fringe.
4. Soil water characteristics curve test: the results from these tests will be used in evaluating existing hydraulic conductivity estimation methods for partially frozen soil that use SWCC as input parameter.

## **ORGANIZATION OF THESIS**

This thesis is presented in the “paper-format” style. Chapters 3, 5, and 6 (check) have been published in peer-reviewed journals and Chapters 2 and 4 have been published in reviewed conferences and/or symposiums. Details of experimental testing programs, analysis, discussion and conclusions for each of the major components of this research are provided in the following chapters.

Chapter 2 presents the four-point bending test (FPBT) supplemented with digital images to measure strains as a test method to measure tensile strength of partially frozen soils. FPBT was conducted on frozen Devon silt at temperatures between 0°C and -10°C, and at different loading rates (0.8 to 8 mm/min). Images taken during testing were used to determine strains thus allowing to follow the stress-strain curve. The results from the test are analysed and presented in this chapter.

Chapter 3 presents result of the FPBT conducted on Devon silt over the temperature range of the frozen fringe. The tensile strength and stress-strain behaviour of partially frozen Devon silt under the frozen fringe temperature conditions is presented. FPBT tests were carried out to determine the tensile strength of the frozen fringe and its stress-strain behaviour. Devon Silt

samples frozen over a range of frozen fringe temperatures (0 to  $-1.5^{\circ}\text{C}$ ) were tested at different deformation rates (0.08 mm/min to 8.0 mm/min).

In Chapter 4 the soil freezing characteristic curve (SFCC) of Devon Silt is discussed. SFCC tests were conducted on samples prepared under different initial void ratios. SFCC tests were also conducted by placing samples in a freezing cell at different subzero temperatures. Hysteresis effect was studied by subjecting the samples to freeze-thaw cycles.

In Chapter 5 a new fundamental approach is proposed to determine the ice lens initiation condition using the soil freezing characteristics curve (SFCC). It is demonstrated that an ice lens initiates close to the so-called ice-entry value defined using the SFCC. Ice lens initiation conditions for different boundary conditions were determined in a laboratory using the SFCC and were then compared with the ice lens initiation conditions from a one-dimensional open system frost heave tests.

Chapter 6 proposes using the soil freezing characteristic curve (SFCC), instead of the soil water characteristic curve (SWCC), to estimate the hydraulic conductivity of partially frozen soils. Shortcomings associated with the use of the SWCC to estimate the hydraulic conductivity function of partially frozen soils are discussed. The hydraulic conductivity function for partially frozen Devon Silt is derived using the SFCC and the empirical relationships for hydraulic conductivity estimation method developed by Fredlund et al (1994). The SFCC for Devon Silt is determined from unfrozen water content measurement using time domain reflectometry and temperature measurements inside the soil sample.

Chapter 7 discusses conceptual model to determine the hydraulic conductivity of the frozen fringe taking into account the presence of the freezing induced cracks. Dual porosity model is proposed to estimate the hydraulic conductivity of the frozen fringe with cracks. The influence of the cracks on the hydraulic

conductivity function of the frozen fringe is investigated using the proposed dual porosity model.

The last chapter, Chapter 8, summarizes the results from this study. It also provides recommendations for future research.

## **PUBLICATIONS RELATED TO THIS RESEARCH**

Journal papers and conference papers were published from the results of this research work. The following is a summary of publications from this research work.

### **Journal Papers**

- Azmatch, T.F., Segó, D.C., Arenson, L.U., and Biggar, K.W., 2012. Using soil freezing characteristic curve to estimate the hydraulic conductivity function of partially frozen soils. *Cold Regions Science and Technology*, 83-84, 103-109
- Azmatch, T.F., Segó, D.C., Arenson, L.U., and Biggar, K.W., 2012. New Ice Lens Initiation Condition for Frost Heave in Fine-Grained Soils. *Cold Regions Science and Technology*. 82, 8–13.
- Azmatch, T.F., Arenson, L.U., Segó, D.C., and Biggar, K.W., 2011. Tensile Strength and Stress-Strain Behaviour of Devon Silt under Frozen Fringe Conditions. *Cold Regions Science and Technology*. 68, 85–90.

### **Conference and Symposium Publications**

- Azmatch, T.F., Arenson, L.U., Segó, D.C., Biggar, K.W., 2012b. Soil freezing characteristic curve of Devon Silt. Published in *Proceedings of the David C. Segó Symposium*, University of Alberta, Edmonton, Alberta, Canada, April 26–27.

- Azmatch, T.F., Arenson, L.U., Segó, D.C., and Biggar, K.W., 2010. Tensile strength of frozen soils using four-point bending test. Proceedings of the 63rd Canadian Geotechnical Conference and 6th Canadian Permafrost Conference, Calgary, Canada (2010), pp. 436–442
- Azmatch, T.F., Arenson, L.U., Segó, D.C., and Biggar, K.W., 2008. Measuring Ice Lens Growth and Development of Soil Strains during Frost Penetration Using Particle Image Velocimetry (GeoPIV), Proceedings of the Ninth International Conference on Permafrost, University of Alaska, Fairbanks, June 29 – July3, 2008, Vol. 1: 89 - 93.
- Arenson, L.U., Azmatch, T.F., and Segó, D.C., 2008. A New Hypothesis on Ice Lens Formation in Frost Susceptible Soils, Proceedings of the Ninth International Conference on Permafrost, University of Alaska, Fairbanks, June 29 – July3, 2008, Vol. 1: 59 - 64.

## **REFERENCES**

- Akagawa, S., 1988. Experimental study of frozen fringe characteristics. *Cold Regions Science and Technology*. 15, 209–223.
- Akagawa, S., Satoh, M., Kanie, S., Mikami, T., 2007. Effects of tensile strength on ice lens initiation temperature. Proceedings of the international conference on cold region engineering. 23-26 July, 2007, Page 43.
- Arenson, L.U., Azmatch, T.F., Segó, D.C., and Biggar, K.W. 2008. A new hypothesis on ice lens formation in frost-susceptible soils. Proceedings of the Ninth International Conference on Permafrost, Fairbanks, Alaska 1: 59-64.

- Azmatch, T.F., Arenson, L.U., Segó, D.C., Biggar, K.W., 2012. Soil freezing characteristic curve of Devon Silt. Published in Proceedings of the David C. Segó Symposium, University of Alberta, Edmonton, Alberta, Canada, April 26-27.
- Azmatch, T.F., Arenson, L.U., Segó, D.C., and Biggar, K.W. 2008. Measuring ice lens growth and development of soil strains during frost penetration using particle image velocimetry (GeoPIV). Proceedings of the Ninth International Conference on Permafrost, Fairbanks, Alaska 1: 89-93
- Beskow, G., 1935. Soil Freezing and frost heaving with special application to roads and railroads. Swed. Geol. Soc., Ser.C, No.375, 26th year book No. 3 (translated by J.O. Osterberg, Northwestern Univ., 1947).
- Black, P. B., Tice, A.R., 1989. Comparison of soil freezing and soil water curve data for Windsor sandy loam, Water Resour. Res., 25, 2205– 2210.
- Burt, T. P., Williams, P. J., 1974. Measurement of hydraulic conductivity of frozen soils. Canadian Geotechnical Journal 11, 647-650.
- Cary, J.W., Maryland, H.F., 1972. Salt and water movement in unsaturated frozen soil. Soil Science Society of America Journal 36, 549-555
- Flerchinger, G. N., Seyfried, M. S., Hardegree, S. P., 2006. Using Soil Freezing Characteristics to Model Multi-Season Soil Water Dynamics. Vadose Zone Journal 5:1143–1153.
- Fredlund, D.G., Xing, A., Huang, S., 1994. Predicting the permeability function for unsaturated soils using the soil-water characteristic curve. Canadian Geotechnical Journal, 31: 533.546.

- Gilpin, R.R., 1980. A model for the prediction of ice lensing and frost heave in soils. *Water Resources Research* 16 (5), 918–930.
- Guymon, G. L., Hromadka 11, T. V., and Berg, R. L. 1980. A one-dimensional frost heave model based upon simulation of simultaneous heat and water flux, *Cold Reg. Sci. Technol.*, 3: 253-262.
- Guymon, G. L., Hromadka 11, T. V., and Berg, R. L. 1984. Two-dimensional model of coupled heat and moisture transport in frost-heaving soils, *J. Energy Resour. Technol.*, 106(3): 336-343.
- Harlan, R.L., 1973. Analysis of coupled heat and mass transfer in partial frozen soil. *Water Resources Research* 9 (5), 1314–1323.
- Hopke, S. 1980. A model for frost heave including overburden, *Cold Reg. Sci. Technol.*, 3: 111-127.
- Horiguchi, K., and Miller, R. D. 1983. Hydraulic conductivity functions of frozen materials, *Proc. 4th Int. Conf. Permafrost*, National Academy Press, Washington, D.C., 504-508.
- Konrad, J.M., 1980. Frost heave mechanics. Ph.D. thesis, Department of Civil Engineering, University of Alberta, Edmonton, AB, Canada, 472 pp.
- Konrad, J.M., Duquennoi, C., 1993. A model for water transport and ice lensing in freezing soils. *Water Resources Research* 29 (9), 3109–3124
- Konrad, J. M., Morgenstern, N. R., 1982. Effect of applied pressure on freezing soils, *Canadian Geotechnical Journal* 19, 494-505.
- Konrad, J. M., and Morgenstern, N. R. 1981. Segregational potential of freezing soil, *Can. Geotech. J.*, 18: 482-491.

- Konrad, J.M., Morgenstern, N.R., 1980. A mechanistic theory of ice lens formation in fine-grained soils. *Canadian Geotechnical Journal* 17, 473–486.
- Koopmans, R.W.R., Miller, R.D., 1966. Soil freezing and soil water characteristic curves, *Soil Sci. Soc. Am. Proc.*, 30, 680-685
- Liu, Z., Zhang, B., Yu, X., Tao, J., 2012. A New Method for Soil Water Characteristic Curve Measurement Based on Similarities Between Soil Freezing and Drying. *Geotechnical Testing Journal*, 35, 1
- Miller, R.D., 1978. Frost heaving in non-colloidal soils. *Proceedings of the Third International Conference on Permafrost*, Edmonton, Alberta, Canada 1, 708-713.
- Miller, R.D., 1972. Freezing and heaving of saturated and unsaturated soils. *Highway Research Rec.* 393, 1-11.
- Mualem, Y., 1976. A new model for predicting the hydraulic conductivity of unsaturated porous media, *Water Resour. Res.* 12, 513–522.
- Newman, G.P., Wilson, G.W., 1997. Heat and mass transfer in unsaturated soils during freezing, *Canadian Geotechnical Journal* 34, 63-70
- Nixon, J.F. 1991. Discrete ice lens theory for frost heave in soils. *Can. Geotech. J.*, 28(6), 843–859.
- O'Neill, K., Miller, R.D., 1985. Exploration of a rigid ice model of frost heave. *Water Resour. Res.*, 21: 1–22.

- O'Neill, K., Miller, R. D., 1980. Numerical solutions for rigid-ice model of secondary frost heave, Proc. 2nd Int. Symp. Ground Freezing, Trondheim, the Norwegian Institute of Technology 1, 656-669.
- Padilla, F., and Villeneuve, J. P. 1992. Modeling and experimental studies of frost heave including solute effects, Cold Reg. Sci. Technol., 20: 183-194.
- Sheng, D., Axelsson, K., and Knutsson, S. 1995. Frost Heave due to Ice Lens Formation in Freezing soils, 1: Theory and Verification, Nordic Hydrology, 26 (2): 125-146.
- Shen, M., and Ladanyi, B. 1987. Modelling of coupled heat, moisture and stress field in freezing soil, Cold Reg. Sci. Technol., 61: 417-429.
- Spaans, E.J.A., Baker, J.M., 1996, The Soil Freezing Characteristic: Its Measurement and Similarity to the Soil Moisture Characteristic, Soil Sci. Soc. Am. J 60, 13-19.
- Taber, S. 1930. The mechanics of frost Heaving. Journal of Geology 38 (4): 303 – 317
- Taber, S., 1929. Frost heaving. Journal of Geology 37, 428–461.
- Tao, Y.X., Gray, D.M. 1994. Prediction of snowmelt infiltration into frozen soils. Numerical Heat Transfer. Part A: Applications 26:643-665
- Tarnawski, V.R., Wagner, B., 1996. On the prediction of hydraulic conductivity of frozen soils. Canadian technical Journal 33, 176 -180
- van Genuchten M.Th., 1980. A closed form equation for predicting the hydraulic conductivity of unsaturated soils. Soil Sci Soc Am J 44:892–898

Watanabe, K., Mizoguchi, M., 2002. Amount of unfrozen water in frozen porous media saturated with solution. *Cold Regions Science and Technology* 34, 103–110.

Williams, P.J., 1964. Unfrozen water content of frozen soils and soil moisture suction. *Geotechnique* 14, 231-246.

Xia, D., 2006. Frost heave studies using digital photographic technique. MSc Thesis, University of Alberta, Edmonton, AB, Canada, 165 pp.

## **CHAPTER 2. TENSILE STRENGTH OF FROZEN SOILS USING FOUR-POINT BENDING TEST**

This paper was previously published in the proceedings of the 63<sup>rd</sup> Canadian Geotechnical Conference. It is modified (formatting only) and presented as published as part of this Ph.D. thesis as Chapter 2.

Reference: Azmatch, T.F., Arenson, L.U., Seg0, D.C., and Biggar, K.W., 2010. Tensile strength of frozen soils using four-point bending test. Proceedings of the 63rd Canadian Geotechnical Conference and 6th Canadian Permafrost Conference, Calgary, Canada (2010), pp. 436–442

## **CHAPTER 2. TENSILE STRENGTH OF FROZEN SOILS USING FOUR-POINT BENDING TEST**

### **ABSTRACT**

The four-point bending test (FPBT) is one possible test method to measure tensile strength of unfrozen soils/rocks. FPBT was conducted on frozen Devon silt at temperatures between 0°C and -10°C, and at different loading rates (0.8 to 8 mm/min). Images taken during testing were used to determine strains thus allowing to follow the stress-strain curve. A clear dependency of the tensile strength on the temperature and on the loading rate could be identified. Frozen Devon silt develops significant tensile strength at temperatures close to 0°C. Furthermore, the elastic modulus increases as the temperature and the loading decrease.

### **INTRODUCTION**

The tensile strength of both unfrozen and frozen soils plays an important role in geotechnical problems involving tensile failure. For tensile failure to occur, the tensile stress in a soil must exceed the tensile strength of the soil. However, not much research has been done on the tensile strength of soils as compared to the compressive strength. This is mainly because tensile strength is considered insignificant and very small as compared to the compressive strength.

Tensile strength becomes more important once the soil is frozen. The limited studies available on frozen soils show that frozen soils have considerable tensile strength (e.g. Zhu and Carbee, 1987). This is due to their phase composition.

Frozen soils are composed of four phases: soil solids, unfrozen water, frozen water (pore ice), and air (if not saturated) (e.g. Andersland and Ladanyi, 1994). The tensile strength of frozen soils depends on the relative proportion of each component.

The tensile strength is an important parameter in the study of ground patterns and ice wedge polygons in permafrost areas (Lachenbruch, 1962). It is also believed to play an important role in the frost heave process during the formation of ice lenses since the frozen fringe has to crack before the ice lenses are formed (Miller, 1978; Arenson et al., 2008; Azmatch et al., 2008). Hence, more research is required in the study of tensile strength of frozen soils especially near 0°C.

The test methods that can be used to determine the tensile strength of soils can be broadly divided into two groups: (i) direct methods such as the direct tension test; and (ii) indirect methods such as split cylinder test, four point bending test, and Brazilian test. Tests proven to provide reliable results for tensile strength tests of unfrozen soils have been applied to test frozen soils: Zhu and Carbee (1985) and Haynes (1978) used direct tension tests; Bragg and Andersland (1980) used split cylinder tests.

Four-point bending test (FPBT) was used successfully to determine the tensile strength of unfrozen soils (Thusyanthan et al., 2007) and also to determine the tensile strength of soft rocks (Coviello et al., 2005). In this study, four-point bending test will be used to study the tensile strength of Devon silt.

The tensile strength of frozen soils depends on temperature, loading rate and unfrozen water content. The effect of each has been investigated by different authors (Zhu and Carbee, 1985; Zhu and Carbee, 1987; Bragg and Andersland, 1980; Haynes et al., 1975; Haynes, 1978).

Bragg and Andersland (1980) used split-cylinder tests to investigate the effect of strain rate on the tensile strength of frozen silica sand at a temperature of  $-6.0^{\circ}\text{C}$ . They found the tensile strength to be nearly independent of the deformation rate for values above  $1.3\text{ mm/min}$  at  $-6.0^{\circ}\text{C}$ . Haynes (1978) conducted direct tension tests to investigate the effect of temperature, loading rate and unfrozen water content on the tensile strength of Fairbanks silt. He conducted the tests over a range of temperature values ( $-0.1^{\circ}\text{C}$  to  $-57.0^{\circ}\text{C}$ ) and over a range of strain rates ( $1.6 \times 10^{-4}\text{ s}^{-1}$  to  $2.9\text{ s}^{-1}$ ). He stated that the tensile strength doubled over the strain rate range and increased about one order of magnitude over the temperature range. Zhu and Carbee (1987) investigated the effect of temperature, strain rate and density of the tensile strength of Fairbanks silt by using direct tension test method. Their investigation was over a temperature range from  $-1.0^{\circ}\text{C}$  to  $-10.0^{\circ}\text{C}$  and over a loading rate range of  $5.9 \times 10^{-4}\text{ mm/min}$  to  $5.9 \times 10^3\text{ mm/min}$ . The peak tensile strength of frozen silt was found to be very sensitive to strain rate. They concluded that for brittle failure, the peak tensile strength slightly decreases with increasing strain rate; and for ductile failure, it significantly decreases with decreasing strain rate. They determined that the peak tensile strength increases with decreasing temperature and that it increases more rapidly when the temperature is lower than  $-5.0^{\circ}\text{C}$ . They also concluded that the initial tangent modulus is independent on strain rate. Christ and Kim (2009) used direct tensile test to investigate the effect of moisture content and temperature on the tensile strength of frozen silt over a temperature ranging from  $-2.0^{\circ}\text{C}$  to  $-20.0^{\circ}\text{C}$ . They observed a strong dependence of the stress-strain behaviour of frozen silt on the moisture content and temperature.

In this study, four-point bending test was used to investigate the influence of temperature, strain rate and unfrozen water content on the tensile strength of frozen Devon silt.

## **EXPERIMENTAL PROGRAM AND MATERIAL STUDIED**

### **Soil Properties and Sample Preparation**

The soil tested is Devon silt with a specific gravity of 2.65, a clay fraction of 25% and a silt fraction of 75%. It has a liquid limit of 32% and plastic limit of 20%. Slurry of the soil sample is prepared at a moisture content of 55% and then consolidated at 100 kPa in a consolidation cell. Soil samples of dimension 304.8 mm x 76.2 mm x 76.2 mm are then cut out for the four-point bending test. The dimensions in the test set-up are as shown in Figure 1.

### **Soil Freezing**

The sample to be used for the FPBT is placed in a freezing cell. The temperature of the freezing cell is controlled by flowing cold fluid through brass coils (placed inside the freezing cell) from a cooling bath. The temperature of the freezing cell is monitored by two RTDs placed at two corners within the cell. The sample is let to freeze isotropically to the desired temperature by placing it in the cell for a minimum of 24 hours.

### **Tensile Strength Test using Four-Point Bending Test**

After the sample is frozen to the desired temperature, the flexural testing (FPBT) is carried out and digital images are taken at regular time interval during the test. A 15.1 megapixel digital camera (Canon EOS 50D) is used to take the images. The test set-up is as shown in Figure 2. The digital images, together with the marks engraved on the sample, are used to determine the strains. The stresses are determined using beam flexure theory. It is assumed that the frozen soil is elastic and elastic analysis is carried out.

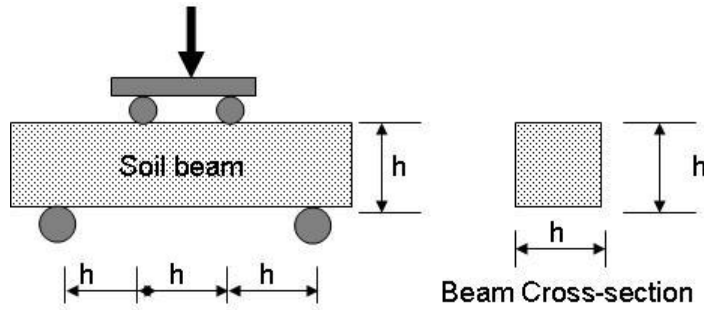


Figure 1. Sample dimensions,  $h = 76.2$  mm.

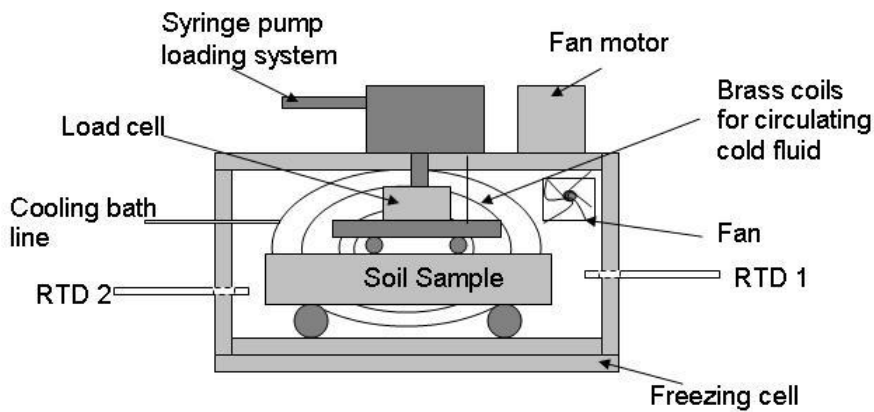


Figure 2. Schematics of (FPBT) tension test set-up.

### Unfrozen Water Content

In a frozen soil, a certain amount of water remains unfrozen at subzero temperatures because of a decrease in the free energy of soil water due to surface forces of soil particles and the pore geometry among soil particles (Dash et al., 1995). There are a number of methods to determine the unfrozen water content (Anderson and Morgenstern, 1973). Some of the methods used are time domain reflectometry (TDR) method, calorimeters method, and nuclear magnetic resonance (NMR) method. For this study, unfrozen water content is measured by TDR. The TDR method measures the dielectric property which is then converted

to volumetric water content by using the empirical equation provided by Topp et al. (1980). The TDR was first used for unfrozen soils. Its use was then extended to frozen soils (e.g. Patterson and Smith, 1980).

The TDR test for this study was carried on samples prepared similar to the samples used in the tensile strength testing. The temperature of the samples is also measured identically by using RTDs placed within the samples. The results were then used to create the soil freezing characteristic curve (which is the unfrozen water content versus temperature).

## **EXPERIMENTAL RESULTS AND DISCUSSION**

Frozen Devon silt showed a significant increase in tensile strength compared to its unfrozen state. The experimental investigations show that frozen Devon silt exhibits considerable tensile strength even at subzero temperature values close to 0°C.

Figure 3 shows a sample loaded to failure. It is seen that the sample cracked just at the middle span. All the samples tested cracked at the middle-third span. The marks engraved on the sample are used to measure the strain development during the test.



Figure 3. Soil sample after loading.

A summary of the tensile test results discussed in this paper is presented in Table 1

Table 1: Tensile strength test results.

Test Number	Temperature, $\theta$ ( $^{\circ}\text{C}$ )	Loading Rate (mm/min)	Peak Tensile Strength, $\sigma_T$ (kPa)
15	+2.25	0.8	7
10	-0.65	0.8	827
4	-0.95	0.8	965
9	-0.95	0.8	982
8	-1.40	0.8	1223
19	-3.9	0.8	1536
20	-5.45	0.8	2413
16	-5.45	3	2855
18	-5.45	8	3175
21	-9.0	0.8	3256

### Effect of Subzero Temperatures on Tensile Strength

To investigate the effect of subzero temperatures on tensile strength of frozen soils, tests were conducted at different temperatures ranging from  $-0.65^{\circ}\text{C}$  to  $-9.0^{\circ}\text{C}$ . These tests were carried out under a loading rate of 0.8 mm/min. The results of these tests are as shown in Table 1. The results show that the peak tensile strength is significantly influenced by the temperature; the tensile strength increases with a decrease in temperature.

The tensile strength of the unfrozen soil was also determined at a temperature of  $+2.25^{\circ}\text{C}$ . Devon silt in the unfrozen state has a peak tensile strength of 7.0 kPa under the test conditions in this study. An increase of two orders of magnitude

(from 7.0 kPa to 827 kPa) is observed as the soil changed from an unfrozen state to a frozen state at a temperature of  $-0.65\text{ }^{\circ}\text{C}$ .

The tensile strength tests carried out over the temperature range of the frozen fringe (zone between  $0\text{ }^{\circ}\text{C}$  isotherm and the base of the warmest ice lens during frost heave) in this study ( $-0.65\text{ }^{\circ}\text{C}$  and  $-0.95\text{ }^{\circ}\text{C}$ ) indicate that the frozen fringe has considerable tensile strength (982 kPa at  $-0.95\text{ }^{\circ}\text{C}$  and 827 kPa at  $-0.65\text{ }^{\circ}\text{C}$ ).

Zhu and Carbee (1987) suggested a relationship for the peak tensile strength of frozen soils as a function of temperature as:

$$\sigma_T = A(\theta/\theta_o)^m \quad (1)$$

Where  $\theta$  is the negative temperature in  $^{\circ}\text{C}$ ,  $\theta_o$  is a reference temperature taken as  $-1.0\text{ }^{\circ}\text{C}$ , and  $A$  (in kPa) and  $m$  are empirical parameters.

Figure 4 shows the variation of the peak tensile strength ( $\sigma_T$ ) with temperature expressed as  $\theta/\theta_o$ . It was determined that for Devon Silt under the conditions of investigation  $A = 997.4\text{ kPa}$  and  $m = 0.49$ , in Eq. 1.

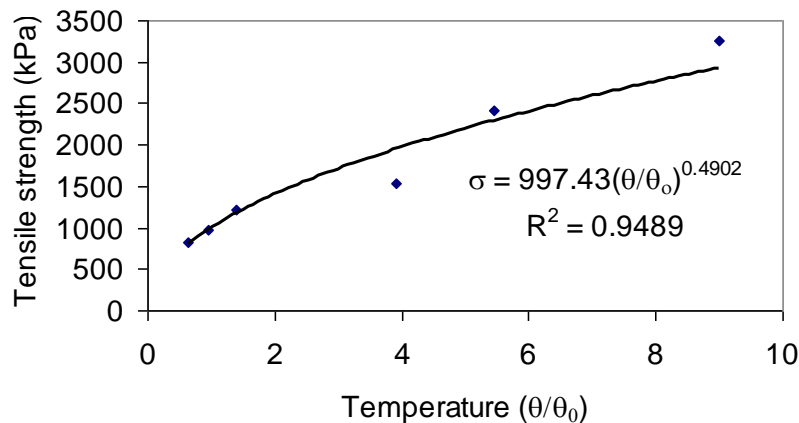


Figure 4. Tensile strength as a function of temperature.

## Effect of Loading Rate on Tensile Strength

To investigate the effect of loading rate on tensile strength, tests at different loading rates were conducted on samples frozen at  $-5.45\text{ }^{\circ}\text{C}$ . The loading rates used were 0.8 mm/min, 3.0 mm/min and 8.0 mm/min. The results from these tests are also presented in Table 1. The results are plotted as shown in Figure 5. Only three data points are available, but the results show that the peak tensile strength is influenced by the loading rate. As the loading rate increases, the tensile strength increases.

Zhu and Carbee (1985) observed that for brittle failure, the peak tensile strength slightly decreases with increasing strain rate; and for ductile failure, it significantly increases with increasing strain rate. For the conditions of investigation in this study, it is observed that the tensile strength increases as the loading rate increases. Hence, it suggests that the soil behaved in a ductile manner under the conditions of investigation.

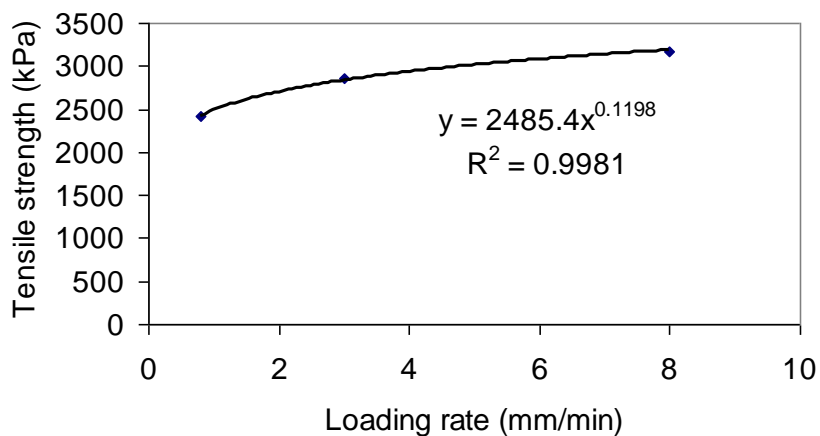


Figure 5. Tensile strength as a function of loading rate.

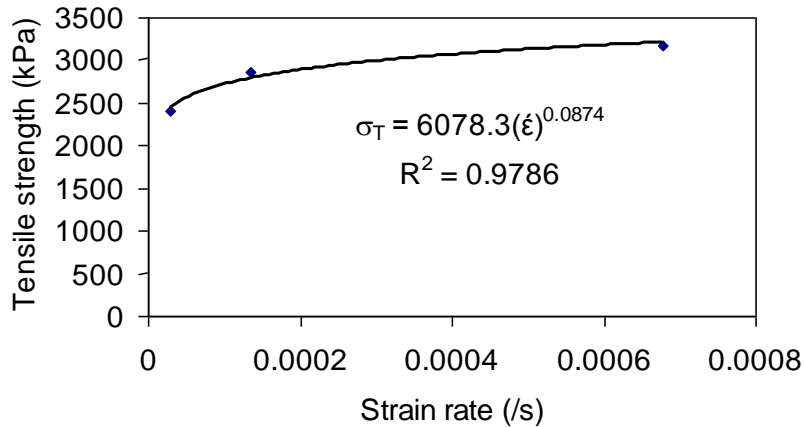


Figure 6. Tensile strength as a function of strain rate.

The variation of peak tensile strength with strain rate is shown in Figure 6. Haynes (1978) expressed the tensile strength as a function of strain rate by:

$$\sigma_T = A\dot{\epsilon}^b \quad (2)$$

Where  $\sigma_T$  is the strength in kPa and  $\dot{\epsilon}$  is the strain rate in  $s^{-1}$ ; A (in kPa) and b are constant for a given temperature. This equation, for Devon Silt, is shown in Figure 6. The values of A and b in Eq. 2 for Devon silt are 6078 kPa and 0.087, respectively.

### **Relationship between Unfrozen Water Content and Tensile Strength**

Unfrozen water content was measured using TDR to establish the relationship between tensile strength and unfrozen water content. The unfrozen water content variation with temperature for Devon silt is shown in Figure 7. The results from this study compared well with the results reported by Konrad (1990), who measured the unfrozen water content for Devon silt using calorimetry method. The unfrozen water content curve indicates that there is a steep decrease in

unfrozen water content in a temperature range from 0 °C to -1.0 °C. The change in unfrozen water content is small from -1.0 °C to -5.0 °C. Then the unfrozen water content remains almost constant at 6.5%.

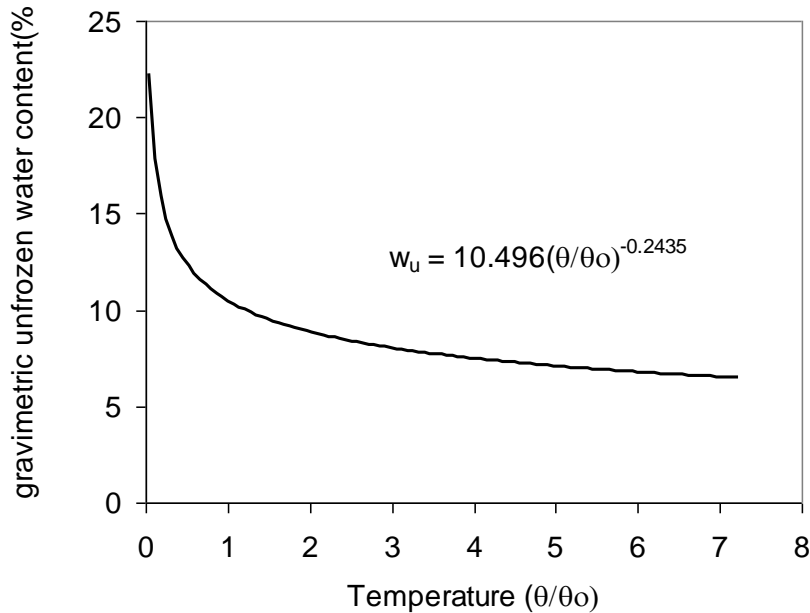


Figure 7. Freezing characteristics (unfrozen water content) curve for Devon Silt.

The dependence of unfrozen water content on temperature can be expressed as (Tice et al., 1976)

$$w_u = \alpha(\theta/\theta_o)^\beta \quad (3)$$

Where  $\theta$  is the negative temperature in °C;  $\theta_o$  is a reference temperature taken as -1.0 °C;  $\alpha$  and  $\beta$  are empirical parameters; and  $w_u$  is the gravimetric unfrozen moisture content expressed in percentage. For Devon silt consolidated at 100 kPa, the values of  $\alpha$  and  $\beta$  in Eq. 3 are 10.50 and -0.244, respectively.

By using the temperature-tensile strength relationship and temperature-unfrozen water content relationship, the relationship between unfrozen water content and tensile strength can be established. This relationship for Devon silt consolidated at 100 kPa is shown in Figure 8. For a small change in unfrozen water content (e.g. from 5.5 % to 10.5%), the tensile strength changes significantly (from 3200 kPa to 800 kPa).

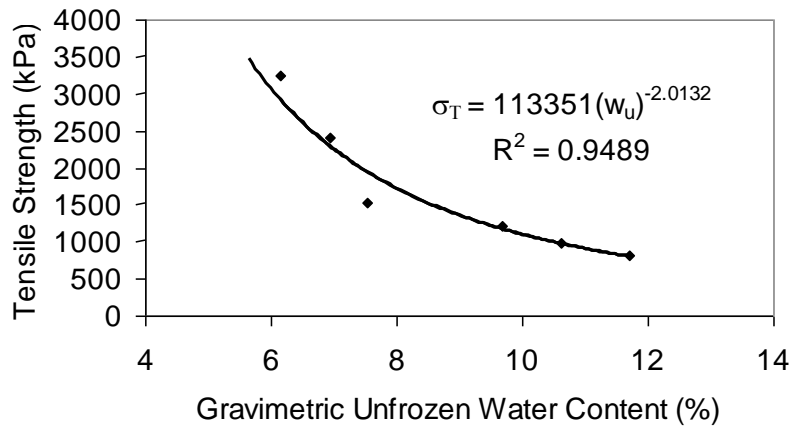


Figure 8. Effect of unfrozen water content on tensile strength.

### **Stress-Strain Relationship and Modulus of Elasticity**

The stress-strain diagrams for the tests conducted at different temperatures but at a loading rate of 0.8 mm/min are shown in Figure 9. Figure 10 shows the stress-strain relationships for the tests conducted at different loading rates at a temperature of -5.45 °C. ImageJ software is used in calculating the strains. The digital images taken at different times during the test together with the linear marks engraved on the soil sample made the strain measurement possible. The change in length of the linear marks was measured using ImageJ software.

## Modulus of Elasticity

The modulus of elasticity values, calculated from the initially linear portion of the stress-strain diagram are shown in Table 2. Figure 11 shows the variation of modulus of elasticity with temperature. The modulus of elasticity increases significantly with a decrease in temperature. It is also influenced by loading rate.

Table 2: Modulus of elasticity values.

Test Number	Loading rate (mm/min)	Temperature (°C)	Modulus of Elasticity (MPa)
10	0.8	-0.65	21.50
8	0.8	-1.40	43.50
19	0.8	-3.90	163.47
20	0.8	-5.45	356.42
16	3.0	-5.45	134.30
18	8.0	-5.45	120.24

## Strain at Failure

The failure strain as a function of temperature for a given loading rate is shown in Figure 12. The failure strain decreases with a decrease in temperature: It decreased from 14.35 % at -0.65 °C to 5.84 % at -5.45 °C. Similar trend was observed by Zhu and Carbee (1987).

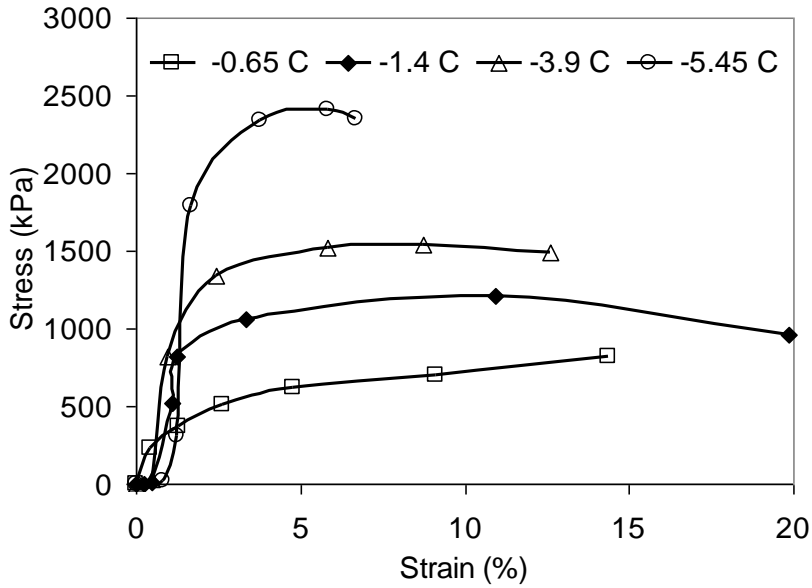


Figure 9. Stress-strain plot for the tension tests at different temperatures for a loading rate of 0.8 mm/min.

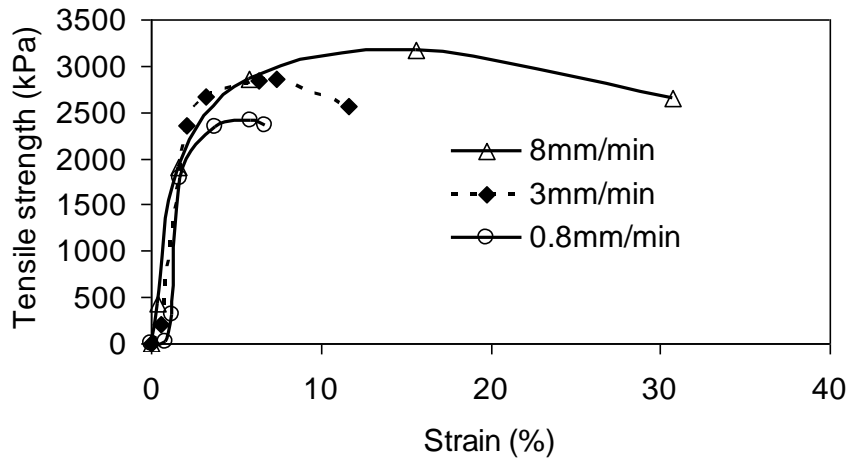


Figure 10. Stress-strain plot for the tension tests at different loading rates at a temperature of -5.45 °C.

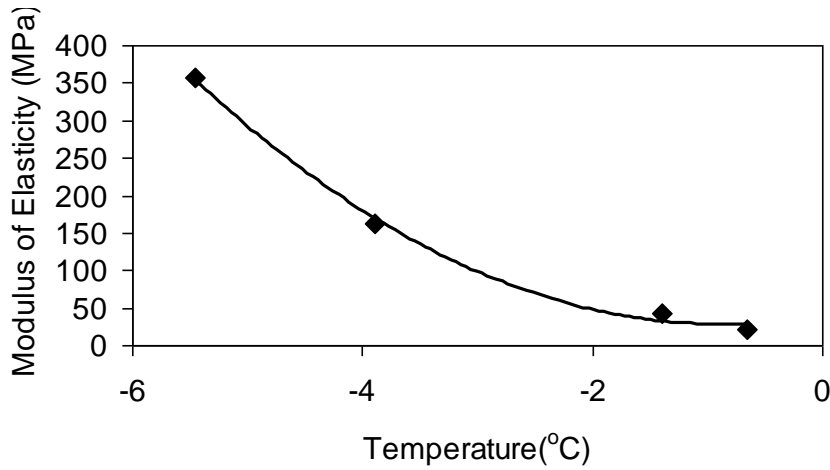


Figure 11. Variation of modulus of elasticity with temperature.

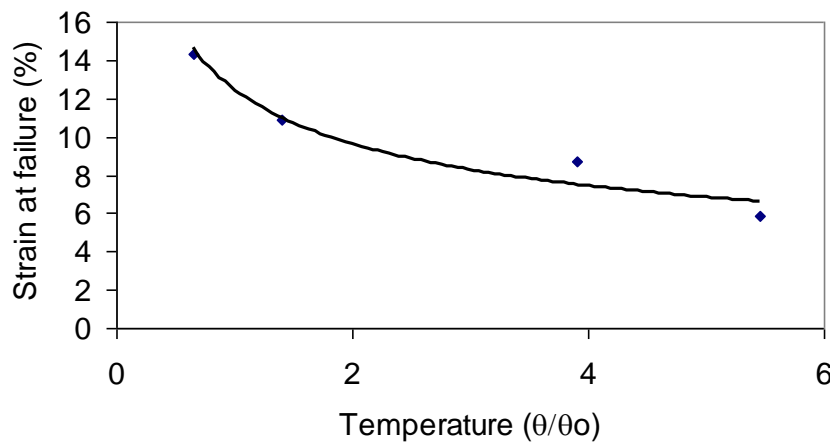


Figure 12. Variation of failure strain with temperature.

## CONCLUSION

Four-point bending test was used to investigate the tensile strength of Devon silt. The tests were conducted on samples prepared by consolidating slurry of Devon silt at 100 kPa. The influence of subzero temperatures, loading rate/strain rate, and unfrozen water content on tensile strength of Devon silt was investigated.

To investigate the influence of subzero temperatures on tensile strength, tests were conducted at temperatures ranging from  $-0.65\text{ }^{\circ}\text{C}$  to  $-9.0\text{ }^{\circ}\text{C}$ . The peak tensile strength increased as the temperature decreased. It changed from 827 kPa at  $-0.65\text{ }^{\circ}\text{C}$  to 3256 kPa at  $-9.0\text{ }^{\circ}\text{C}$ .

To investigate the influence of loading rate on tensile strength, tests were carried out at loading rates of 0.8 mm/min, 3.0 mm/min and 8.0 mm/min on samples frozen at  $-5.45\text{ }^{\circ}\text{C}$ . The results showed that the peak tensile strength increased as the loading rate increased. It increased from 2413 kPa at 0.8 mm/min to 3175 kPa at 8.0 mm/min.

Frozen Devon silt has significant tensile strength even at negative temperatures close to  $0\text{ }^{\circ}\text{C}$ . Devon silt at unfrozen state possessed a tensile strength of 7 kPa. It showed a peak tensile strength of 827 kPa at a temperature of  $-0.65\text{ }^{\circ}\text{C}$ .

The influence of unfrozen water content on tensile strength was examined by determining the unfrozen water content using TDR. From the relationship established between gravimetric unfrozen water content and tensile strength, it is observed that a small change in unfrozen water content produced a significant change in tensile strength. For example, a change in gravimetric water content from 10.5 % to 5.5 % results in a change in the peak tensile strength from 800 kPa to 3200 kPa.

The tests carried out over the temperature range of the frozen fringe ( $-0.65\text{ }^{\circ}\text{C}$  and  $-0.95\text{ }^{\circ}\text{C}$ ) indicate that the frozen fringe possesses considerable tensile strength: 827 kPa at  $-0.65\text{ }^{\circ}\text{C}$  and 982 kPa at  $-0.95\text{ }^{\circ}\text{C}$ . Additional tests are being carried out on the tensile strength under temperatures found in the frozen fringe.

The stress-strain plots showed that the modulus of elasticity is influenced by the freezing temperature and the loading rate: it increased from 21.5 MPa at  $-0.65\text{ }^{\circ}\text{C}$

to 356.4 MPa at -5.45 °C; it decreased from 356.4 MPa at 0.8 mm/min to 120.4 MPa at 8.0 mm/min.

The failure strain was influenced by the freezing temperature. It decreased from 14.35 % at -0.65 °C to 5.84 % at -5.45 °C.

## ACKNOWLEDGEMENTS

The authors would like to thank Steve Gamble and Christine Hereygers at the UofA Geotechnical Centre for their assistance during the lab works. Tezera Firew Azmatch appreciated the funding through the NSERC Discovery Grant held by Dr. Sego and Dr. Biggar.

## REFERENCES

- Andersland, O.B. and Ladanyi, B. 1994. An introduction to frozen ground engineering. Chapman and Hall, New York, NY, USA.
- Anderson, D.M. and Morgenstern, N.R. 1973. Physics, chemistry and mechanics of frozen ground. 2nd International Conference on Permafrost, Yakutsk, USSR, 257-288.
- Arenson, L.U., Azmatch, T.F., Sego, D.C., and Biggar, K.W. 2008. A new hypothesis on ice lens formation in frost-susceptible soils. Proceedings of the Ninth International Conference on Permafrost, Fairbanks, Alaska 1: 59-64.
- Azmatch, T.F., Arenson, L.U., Sego, D.C., and Biggar, K.W. 2008. Measuring ice lens growth and development of soil strains during frost penetration using particle image velocimetry (GeoPIV). Proceedings of the Ninth International Conference on Permafrost, Fairbanks, Alaska 1: 89-93.

- Bragg, R.A. and Andersland, O.B. 1980. Strain rate, temperature, and sample size effects on compression and tensile properties of frozen sand. Proceedings of the Second International Symposium on Ground Freezing, Trondheim, Norway, 34–47.
- Christ, M. and Kim, Y. 2009. Experimental Study on the Physical-Mechanical Properties of Frozen Silt. *KSCE Journal of Civil Engineering*. 13(5):317-324.
- Coviello, A., Lagioia, R., and Nova, R. 2005. On the measurement of the tensile strength of soft rocks. *Rock Mech. Rock Engng.* 38(4), 251-273.
- Dash, J.G., Fu, H., and Wettlaufer, J.S., 1995. The premelting of ice and its environmental consequences. *Rep. Prog. Phys.* 58, 115-167.
- Haynes, F.D., Karalius, J.A., and Kalafut, J., 1975. Strain rate effect on the strength of frozen silt. US Army Cold Regions Research and Engineering Laboratory. CRREL Research Report, vol. 350.
- Haynes, F.D., 1978. Strength and deformation of frozen silt. Proceedings of the Third International Conference on Permafrost, Edmonton, Alberta, Canada, 1:655–661.
- Konrad, J.M. 1990. Unfrozen water as a function of void ratio in a clayey silt. *Cold Regions Science and Technology*, 18: 49-55.
- Lachenbruch, A.H., 1962. Mechanics of thermal contraction cracks and ice-wedge polygons in permafrost. *Geophysical Society of America Special Papers*, 70:1-69.

- Miller, R.D. 1978. Frost heaving in non-colloidal soils. Proceedings of the Third International Conference on Permafrost, Edmonton, Alberta, Canada, 1:708-713.
- Patterson, D.E., and Smith, M.W. 1980. The use of Time Domain Reflectometry for the Measurement of Unfrozen Water Content in Frozen Soils. *Cold Regions Science and Technology*, 3:205-210
- Thusyanthan, N.I., Take, W.A., Madabhushi, S.P.G., and Bolton, M.D., 2007. Crack initiation in clay observed in beam bending. *Geotechnique* 57 (7): 581-594
- Tice, A.R., Anderson, D.M., and A. Banin. 1976. The prediction of unfrozen water content in frozen soils from liquid limit determinations, US Army Cold Regions Research. Engineering Laboratory, CRREL Rep. 76-8
- Topp, G.C., Davis, J.L, and Annan, A.P. 1980. Electromagnetic determination of soil water content: measurements in coaxial transmission lines. *Water Resources Research*, 16(3):574-582
- Zhu, Y., and Carbee, D.L. 1985. Strain rate effect on the tensile strength of frozen silt, Fourth International Symposium on Ground Freezing, Sapporo, Japan: 153 – 157
- Zhu, Y. and Carbee, D.L., 1987. Tensile strength of frozen silt. US Army Cold Regions Research and Engineering Laboratory, CRREL Report 87-15

### **CHAPTER 3. TENSILE STRENGTH AND STRESS-STRAIN BEHAVIOUR OF DEVON SILT UNDER FROZEN FRINGE CONDITIONS**

This paper was previously reviewed, accepted and published in the Cold Regions Science and Technology journal. It is modified (formatting only) and presented as published as part of this Ph.D. thesis as Chapter 3.

Reference: Azmatch, T.F., Arenson, L.U., Sego, D.C., and Biggar, K.W., 2011. Tensile Strength and Stress-Strain Behaviour of Devon Silt under Frozen Fringe Conditions. Cold Regions Science and Technology. 68, 85–90.

## CHAPTER 3. TENSILE STRENGTH AND STRESS-STRAIN BEHAVIOUR OF DEVON SILT UNDER FROZEN FRINGE CONDITIONS

### ABSTRACT

Frost heave is attributed to the segregation of ice and ice lens formation as a soil freezes. Ice lens formation and hence frost heave starts with the cracking of the frozen fringe. In order for these cracks to initiate and open, the tensile strength of the soil has to be exceeded. Therefore, any evaluation of the ice lens initiation condition requires the determination of the tensile strength in the frozen fringe. Four point bending tests were carried out to determine the tensile strength of the frozen fringe and its stress-strain behaviour. Devon Silt samples frozen over a range of frozen fringe temperatures (0 to  $-1.5^{\circ}\text{C}$ ) were tested at different deformation rates (0.08 mm/min to 8.0 mm/min). The frozen fringe of Devon silt has considerable tensile strength. The results show the dependency of the tensile strength on the temperature, the deformation rate, and the unfrozen water content. A unique strain rate dependency was determined for the frozen fringe. Further, it was observed that the stress-strain behaviour is influenced by the deformation rate and the subzero temperatures.

*Key words: frozen fringe, tensile strength, frost heave, stress-strain, unfrozen water content, cracks*

### INTRODUCTION

The phenomenon of frost heave has been studied both experimentally and theoretically for decades (e.g. Taber, 1929; Beskow, 1935; Harlan, 1973; Konrad and Morgenstern, 1980; Gilpin, 1980). Experimental observations indicate that

significant frost heave observed in field or laboratory is attributed to ice segregation and ice lens formation associated with water migration. Horizontal ice lenses and vertical ice veins are formed during freezing giving the reticulate ice lens structure observed in Figure 1. Freezing-induced cracks are also formed during freezing as shown in Figure 1. The presence of cracks during the freezing process has been observed by researchers such as Chamberlain and Gow (1979) and Arenson et al (2008).

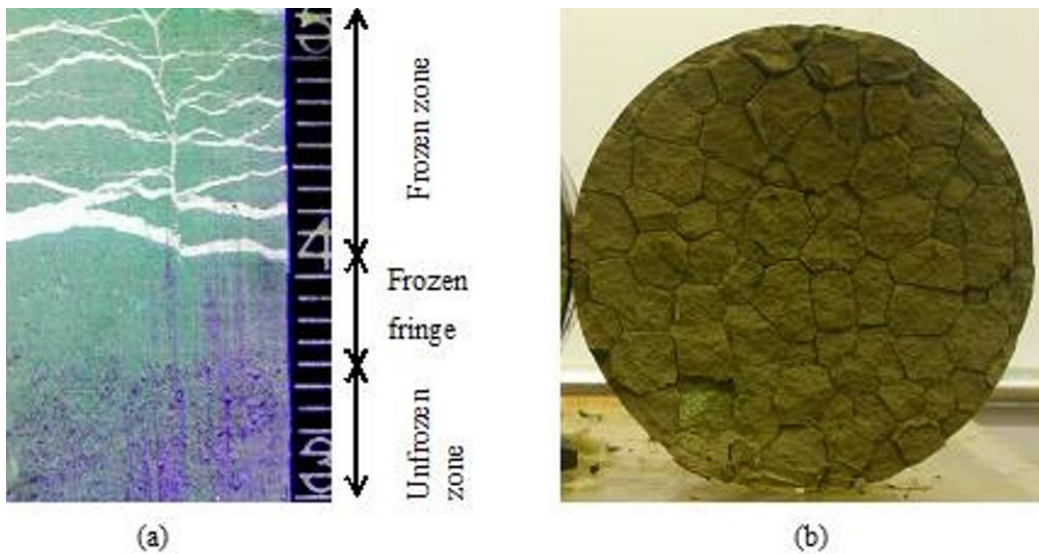


Figure 1: Frost heave features: (a) Reticulate Ice lens structure and, (b) freezing-induced cracks in the frozen fringe (Xia, 2006)

Three distinct zones exist in a freezing soil during frost heave: the passive frozen zone, the active unfrozen zone and the frozen fringe. These zones are shown in Figure 1. The frozen fringe is the zone between the growing ice lens and the frost front where the warmest pore ice exists. Since the concept of frozen fringe was presented (Miller, 1972), it has been realized that the characteristics of the frozen fringe play a very important role in frost heave process. One-dimensional freezing tests by Xia (2006) showed the existence of freezing-induced cracks in the frozen fringe in tests carried out under various boundary conditions (Figure 1). The

freezing-induced cracks in the frozen fringe are very important features since they affect the rate of moisture migration through the frozen fringe during freezing and subsequently the formation of both vertical ice veins and horizontal ice lenses (Arenson et al. 2008, Azmatch et al. 2008). Hence, the damage caused by frost heave is affected by the presence and size of freezing-induced cracks.

To date, the exact nature of the formation of these cracks is not yet fully understood. They could be formed as a result of the moisture migration process, which may desiccate the unfrozen zone in the soil, in which case they may be referred to as desiccation cracks (Chamberlain and Gow, 1979), or they could be a result of the decrease in temperature, which results in thermal stress that may lead to cracking, in which case they may be referred to as thermal contraction cracks (Lachenbruch, 1962). However, there is not any published research that has established the exact nature of the formation of the cracks in the frozen fringe. Hence, we coined the term “freezing-induced cracks” to describe them, since the cracks are a result of the freezing process which can result in desiccation cracks or thermal cracks.

Independent on the nature of the cracks, i.e. desiccation cracks or thermal cracks, in order for the cracks to initiate, the tensile strength of the soil has to be exceeded. Hence, investigation of the crack initiation process requires determination of the tensile strength of the soil over the temperature range of the frozen fringe.

Different properties of the frozen fringe were investigated by researchers such as Ping and Xiaozu (2000), Xiaozu et al (1997), Akagawa (1988), and Konrad and Morgenstern (1982). However, the tensile strength of the frozen fringe was not studied except by Akagawa and Nishisato (2009). It, however, is a very important parameter of the frozen fringe that needs farther investigation since it is thought to affect the cracking of the frozen fringe and hence the ice lens initiation condition

and the hydraulic conductivity of the frozen fringe (Azmatch et al. 2008, Arenson et al. 2008). Hence, the tensile strength of the frozen fringe is investigated in this study.

Most of the research carried out on tensile strength of frozen soils has been at temperatures colder than found in the frozen fringe. It has been mainly at temperature colder than  $-5.0\text{ }^{\circ}\text{C}$  (Haynes et al., 1975; Bragg and Andersland, 1980; and Zhu and Carbee (1985). Haynes (1978) conducted tensile strength tests on frozen silt at  $-0.1$  and  $-1.7\text{ }^{\circ}\text{C}$ . However, no effort has been made to specifically measure the tensile strength of the frozen fringe over the temperature range typically found in the fringe. An exception is the work by Akagawa and Nishisato (2009), who investigated the tensile strength of frozen soils over the temperature range of the frozen fringe. However, the tensile strength data they provided is widely scattered and does not show a well defined relationship with subzero temperature and the influence of strain rate and unfrozen water content was not investigated.

The tensile strength of frozen soils depends on temperature, loading rate and unfrozen water content. The effect of each has been investigated by different authors (Zhu and Carbee, 1985 and 1987; Bragg and Andersland, 1980; Haynes et al., 1975; Haynes, 1978). Bragg and Andersland (1980) used split-cylinder tests to investigate the effect of strain rate on the tensile strength of frozen silica sand at a temperature of  $-6.0^{\circ}\text{C}$ . They found the tensile strength to be nearly independent of the deformation rate for values above  $1.3\text{ mm/min}$  and at  $-6.0^{\circ}\text{C}$ . Haynes (1978) conducted direct tension tests to investigate the effect of temperature, loading rate and unfrozen water content on the tensile strength of Fairbanks silt. He conducted the tests over a range of temperature values ( $-0.1^{\circ}\text{C}$  to  $-57.0^{\circ}\text{C}$ ) and over a range of strain rates ( $1.6 \times 10^{-4}\text{ s}^{-1}$  to  $2.9\text{ s}^{-1}$ ). He stated that the tensile strength doubled over the strain rate range and increased about one order of magnitude over the temperature range. Zhu and Carbee (1987) investigated the

effect of temperature, strain rate and density on the tensile strength of Fairbanks silt by using direct tension test method. Their investigation was over a temperature range from  $-1.0^{\circ}\text{C}$  to  $-10.0^{\circ}\text{C}$  and over a deformation rate range of  $5.9 \times 10^{-4}$  mm/min to  $5.9 \times 10^3$  mm/min. The peak tensile strength of frozen silt was found to be very sensitive to strain rate. They concluded that for brittle failure, the peak tensile strength decreases slightly with increasing strain rate; and for ductile failure, it significantly decreases with decreasing strain rate. They determined that the peak tensile strength increases with decreasing temperature and that it increases more rapidly for temperatures colder than  $-5.0^{\circ}\text{C}$ . They also concluded that the initial tangent modulus is independent on strain rate. Christ and Kim (2009) used direct tensile test to investigate the effect of moisture content and temperature on the tensile strength of frozen silt over a temperature ranging from  $-2.0^{\circ}\text{C}$  to  $-20.0^{\circ}\text{C}$ . They observed a strong dependence of the stress-strain behaviour of frozen silt on the moisture content and temperature. Azmatch et al (2010) investigated the tensile strength of frozen Devon silt using four-point bending test over a temperature range from  $-0.70^{\circ}\text{C}$  to  $-9.5^{\circ}\text{C}$  and using deformation rate from 0.8 mm/min to 8 mm/min. They observed an increase in tensile strength as the temperature decreased; and also that the tensile strength increased as the deformation rate increased.

Akagawa and Nishisato (2009) carried out tensile strength tests over the temperature range of the frozen fringe. They determined that there is a significant increase in tensile strength with a decrease in temperature. However, the tensile strength data they provided is widely scattered and does not show a well defined relationship with temperature and effect of strain rate was not investigated.

In this study, four-point bending test was used to investigate the tensile strength of the frozen fringe. The influence of temperature, strain rate and unfrozen water content on the tensile strength of the frozen fringe is investigated. Tests were also

carried out at temperatures colder than the frozen fringe temperature range for the purpose of comparison.

## SOIL PROPERTIES AND SAMPLE PREPARATION

The soil tested is Devon silt with a specific gravity of 2.65, a clay fraction of 25% and a silt fraction of 75%. It has a liquid limit of 32% and plastic limit of 20%. Slurry of the soil is prepared at a moisture content of 55% and then consolidated at 100 kPa in a consolidation cell. The moisture content at the end of consolidation is 27%. Soil samples of dimension 304.8 mm x 76.2 mm x 76.2 mm are then trimmed for the four-point bending test (FPBT). The dimensions in the test set-up are as shown in Figure 2.

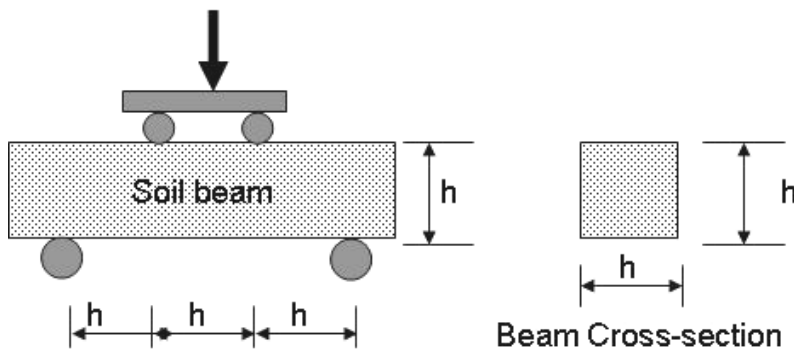


Figure 2. Sample dimensions,  $h = 76.2$  mm.

### Soil Sample Freezing and Freezing Temperatures

The sample to be used for the FPBT is placed in a freezing cell. The temperature of the freezing cell is controlled by flowing cold fluid through brass coils (placed inside the freezing cell) from a cooling bath. The temperature of the freezing cell is monitored by two RTDs placed at two corners within the cell. The sample is let to freeze isotropically to the desired temperature once placed in the cell. The samples are first frozen at  $-4.0$  °C for about 16 hours and then the temperature is

raised to the desired temperature and the sample is left to equilibrate at the desired test temperature for a minimum of 24 hours. The samples are always inspected visually to see if there are any freezing-induced cracks that might influence the tensile strength of the sample. Cross sections along crack surface were also observed after testing to see if there are any special structures that may indicate presence of ice lenses at the center of the test specimen. In all the tests, no such features were observed.

### **Temperature range of the frozen fringe**

The temperature in the frozen fringe decreases from the water freezing point at the frost front to the segregational temperature at the warm side of the ice lens. The segregation temperature is influenced by the overall temperature gradient in the sample (Xiaozu et al 1997), the freezing rate (Konrad, 1989), the external load (Konrad and Morgenstern, 1982), the tensile strength of the soil (Akagawa et al., 2007) and the soil type (Konrad, 2005). Based on the segregation temperature values reported by Konrad (1989) for Devon silt, Ping and Xiaozu (2000) for Hebei Loam, and by Akagawa et al. (2007) for diluvial Dotan silt, temperatures ranging from 0°C to -1.5 °C were used to carry out the tensile strength tests.

### **Tensile Strength Test using Four-Point Bending Test**

After the sample reached the desired temperature, the flexural testing (FPBT) is carried out and digital images were taken at regular time interval during the test. A 15.1 megapixel digital camera (Canon EOS 50D) was used to take the images. The test set-up is as shown in Figure 3. The digital images, together with the markers engraved on the sample, were used to determine the strains. The stresses were determined using beam flexure theory. It is assumed that the frozen soil is elastic; hence, an elastic analysis was carried out.

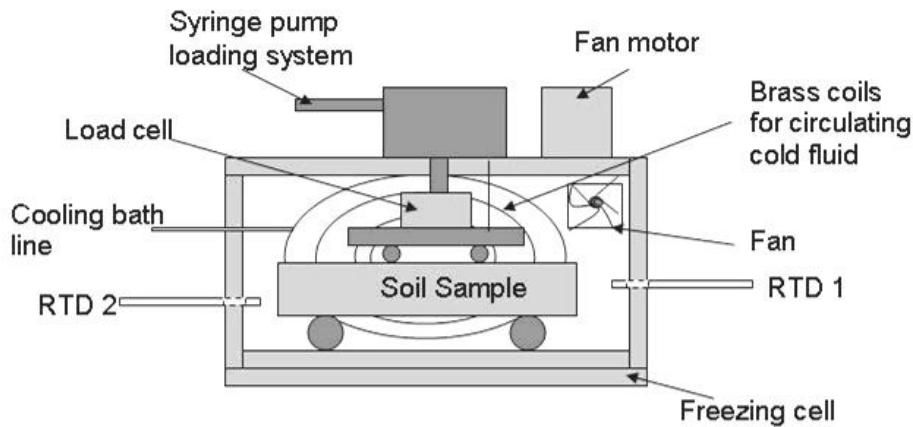


Figure 3. Schematics of Four-Point Bending Test tension test set-up.

### Unfrozen Water Content

Within a frozen soil, a certain amount of water remains unfrozen at subzero temperatures because of a decrease in the free energy of soil water due to surface forces associated with soil particles and the pore geometry among soil particles (Dash et al., 1995). The unfrozen water content was measured using time domain reflectometry (TDR). The TDR method measures the soil's dielectric property, which is converted to volumetric water content using the empirical equation described by Topp et al. (1980).

The TDR test was carried out on samples prepared in a similar manner to the samples used in the tensile strength testing. The temperature of the samples was measured by using RTDs placed within the samples. The results were then used to create the soil freezing characteristic curve (which is the unfrozen water content versus temperature). The unfrozen water content variation with temperature for Devon silt is shown in Figure 4. The unfrozen water content curve indicates that there is a steep decrease in unfrozen water content in a temperature range from 0°C to -1.0°C. The change in unfrozen water content is small from -1.0°C to -5.0°C. Then the unfrozen water content remains almost constant at 6.5%.

The unfrozen water content changes drastically for temperature changes within the temperature range of the frozen-fringe. As the temperature changes from 0°C to -1.5°C, the unfrozen water content changes from 25% to 9.5%.

The dependence of unfrozen water content on temperature can be expressed as (Tice et al., 1976)

$$w_u = \alpha(\theta/\theta_o)^\beta$$

Where  $\theta$  is the negative temperature in °C;  $\theta_o$  is a reference temperature taken as -1.0°C;  $\alpha$  and  $\beta$  are empirical parameters; and  $w_u$  is the gravimetric unfrozen moisture content expressed in percentage. For Devon silt consolidated at 100 kPa, the values of  $\alpha$  and  $\beta$  are 10.5 and -0.244, respectively.

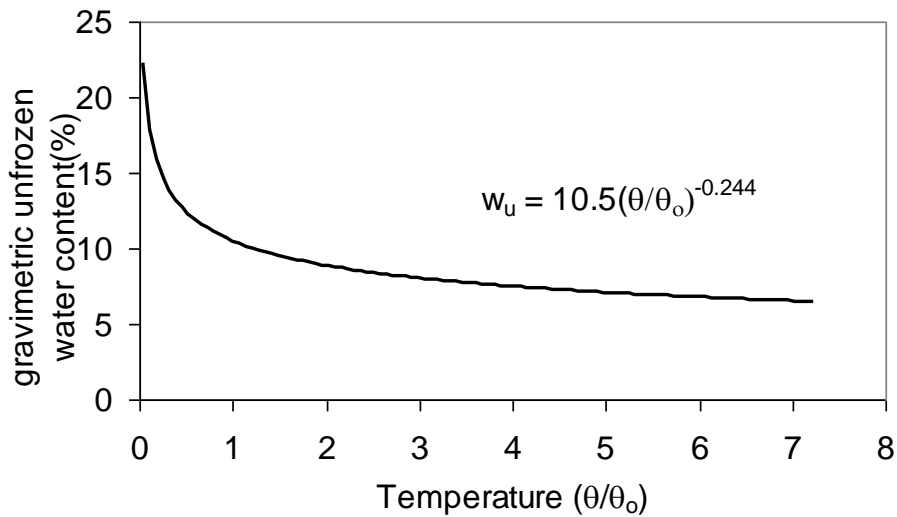


Figure 4. Freezing characteristics (unfrozen water content) curve for Devon Silt ( $\theta$  is the temperature at which the sample is frozen and  $\theta_o$  is a reference temperature taken as -1.0°C).

## EXPERIMENTAL RESULTS AND DISCUSSION

The frozen Devon silt showed a significant increase in tensile strength compared to its unfrozen state. The results from the tests carried out over the temperature range of the frozen fringe showed that the frozen fringe exhibits considerable tensile strength. Figure 5 shows a sample loaded to failure. It is seen that the sample cracked in the middle span. All the samples tested cracked in this manner. The marks engraved on the sample are used to measure the strain development during the test.



Figure 5. Soil sample after loading

### Effect of Subzero Temperatures on Tensile Strength

To investigate the effect of subzero temperatures on tensile strength, tests were conducted at different temperatures ranging from  $-0.30^{\circ}\text{C}$  to  $-1.40^{\circ}\text{C}$ . These tests were carried out under a deformation rate of  $0.8\text{ mm/min}$ . The temperature dependence of the tensile strength of the frozen fringe is shown in Figure 6. The results show that the peak tensile strength of the frozen fringe is significantly influenced by the temperature; the tensile strength increases with decreasing in temperature.

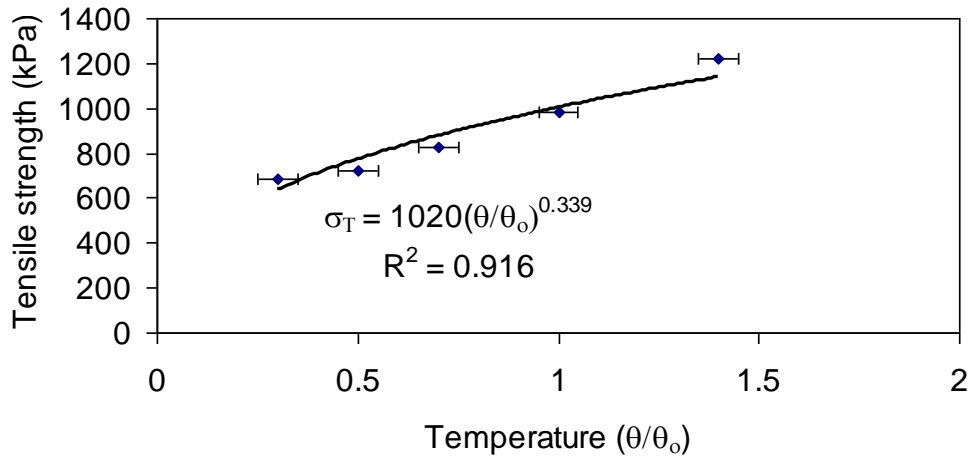


Figure 6. Tensile strength as a function of temperature ( $\theta$  is the temperature at which the sample is frozen and  $\theta_0$  is a reference temperature taken as  $-1.0^\circ\text{C}$ ).

The tensile strength of the unfrozen soil was also determined at a temperature of  $+2.25^\circ\text{C}$ . Devon silt in the unfrozen state has a peak tensile strength of 7.0 kPa under the test conditions in this study. An increase of two orders of magnitude (from 7.0 kPa to 686 kPa) is observed as the soil changed from an unfrozen state to a frozen state at a temperature of only  $-0.30^\circ\text{C}$ . This shows that the frozen fringe possesses considerable tensile strength.

Zhu and Carbee (1987) suggested a relationship for the peak tensile strength of frozen soils as a function of temperature as:

$$\sigma_T = A(\theta/\theta_0)^m$$

Where  $\theta$  is the negative temperature in  $^\circ\text{C}$ ,  $\theta_0$  is a reference temperature taken as  $-1.0^\circ\text{C}$ , and  $A$  (in kPa) and  $m$  are empirical parameters.

Figure 6 shows the variation of the peak tensile strength ( $\sigma_T$ ) with temperature expressed as  $\theta/\theta_0$ . It is determined that for the frozen fringe in Devon Silt under the conditions of investigation  $A = 1020$  kPa and  $m = 0.339$ .

### Effect of Deformation Rate on Tensile Strength of the Frozen Fringe

To investigate the effect of deformation rate on tensile strength of the frozen fringe, tests were conducted at different rates on samples frozen at  $-0.70^\circ\text{C}$ . The rates used were 0.08 mm/min, 0.8 mm/min, 3.0 mm/min and 8.0 mm/min. The results from these tests are presented in Table 1. The results are also plotted in Figure 7.

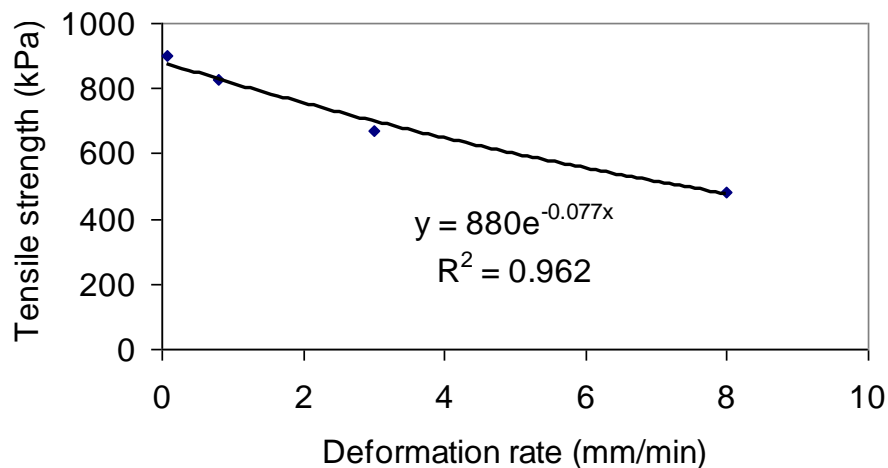


Figure 7. Influence of deformation rate on the tensile strength of the frozen fringe. The deformation rate is the rate of displacement of compression test machine.

The results show that the peak tensile strength is influenced by the deformation rate. For the tests carried out over the temperature range of the frozen fringe (at  $-0.70^\circ\text{C}$ ), as the deformation rate increases, the tensile strength decreases (Figure 7). This is contrary to existing knowledge on the influence of deformation rate on tensile strength of frozen soils (Haynes, 1978; Bragg and Andersland, 1980; Zhu and Carbee, 1987). However, the investigation on the influence of deformation

rate by these researchers was carried out at colder temperatures; typically,  $-5.0^{\circ}\text{C}$ . To address this issue, tests were conducted tests at  $-5.45^{\circ}\text{C}$  for comparison to findings from the literature. The results from the tests carried out at  $-5.45^{\circ}\text{C}$  indicate that the tensile strength increases as the deformation rate increases (Figure 8), which is in agreement with the results presented by other researchers. Figure 8 shows that the effect of deformation rate on tensile strength is temperature dependent. The data by Akagawa and Nishisato (2009) supports the finding from this research. Akagawa and Nishisato (2009) conducted tensile strength tests at deformation rates of 0.34 mm/min and 2.31 mm/min on samples frozen at  $-0.16^{\circ}\text{C}$  and  $-0.15^{\circ}\text{C}$ , respectively. They found that the tensile strength under the lower deformation rate was about 30% higher than that under the higher deformation rate. However, they did not reach a similar conclusion for they had only two data points with a temperature difference of  $-0.01^{\circ}\text{C}$ . Hence, they suggested that the trend was due to small difference in freezing temperature. However, using the relationship established between temperature and tensile strength, it can be verified that a difference of  $-0.01^{\circ}\text{C}$  would not produce this much change in measured tensile strength.

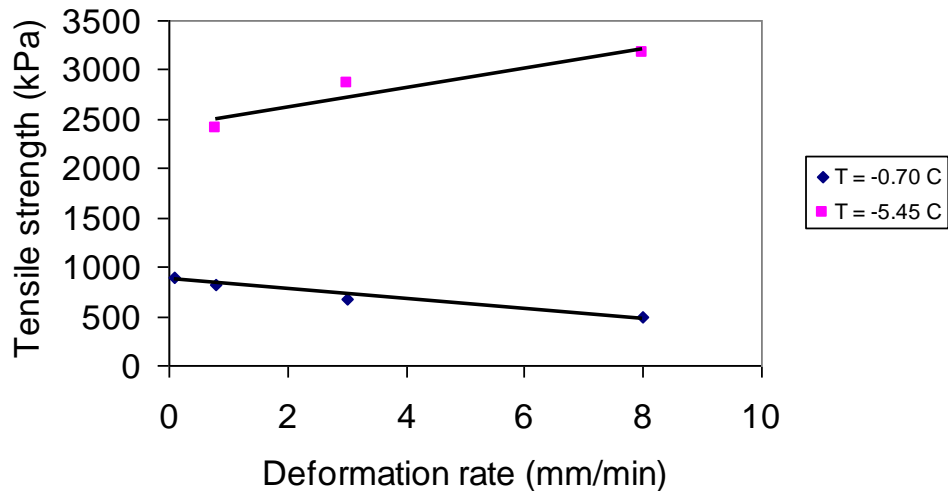


Figure 8. Temperature dependence of the influence of deformation rate on the tensile strength of the frozen fringe.

Hence, the behavior of frozen Devon silt under the frozen fringe temperature range is different from its behavior under colder temperatures. This behaviour is attributed to the change in unfrozen water content. There is a 67% increase in gravimetric water content as the temperature increases from  $-5.45^{\circ}\text{C}$  to  $-0.70^{\circ}\text{C}$  (from 7.0 % to 11.7%). This change in water content could lead to a change in pore water pressure and hence a change in behaviour.

The variation of peak tensile strength with strain rate is shown in Figure 9. Haynes (1978) expressed the tensile strength as a function of strain rate using:

$$\sigma_T = A\dot{\epsilon}^b$$

Where  $\sigma_T$  is the strength in kPa and  $\dot{\epsilon}$  is the strain rate in  $\text{s}^{-1}$ ;  $A$  (in kPa) and  $b$  are constant for a given temperature. This equation, for Devon Silt, is presented in Figure 9. The values of  $A$  and  $b$  are 297 kPa and  $-0.085$ , respectively.

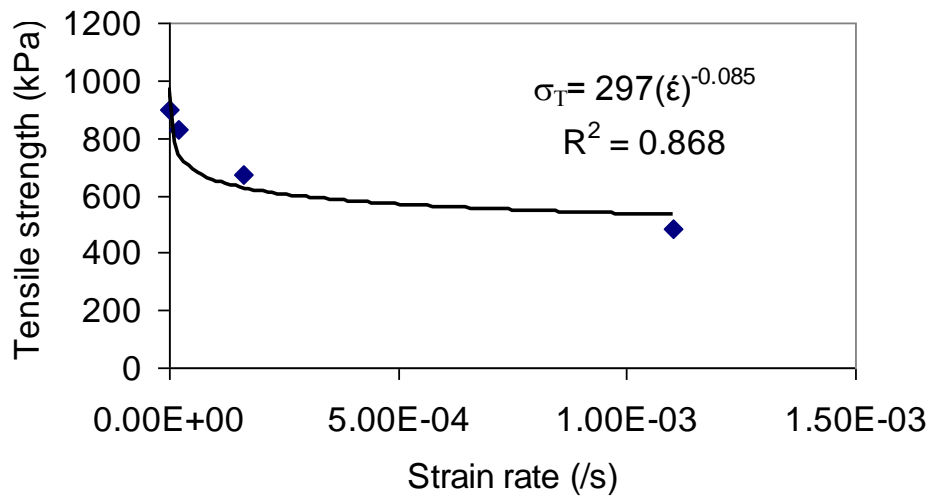


Figure 9. Tensile strength as a function of strain rate at a temperature of  $-0.70^{\circ}\text{C}$ .

### Relationship between Unfrozen Water Content and Tensile Strength

Using the temperature-tensile strength and temperature-unfrozen water content relationships, the relationship between unfrozen water content and tensile strength can be established. This relationship for Devon silt consolidated at 100 kPa is shown in Figure 10. A change in unfrozen water content from 9.70 % to 14.70 % resulted in a change in tensile strength from 1220 kPa to 686 kPa.

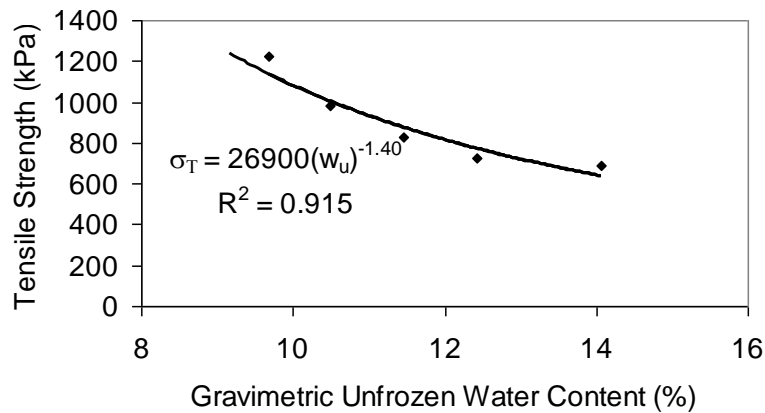


Figure 10. Effect of unfrozen water content on tensile strength of the frozen fringe.

### Relationship between Volumetric Ice Content and Tensile Strength

The relationship between volumetric ice content and tensile strength is shown in Figure 11.

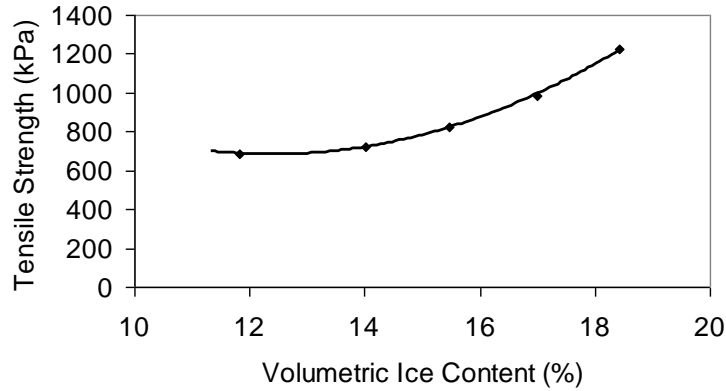


Figure 11. Relationship between volumetric ice content and tensile strength

### Stress-Strain Relationship and Modulus of Elasticity

The stress-strain diagrams for the tests conducted at different temperatures but at a deformation rate of 0.8 mm/min are shown in Figure 12. Figure 13 shows the stress-strain relationships for the tests conducted at different deformation rates at a temperature of  $-0.70^{\circ}\text{C}$ . The digital images taken at different times during the test together with the linear marks engraved on the soil sample made the strain measurement possible. The change in length of the linear marks was measured using the ImageJ software.

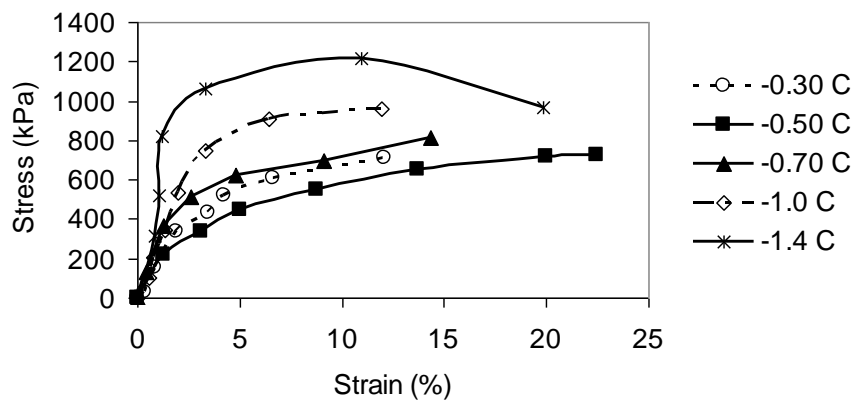


Figure 12. Stress-strain plot for the tension tests at different temperatures for a deformation rate of 0.8 mm/min.

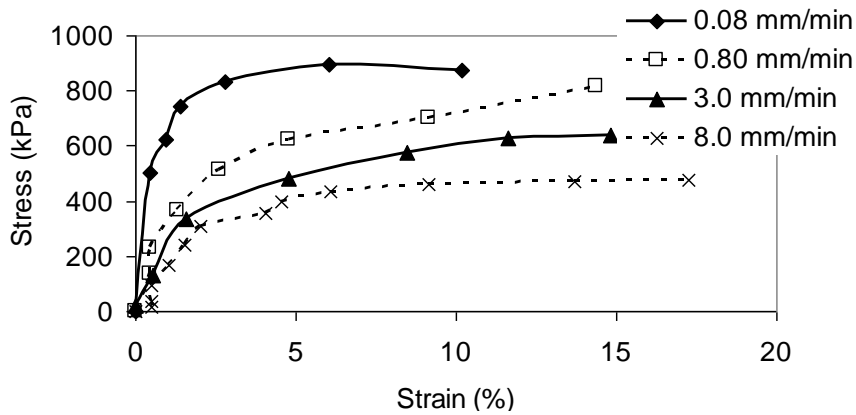


Figure 13. Stress-strain plot for the tension tests at different deformation rates at a temperature of  $-0.70\text{ }^{\circ}\text{C}$ .

### Modulus of Elasticity

The modulus of elasticity values were calculated from the initially linear portion of the stress-strain diagram. Figure 14 shows the variation of modulus of elasticity with temperature. The modulus of elasticity increases significantly with a decrease in temperature. It is also influenced by deformation rate (Figure 15).

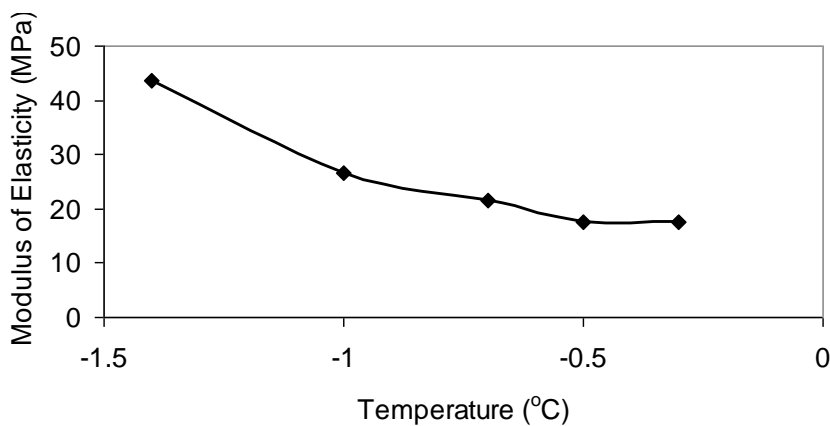


Figure 14. Variation of modulus of elasticity with temperature for a deformation rate of  $0.8\text{ mm/min}$

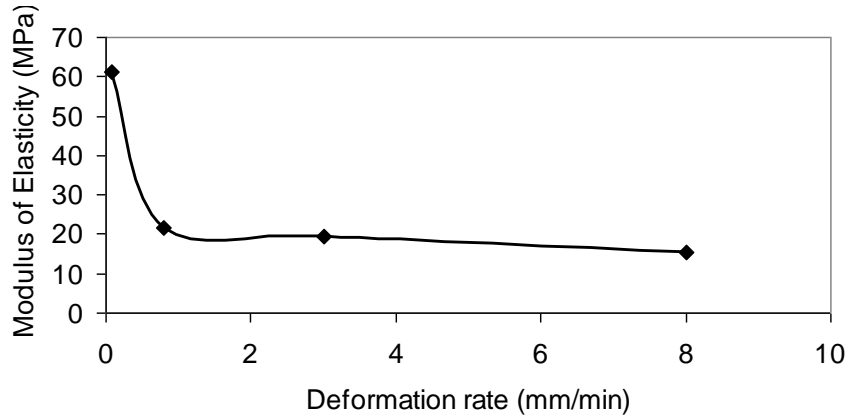


Figure 15. Variation of modulus of elasticity with deformation rate for samples frozen at  $-0.70\text{ }^{\circ}\text{C}$ .

## CONCLUSION

Four-point bending test was used to investigate the tensile strength and the stress-strain behaviour of the frozen fringe of Devon silt. The tests were conducted on samples prepared by consolidating slurry of Devon silt at 100 kPa. The influence of subzero temperatures, deformation rate/strain rate, and unfrozen water content on tensile strength of the frozen fringe of Devon silt was investigated.

The tests established that the frozen fringe possessed considerable tensile strength. Devon silt in the unfrozen state has a tensile strength of 7kPa whereas it developed a tensile strength of 686 kPa at  $-0.30^{\circ}\text{C}$ .

To investigate the influence of subzero temperatures on tensile strength of the frozen fringe, tests were conducted at temperature values from  $-0.30^{\circ}\text{C}$  to  $-1.40^{\circ}\text{C}$ . The peak tensile strength increased as the temperature decreased. It changed from 686 kPa at  $-0.30\text{ }^{\circ}\text{C}$  to 1220 kPa at  $-1.40\text{ }^{\circ}\text{C}$ .

The influence of deformation rate on the tensile strength of the frozen fringe was investigated by carrying out tests at deformation rates of 0.08 mm/min, 0.80 mm/min, 3.0 mm/min and 8.0 mm/min on samples frozen at  $-0.70^{\circ}\text{C}$ . A unique behaviour of the frozen fringe was observed: the results showed that the peak tensile strength decreased as the deformation rate increased. It decreased from 900 kPa at 0.08 mm/min to 484 kPa at 8.0 mm/min.

The relationship established between gravimetric unfrozen water content and tensile strength showed that the tensile strength is influenced by the unfrozen water content. A small change in unfrozen water content produced a significant change in tensile strength. As the unfrozen water content decreased from 14.70 % to 9.70 %, the tensile strength increased by 78% (from 686 kPa to 1220 kPa).

The stress-strain plots showed that the modulus of elasticity is influenced by the temperature and the deformation rate: it increased from 17.60 MPa at  $-0.30^{\circ}\text{C}$  to 43.50 MPa at  $-1.4^{\circ}\text{C}$ ; it decreased from 61.30 MPa at 0.08 mm/min to 15.70 MPa at 8.0 mm/min.

Additional tensile strength tests and one-dimensional freezing tests are currently being carried out to investigate the ice lens initiation condition and the formation of the freezing-induced cracks.

## ACKNOWLEDGEMENTS

The authors would like to thank Steve Gamble and Christine Hereygers at the UofA Geotechnical Centre for their assistance during the lab works. Tezera Firew Azmatch appreciated the funding through the NSERC Discovery Grants held by Dr. Sego and Dr. Biggar.

## REFERENCES

- Andersland, O.B., Ladanyi, B., 1994. An introduction to frozen ground engineering. Chapman and Hall, New York, NY, USA.
- Anderson, D.M., Morgenstern, N.R., 1973. Physics, chemistry and mechanics of frozen ground. 2nd International Conference on Permafrost, Yakutsk, USSR, 257-288.
- Akagawa, S., 1988. Experimental study of frozen fringe characteristics. Cold Regions Science and Technology. 15:209-223
- Akagawa, S., Nishisato, K., 2009. Tensile strength of frozen soil in the temperature range of the frozen fringe. Cold Regions Science and Technology. 57:13-22.
- Akagawa, S., Satoh, M., Kanie, S., Mikami, T., 2007. Effect of tensile strength on ice lens initiation temperature. Proceedings of the international conference on cold region engineering. 23-26 July, 2007, Page 43
- Arenson, L.U., Azmatch, T.F., Segó, D.C., Biggar, K.W., 2008. A new hypothesis on ice lens formation in frost-susceptible soils. Proceedings of the Ninth International Conference on Permafrost, Fairbanks, Alaska 1: 59-64.
- Azmatch, T.F., Arenson, L.U., Segó, D.C., Biggar, K.W., 2008. Measuring ice lens growth and development of soil strains during frost penetration using particle image velocimetry (GeoPIV). Proceedings of the Ninth International Conference on Permafrost, Fairbanks, Alaska 1: 89-93.

- Azmatch, T.F., Sego, D.C., Arenson, L.U., Biggar, K.W., 2010. Tensile strength of frozen soils using four-point bending test. Proceedings of the 63<sup>rd</sup> Canadian Geotechnical Conference and 6<sup>th</sup> Canadian Permafrost Conference, Calgary, Canada. 436-442.
- Bragg, R.A., Andersland, O.B., 1980. Strain rate, temperature, and sample size effects on compression and tensile properties of frozen sand. Proceedings of the Second International Symposium on Ground Freezing, Trondheim, Norway, 34–47.
- Chamberlain EJ, Gow AJ. 1979. Effect of freezing and thawing on the permeability and structure of soils. *Engineering Geology* 13: 73–92.
- Christ, M., Kim, Y., 2009. Experimental Study on the Physical-Mechanical Properties of Frozen Silt. *KSCE Journal of Civil Engineering*. 13(5):317-324.
- Coviello, A., Lagioia, R., Nova, R., 2005. On the measurement of the tensile strength of soft rocks. *Rock Mech. Rock Engng.* 38(4), 251-273.
- Dash, J.G., Fu, H., Wettlaufer, J.S., 1995. The premelting of ice and its environmental consequences. *Rep. Prog. Phys.* 58, 115-167.
- Haynes, F.D., Karalius, J.A., Kalafut, J., 1975. Strain rate effect on the strength of frozen silt. US Army Cold Regions Research and Engineering Laboratory. CRREL Research Report, vol. 350.
- Haynes, F.D., 1978. Strength and deformation of frozen silt. Proceedings of the Third International Conference on Permafrost, Edmonton, Alberta, Canada, 1:655–661.

Konrad, J. M., 2005. Estimation of the segregation potential of fine-grained soils using the frost heave response of two reference soils. *Can. Geotech. J.*, Vol. 42, pp. 38-50.

Konrad, J.M., 1990. Unfrozen water as a function of void ratio in a clayey silt. *Cold Regions Science and Technology*, 18: 49-55.

Konrad, J.M., 1989. "Influence of cooling rate on the temperature of ice lens formation", *Cold regions science and technology*. 16:25-36

Konrad, J.M., Morgenstern, N.R., 1982. Effects of applied pressure on freezing soils. *Canadian Geotechnical Journal*, 19: 494-505.

Kujala, K., 1997. Estimation of frost heave and thaw weakening by statistical analyses. *Ground Freezing 97*, ed. Knutsson, Rotterdam, A.A. Balkema, pp. 31-41.

Lachenbruch, A.H., 1962. Mechanics of thermal contraction cracks and ice-wedge polygons in permafrost. *Geophysical Society of America Special Papers*, 70:1-69.

Miller, R.D., 1972. Freezing and heaving of saturated and unsaturated soils. *Highway Research Rec.* 393:1-11

Miller, R.D., 1978. Frost heaving in non-colloidal soils. *Proceedings of the Third International Conference on Permafrost*, Edmonton, Alberta, Canada, 1:708-713.

Patterson, D.E., Smith, M.W., 1980. The use of Time Domain Reflectometry for the Measurement of Unfrozen Water Content in Frozen Soils. *Cold Regions Science and Technology*, 3:205-210

- Ping, L., Xiaozu, X., 2000. Application of experimental inversion method to analyzing the characteristics of the frozen fringe. *Ground Freezing 2000*, Balkema, Rotterdam. 105-110
- Thusyanthan, N.I., Take, W.A., Madabhushi, S.P.G., Bolton, M.D., 2007. Crack initiation in clay observed in beam bending. *Geotechnique* 57 (7): 581-594
- Tice, A.R., Anderson, D.M., A. Banin., 1976. The prediction of unfrozen water content in frozen soils from liquid limit determinations, US Army Cold Regions Research. Engineering Laboratory, CRREL Rep. 76-8
- Topp, G.C., Davis, J.L, Annan, A.P., 1980. Electromagnetic determination of soil water content: measurements in coaxial transmission lines. *Water Resources Research*, 16(3):574-582
- Watanabe, K., Mizoguchi, M., Ishizaki, T., Fukuda, M., 1997. Experimental study on microstructure near freezing front during soil freezing. *Ground Freezing 97*, ed. Knutsson, Rotterdam, A.A. Balkema, pp. 187 - 192
- Xia, D., 2006. Frost heave studies using digital photographic technique. MSc Thesis, University of Alberta, Edmonton, AB, Canada, 165 pp.
- Xiaozu, X., Ziawang W., 1997. Essential characteristics of frozen fringe and determination of its parameters. *Ground Freezing*. 203-207
- Zhu, Y., Carbee, D.L., 1985. Strain rate effect on the tensile strength of frozen silt, *Fourth International Symposium on Ground Freezing*, Sapporo, Japan: 153 – 157
- Zhu, Y., Carbee, D.L., 1987. Tensile strength of frozen silt. US Army Cold Regions Research and Engineering Laboratory, CRREL Report 87-15

## **ADDENDUM TO CHAPTER 3**

### **Ice Lens Initiation condition based on the tensile strength of frozen fringe**

Arenson et al (2008) and Azmatch et al. (2008) have indicated that ice lens initiation and hence frost heave starts with the cracking of the frozen fringe. In order for the frozen fringe to crack, its tensile strength needs to be exceeded. Therefore, ice lens initiation is related to tensile strength within the frozen fringe.

The original intention of this study was to propose ice lens initiation condition as a function of the tensile strength of the frozen fringe as indicated in Azmatch et al (2011), Arenson et al. (2008) and Azmatch et al (2008). However, later on it was discovered that the criterion using the soil freezing characteristics curve is a much simpler and more straightforward approach to determine the ice lens initiation condition. Hence, the research was redirected to evaluation of this important ice lens initiation condition.

In here, however, the importance of the tensile strength criterion as another option to define ice lens initiation condition is presented. Therefore, we will use the tensile strength data together with equations provided by Style et al. (2011) to show that ice lens initiation condition depends on the tensile strength of the soil.

As discussed in Chapter 3, it is proposed that ice lens initiation condition is related to the tensile strength of the frozen fringe. The tensile strength tests were carried out to verify this.

A new ice lens initiation condition that accounts for the tensile strength of the frozen fringe, and citing our previous publication (Arenson et al., 2008), was recently published by Style et al. (2011). According to this work, a new ice lens initiates when the following condition is satisfied:

$$T_m - T = \frac{T_m \sigma_t}{\rho L_m} \quad (3A.1)$$

Where  $T$  is temperature,  $T_m$  is the bulk melting temperature of pure water,  $\rho$  is the density of water,  $L_m$  is the latent heat of melting of ice,  $\sigma_t$  is the tensile strength of the soil.

However, Style et al. (2011) did not provide experimental evidence to prove that equation (3A.1) controlled this initiation condition since they did not have tensile strength data. Experimental results from this study are used to establish the validity of this criterion. The stress-strain behavior is modeled as bi-linear and it is assumed that the cracks initiate at a stress corresponding to 2% strain.

Using tensile strength and stress-strain behavior of a sample consolidated to 100 kPa, the ice lens initiation temperature from a one-dimensional frost heave test are compared with the result determined by using the tensile strength of the frozen fringe. The tensile strength (determined at 2% strain) variation with temperature is shown in Figure 3A.1.

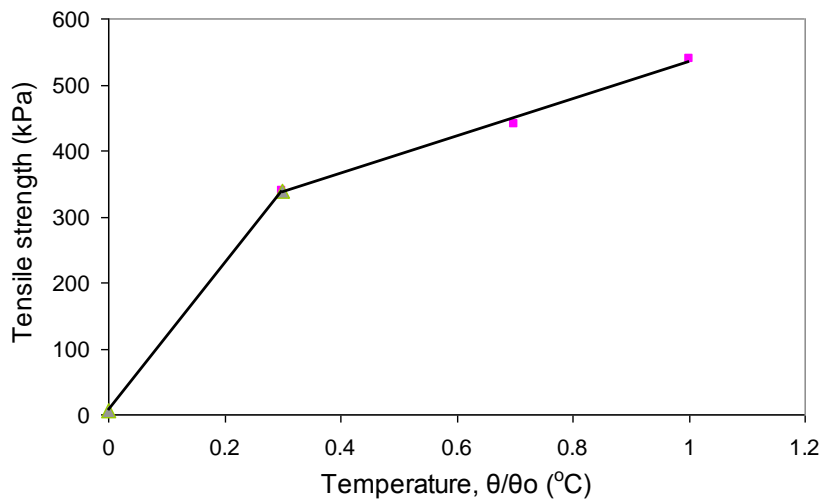


Figure 3A.1. Tensile strength (at 2% tensile strain value) variation with temperature ( $\theta$  is the temperature at which the sample is frozen and  $\theta_0$  is a reference temperature taken as  $-1.0^\circ\text{C}$ ).

The ice lens initiation temperature from the one-dimensional frost heave test is  $-0.16\text{ }^{\circ}\text{C}$ . Substituting this value in the above equation and solving for the corresponding tensile strength gives a value of 193 kPa. The tensile strength at a temperature of  $-0.16\text{ }^{\circ}\text{C}$  from Figure 3A.1 is 185 kPa.

Comparing the two values shows that the ice lens initiation criterion proposed above by Style et al (2011) gives a result close to the experimental values. Therefore, the results from this study support the hypothesis (Presented in Azmatch et al., 2008; Arenson et al., 2008) that crack initiation is related to the tensile strength within the frozen fringe in a particular soil.

## **REFERENCE**

Arenson, L.U., Azmatch, T.F., Segó, D.C., and Biggar, K.W. 2008. A new hypothesis on ice lens formation in frost-susceptible soils. Proceedings of the Ninth International Conference on Permafrost, Fairbanks, Alaska 1: 59-64.

Azmatch, T.F., Arenson, L.U., Segó, D.C., and Biggar, K.W., 2011. Tensile Strength and Stress-Strain Behaviour of Devon Silt under Frozen Fringe Conditions. Cold Regions Science and Technology. 68, 85–90.

Azmatch, T.F., Arenson, L.U., Segó, D.C., and Biggar, K.W. 2008. Measuring ice lens growth and development of soil strains during frost penetration using particle image velocimetry (GeoPIV). Proceedings of the Ninth International Conference on Permafrost, Fairbanks, Alaska 1: 89-93

Style, R.W., Peppinn, S.S. L., Cocks, A.C.F., Wettlaufer, J.S., 2011. Ice-lens formation and geometrical supercooling in soils and other colloidal materials. Physical Review E84, 041402, 1-12

## **CHAPTER 4. SOIL FREEZING CHARACTERISTIC CURVE OF DEVON SILT**

This paper was previously published in the Proceedings of the David C. Segó Symposium. It is modified (formatting only) and presented as published as part of this Ph.D. thesis as Chapter 4.

Reference: Azmatch, T.F., Arenson, L.U., Segó, D.C., Biggar, K.W., 2012. Soil freezing characteristic curve of Devon Silt. Published in Proceedings of the David C. Segó Symposium, University of Alberta, Edmonton, Alberta, Canada, April 26–27.

## **CHAPTER 4. SOIL FREEZING CHARACTERISTIC CURVE OF DEVON SILT**

### **ABSTRACT**

The soil freezing characteristic curve (SFCC) of Devon Silt is discussed. SFCC tests were conducted on samples prepared under different initial void ratios. SFCC tests were also conducted by placing samples in a freezing cell at different subzero temperatures. Hysteresis effect was studied by subjecting the samples to freeze-thaw cycles. The results showed that the shape of the SFCC depends on the initial void ratio, the cooling rate, and the freeze-thaw cycle. The ice entry value (IEV) increases with a decrease in initial void ratio and it also increases with an increase in cooling rate. The IEV further changes with each freeze-thaw cycle. The IEV is larger for the first cycle of freezing when compared to the second and third freezing cycle. This behaviour is attributed to the structural changes that occur during the first freeze-thaw cycle.

### **INTRODUCTION**

Pore water in soil can remain unfrozen at temperatures well below the freezing point temperatures because of a decrease in the free energy of the water due to surface forces associated with soil particles and the pore geometry among soil particles (Dash et al., 1995). The existence of unfrozen water in a soil below the freezing point has significant consequences for the transport of water, solutes, and heat in a freezing soil (Spaans and Baker, 1996).

In a frozen soil, where liquid water and pore ice coexist, the water potential is strongly dependent on temperature. The relationship between unfrozen water content and temperature (or, unfrozen water content and suction) in a partially

frozen soil is characterized through the so-called soil freezing characteristics curve (SFCC). A complete SFCC is required to understand heat, water, and solute transport in frozen soils (Spaans and Baker, 1996). SFCC has also been used to analyze the freeze-thaw behavior of frozen soils, for example as recently presented by Liu et al. (2012).

SFCC was further used to determine the soil-water characteristic curve (SWCC) of unfrozen, unsaturated soils for modeling multi-season soil water dynamics (Flerchinger et al., 2006). Such a use is based on the similarity of drying and wetting phenomena in unfrozen soil to freezing and thawing phenomena in frozen soil (Spaans and Baker, 1996). In drying soils, water is removed and replaced by air leaving the remaining water at an increasingly lower matric potential. The same occurs in freezing soils, except that liquid water changes phase and becomes ice. The same forces that prevent soil water from draining also prevent it from freezing (Spaans and Baker, 1996). Hence, frozen soils have been assumed to behave in a similar fashion as unfrozen, unsaturated soils with the air phase in non-frozen soil replaced by the ice phase in a frozen soil. This assumption has been used by different authors such as Spaans and Baker, 1996; Koopmans and Miller, 1966; Black and Tice, 1989; and Williams, 1964. Flerchinger et al. (2006) have presented the SWCC from the SFCC and used it to model multi-season soil water dynamics in unfrozen soils with reasonable accuracy.

SFCC can be plotted as unfrozen water content versus temperature or as unfrozen water content versus suction. Figure 1 show typical SFCC plotted as unfrozen volumetric water content ( $\theta$ ) versus suction. If similarity between drying and freezing processes is assumed, then the soil water characteristics curve (SWCC) and SFCC will be assumed to be similar; and hence the terminologies used in unsaturated soil can be modified to fit partially frozen soils. The ice entry value (IEV), which is the analogue to air-entry value (AEV), is defined as the suction/temperature at which ice first begins to enter the largest soil pores. The



## **EXPERIMENTAL PROGRAM**

### **Soil Properties and Sample Preparation**

The soil tested is Devon Silt with a specific gravity of 2.65, a clay fraction of 25% and a silt fraction of 75%. It has a liquid limit of 32% and plastic limit of 20%. Slurry of the soil is prepared at a moisture content of 60% and then consolidated under a specific consolidation pressure.

### **Test for Soil Freezing Characteristics Curve**

There are a number of methods to determine the unfrozen water content (Anderson and Morgenstern, 1973). Some of the methods used are time domain reflectometry (TDR), calorimeters, and nuclear magnetic resonance (NMR). For this study, unfrozen water content is measured by TDR. The TDR method measures the dielectric property which is then converted to volumetric water content by using the empirical equation provided by Topp et al. (1980). The TDR was first used for unfrozen soils and later extended to frozen soils (e.g. Patterson and Smith, 1980).

The unfrozen water content of Devon Silt was measured using TDR. The soil sample was placed in a freezing cell. The temperature of the freezing cell was controlled separately using a temperature control bath. The temperature of the freezing cell is monitored using two resistance temperature detectors (RTDs) placed at two corners within the cell. The sample froze isotropically once placed in the cell. An RTD and a TDR were placed inside the sample to monitor the temperature and the unfrozen water content, respectively, during freezing. The TDR test was carried out on samples prepared from slurry and consolidated under different pressures. These results were then used to create the SFCC for Devon Silt.

## EXPERIMENTAL RESULTS AND DISCUSSION

The results from the laboratory tests for the SFCCs are shown in Figure 2. In Figure 2 the SFCC is presented as a plot of unfrozen water content versus temperature. However, to get the IEV from a SFCC, the SFCC has to be plotted as unfrozen water content versus suction. To be able to do this we need to correlate temperature with suction. For this, it is assumed that the general Clausius-Clapeyron equation is valid. The equation is used to correlate suction with temperature by assuming the ice phase to be under atmospheric pressure. Hence, the relation provided by Konrad (1994), which states that the suction increases linearly with decreasing temperature at a rate of 1250 kPa/°C, is used herein. This relationship was used in plotting the SFCCs (unfrozen water content versus suction) as shown in Figure 3.

### Influence of Initial Void Ratio

The IEV was determined using the procedure shown in Figure 1. The IEVs determined from the SFCCs for the different samples are summarized in Table 1. Figure 4 presents the variation of IEV with initial void ratio. It is observed that IEV increases as the initial void ratio decreases.

Table 1. IEVs determined from the SFCCs.

Consolidation Pressure (kPa)	50	100	200	400
Initial Void ratio, $e$ (-)	0.795	0.702	0.623	0.583
Ice Entry Value, IEV(kPa)	85	175	250	450

Figure 3 also shows that the slope of the SFCC, in the zone where there is a sharp decrease in unfrozen water content, changes with a change in initial void ratio. The sample consolidated to 50 kPa has a steeper slope in this zone when

compared to the sample consolidated to 400 kPa. Hence, the shape of the SFCC depends on the consolidation pressure at which the sample was prepared or on the initial void ratio of the soil sample.

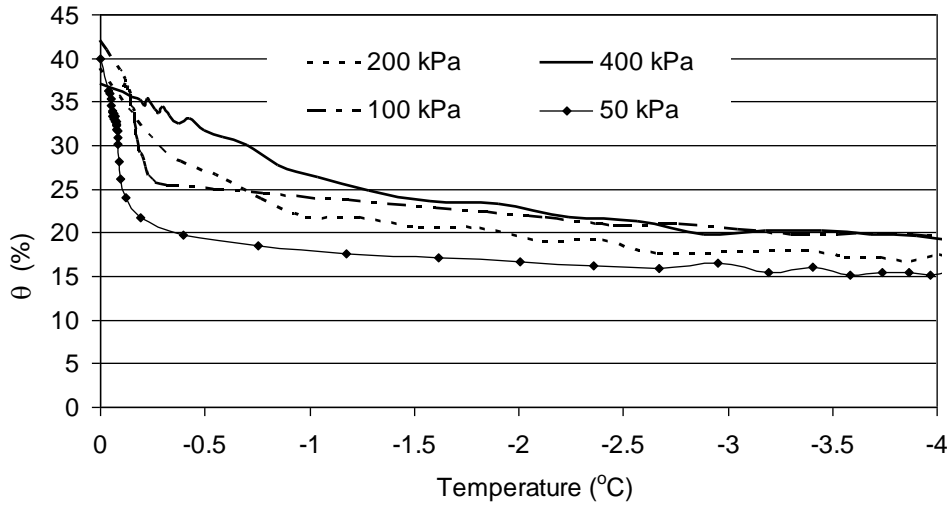


Figure 2. SFCC (volumetric water content,  $\theta$ , versus temperature) for samples consolidated at different pressures.

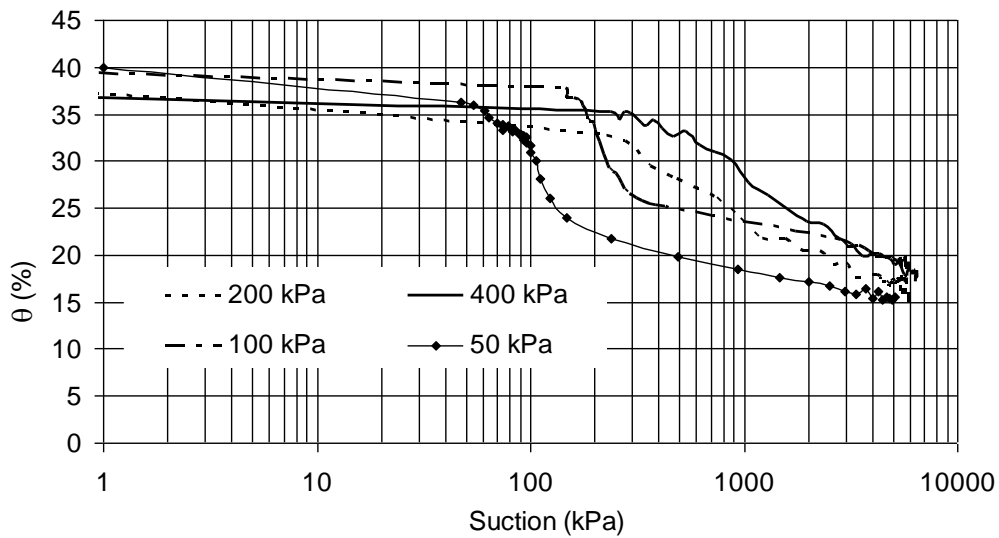


Figure 3. SFCC curve (volumetric water content,  $\theta$ , versus suction) for samples consolidated at different pressures.

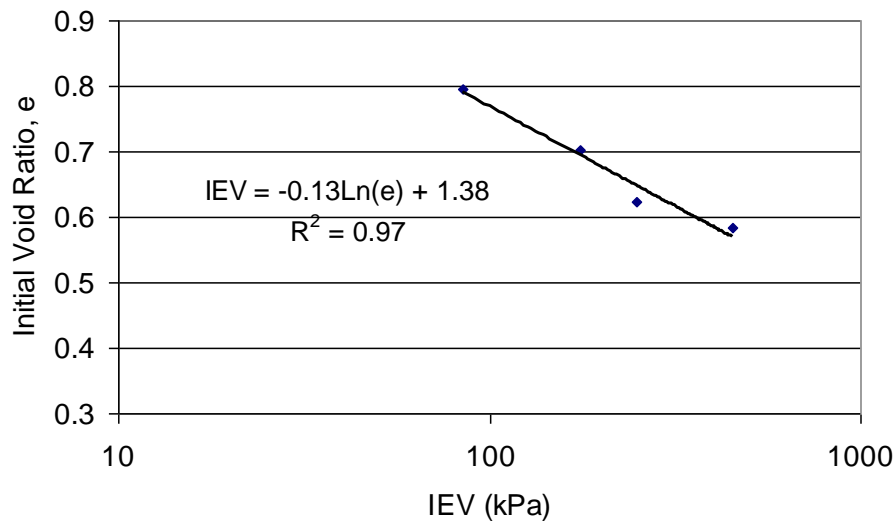


Figure 4. Variation in the IEV with initial void ratio.

### **Influence of Freezing Temperature and Cooling Rate**

To investigate the influence of temperatures on the freezing characteristic, tests were carried out on samples consolidated at 50 kPa and frozen by placing them in a freezing cell at different temperatures. The first sample was placed in a freezing cell at a temperature of  $-4\text{ }^{\circ}\text{C}$ , the second sample was frozen at a temperature of  $-10\text{ }^{\circ}\text{C}$ , and the third sample at a temperature of  $-18\text{ }^{\circ}\text{C}$ . The temperatures and the volumetric water contents were measured using RTD and TDR, respectively. The SFCCs from these tests are shown in Figure 5. It is observed that the IEV changes with change in freezing temperature. The IEVs were 70 kPa, 80 kPa and 100 kPa for samples frozen in a freezing cell at  $-4\text{ }^{\circ}\text{C}$ ,  $-10\text{ }^{\circ}\text{C}$  and  $-18\text{ }^{\circ}\text{C}$ , respectively. Even though constant rate of cooling was not used during these tests, it is expected that the cooling rate changes as a function of the freezing cell temperature. Therefore, it can be concluded that the IEV increases with increasing cooling rate.

## **Influence of Freeze-Thaw Cycles**

A sample consolidated at 100 kPa was subjected to three freeze-thaw cycles to investigate that influence on the SFCC. Figure 6 shows the first cycle of freezing and thawing. It is noted that there is a hysteresis in the volumetric water content curve. A different unfrozen water content was measured for the same suction value under freezing compared to thawing. The results of the subsequent freeze-thaw cycles are presented in Figure 7 and Figure 8, for the freezing cycles and for the thawing cycles, respectively.

Figure 7 shows that the SFCC corresponding to the first freezing is different from the second and the third cycles. It is observed that the IEV during the first cycle of freezing is higher than the IEVs during the second and third freezing cycles. This shows that a lower suction, hence a warmer temperature, is required for ice to penetrate the soil during the second cycle of freezing (100 kPa,  $-0.08\text{ }^{\circ}\text{C}$ ) compared with the first cycle (175 kPa,  $-0.14\text{ }^{\circ}\text{C}$ ). This is believed to be caused by some changes in the soil structure during the first freezing cycle, which might have increased the void ratio of the soil resulting in a reduced IEV (suction) being required for ice to enter the soil pores during subsequent freeze-thaw cycles. Figure 7 also indicates that the SFCC of the second and third freezing cycles is almost identical. These observations indicate that most of the structural changes occur when a soil is subjected to freezing and thawing for the first time.

An interesting observation from Figure 8 is that all thawing cycle results indicate almost identical SFCCs.

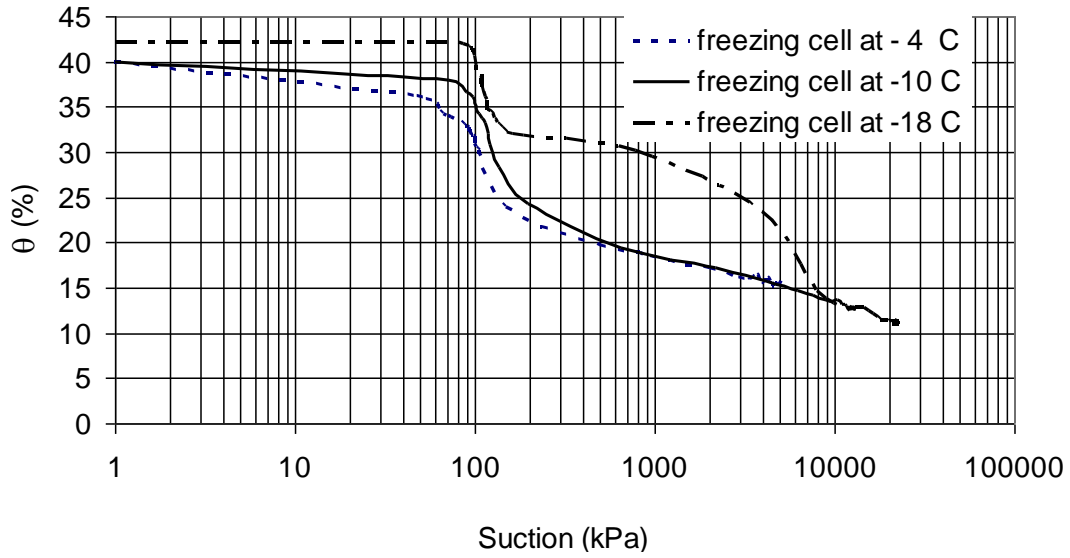


Figure 5. SFCC under different freezing temperatures.

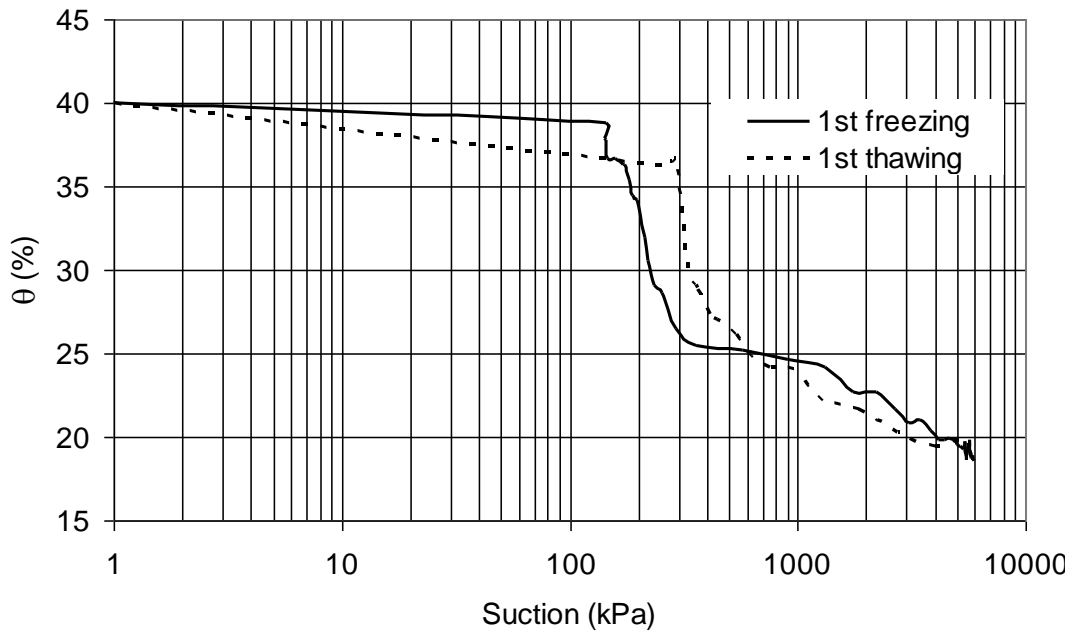


Figure 6. SFCC of Devon Silt during first freezing and first thawing stages.

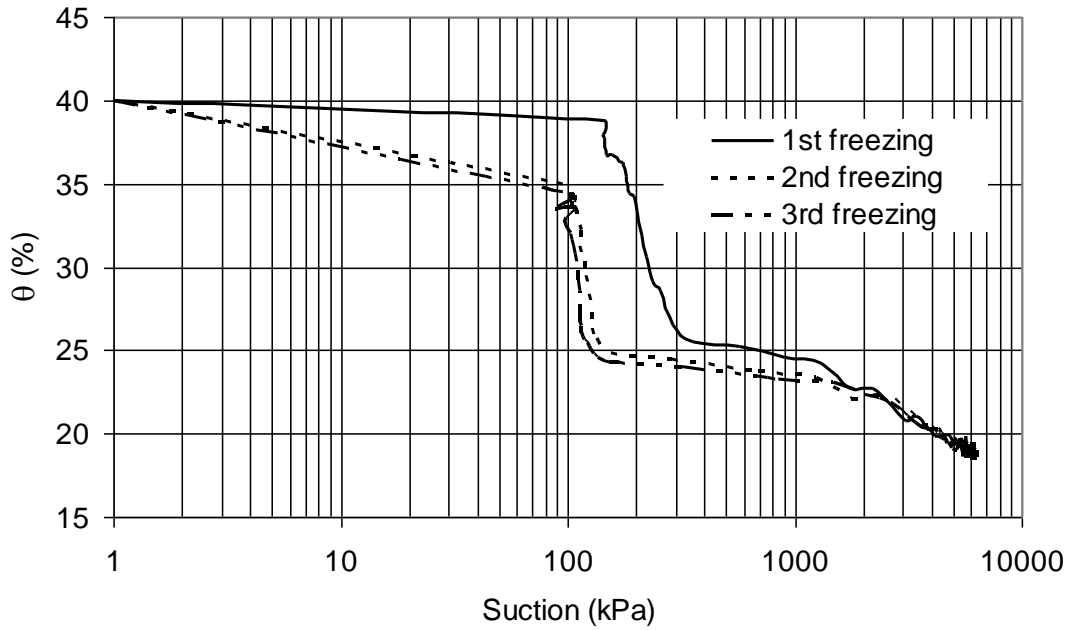


Figure 7. SFCC of Devon Silt during cycles of freezing.

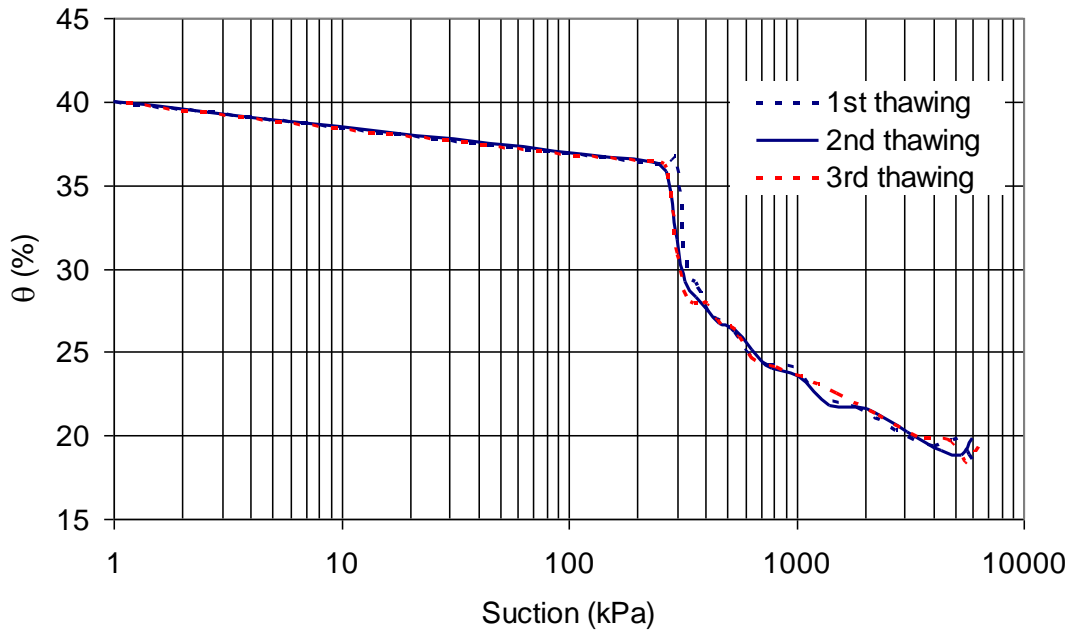


Figure 8. SFCC of Devon Silt during cycles of thawing.

## **CONCLUSION**

The soil freezing characteristic curve (SFCC) of Devon silt was determined on samples prepared at different initial void ratios. To investigate the influence of cooling rate on the SFCC, tests were carried out on samples placed in a freezing cell at different temperatures. Multi cycle freeze-thaw tests were also carried out on some of the soil samples to investigate the influence of freeze-thaw cycles on the SFCC and the ice entry value (IEV). The results show that the shape of the SFCC depends on initial void ratio as well as temperature, i.e. the cooling rate.

The IEV increases with a decrease in initial void ratio and it also increases with an increase in cooling rate (cooling). In addition, the IEV changed from the first to the subsequent freeze-thaw cycles. The IEV was higher for the first cycle in comparison with the second and third freeze cycles. The experimental results showed that a lower suction, hence a higher temperature, is required for ice to penetrate the soil during the second cycle of freezing (100 kPa, -0.08 °C) than the first cycle (175 kPa, -0.14 °C). This is attributed to potential structural changes that occur during initial freezing.

## **ACKNOWLEDGEMENT**

The research was funded from Discovery Grants provided by the Natural Science and Engineering Research Council of Canada.

## **REFERENCES**

Anderson, D.M., Morgenstern, N.R. 1973. Physics, chemistry and mechanics of frozen ground. 2nd International Conference on Permafrost, Yakutsk, USSR, 257-288.

- Black, P.B., Tice, A.R. 1989. Comparison of soil freezing curve and soil water curve data for Windsor Sandy Loam. *Water Resources Research* 25, 2205-2210.
- Dash, J.G., Fu, H., Wettlaufer, J.S. 1995. The premelting of ice and its environmental consequences. *Rep. Prog. Phys.* 58, 115-167.
- Flerchinger, G.N., Seyfried, M.S., Hardegree, S.P. 2006. Using soil freezing characteristics to model multi-season soil water dynamics. *Vadose Zone Journal* 5:1143–1153.
- Konrad, J.M. 1994. 16th Canadian Geotechnical Colloquium-Frost heave in soils-concepts and engineering. *Canadian Geotechnical Journal* 31(2), 223-245.
- Koopmans, R.W.R. Miller, R.D. 1966. Soil freezing and soil water characteristic curves. *Soil Sci. Soc. Am Proc.* 30, 680-685.
- Liu, Z., Yu, X., Yu, X., Gonzalez, J. 2012. Time domain reflectometry sensor-assisted freeze/thaw analysis in geomaterials. *Cold Regions Science and Technology* 71:84-89
- Patterson, D.E., Smith, M.W. 1980. The use of time domain reflectometry for the measurement of unfrozen water content in frozen soils. *Cold Regions Science and Technology*, 3:205-210
- Spaans, E.J.A., Baker, J.M. 1996, The soil freezing characteristic: Its measurement and similarity to the soil moisture characteristic, *Soil Sci. Soc. Am. J* 60, 13-19.

Topp, G.C., Davis, J.L., Annan, A.P. 1980. Electromagnetic determination of soil water content: measurements in coaxial transmission lines. *Water Resources Research*, 16(3):574-582

Williams, P.J. 1964. Unfrozen water content of frozen soils and soil moisture suction. *Geotechnique* 14, 231-246.

## **CHAPTER 5. NEW ICE LENS INITIATION CONDITION FOR FROST HEAVE IN FINE-GRAINED SOILS**

This paper was previously reviewed, accepted and published in the Cold Regions Science and Technology journal. It is modified (formatting only) and presented as published as part of this Ph.D. thesis as Chapter 5.

Reference: Azmatch, T.F., Segó, D.C., Arenson, L.U., and Biggar, K.W., 2012. New Ice Lens Initiation Condition for Frost Heave in Fine-Grained Soils. Cold Regions Science and Technology. 82, 8–13.

## **CHAPTER 5. NEW ICE LENS INITIATION CONDITION FOR FROST HEAVE IN FINE-GRAINED SOILS**

### **ABSTRACT**

Frost heave results from ice segregation and ice lens formation and growth as a soil freezes. This formation is initiated by cracking of the soil in the frozen fringe. Therefore, evaluation of the ice lens initiation requires the determination of the crack initiation condition in the frozen fringe. A new fundamental approach is proposed to determine the ice lens initiation condition using the soil freezing characteristics curve (SFCC). It is demonstrated that an ice lens initiates close to the so-called ice-entry value defined using the SFCC. Ice lens initiation conditions for different boundary conditions were determined in a laboratory using the SFCC and were then compared with the ice lens initiation conditions from a one-dimensional open system frost heave tests. The results using the SFCC showed good agreement with the values determined experimentally. It was therefore concluded that the SFCC derived information can be used as an input parameter in existing frost heave models to establish the segregation temperature.

*Key words: Frost heave, ice lens, frozen fringe, ice-entry value, soil freezing characteristics curve, segregation temperature*

### **INTRODUCTION**

Studies to understand the frost heave process have been carried out by many researchers for nearly a century (e.g. Taber, 1929; Beskow, 1935; Harlan, 1973; Konrad and Morgenstern, 1980; Gilpin, 1980; Bronfenbrener and Bronfenbrener, 2010). Horizontal ice lenses and vertical ice veins are formed during freezing forming a reticulate ice lens structure as observed in Figure 1. Three distinct zones exist in a freezing soil during frost heave: the frozen zone, the unfrozen zone and the frozen fringe. These zones are as shown in Figure 1. The frozen

fringe is the zone between the growing (warmest) horizontal ice lens and the frost front (zero degree isotherm), i.e., it is the zone where the warmest pore ice exists. Since, the concept of the frozen fringe was first presented by Miller (1972), it has been realized that the characteristics of the frozen fringe play a very important role in the frost heave process.

One-dimensional freezing tests using Devon Silt and carried out by Xia (2006) showed the existence of cracks in and/or through the frozen fringe from tests carried out under various boundary conditions (Figure 1). These cracks that precede the formation of horizontal ice lenses and vertical ice veins are important features associated with the frost heave process since they are believed to influence both the magnitude of frost heave and the moisture transfer rate or the hydraulic conductivity within the frozen fringe (Azmatch et al., 2008; Arenson et al., 2008).

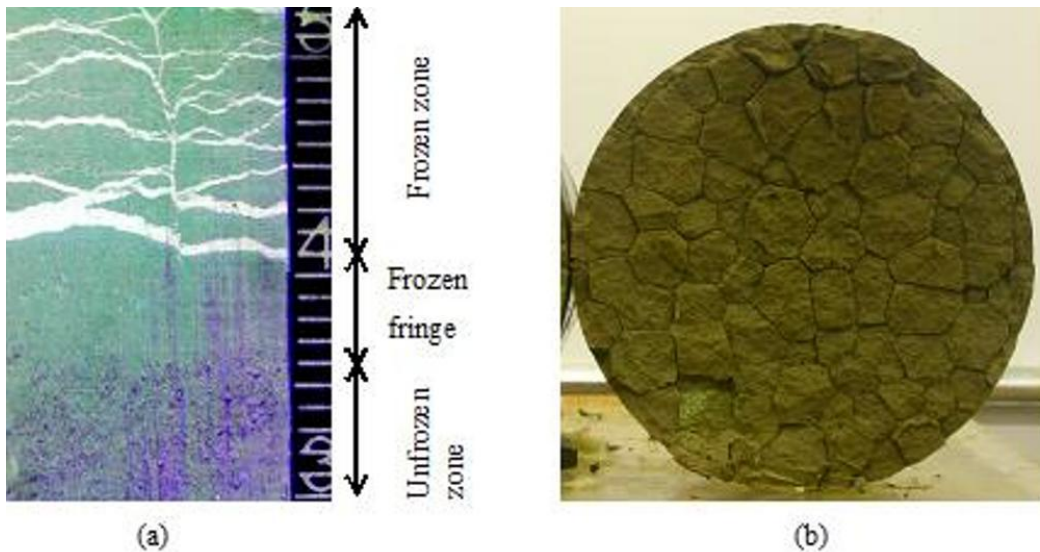


Figure 1: Frost heave features: (a) Reticulate ice structure viewed in vertical sample section and, (b) freezing-induced cracks within the frozen fringe viewed on a horizontal sample cross section at the base of the final ice lens (Xia, 2006). Sample diameter = 10.0 cm.

The results from previous studies on frost heave (e.g., Taber, 1929; Beskow, 1935; Harlan, 1973; Konrad and Morgenstern, 1980; Gilpin, 1980; Bronfenbrener and Bronfenbrener, 2010) indicate that significant frost heave observed in the field or laboratory is attributed to ice lens formation associated with water migration to the freezing front and the segregational ice that develops. Hence frost heave prediction models require ice lens initiation criteria. Observations by different researchers (Azmatch et al., 2011; Konrad and Duquennoi, 1993) indicate that ice lens initiation is related to cracking of the soil in the frozen fringe.

In this paper, the crack initiation condition is first defined and it is then used to subsequently define the ice lens initiation condition for frost heave to develop. It is assumed that the ice lens initiation is related to this crack initiation condition.

### **ICE LENS INITIATION CONDITION IN FROZEN SOILS**

The criteria governing ice lens initiation has been studied by different researchers. Miller (1972, 1978) pointed out that ice lenses do not form until the pore water pressure is sufficient to separate soil particles. Gilpin (1980) suggested that a new ice lens appears when and where the maximum ice pressure reaches the separation pressure. O'Neill and Miller (1980) used a neutral stress defined as the difference between the overburden pressure and the effective stress instead of the ice pressure to define this initiation condition. A new ice lens appears when and where the maximum neutral stress reaches the overburden pressure, i.e., the effective stress approaches zero.

The generalized Clausius-Clapeyron equation is used to relate the water pressure and ice pressure to the temperature within the frozen fringe under these conditions. The neutral stress is equal to a weighted sum of the water and ice pressure. The weight factor depends on the unfrozen water content and porosity. Sheng et al. (1995) have used a similar approach but have calculated the weight

factors differently. According to Akagawa et al. (2007) a new ice lens initiates when the ice pressure exceeds both the sum of the overburden pressure and the tensile strength of the freezing soil.

Konrad and Duquennoi (1993) stated that a new ice lens is initiated when the strain exceeds the instantaneous tensile failure strain of the frozen soil. Konrad and Morgenstem (1980) stated that the starting position of a new ice lens is governed by the local permeability within the current frozen fringe, which is associated with the segregation temperature. As the temperature at the base of the warmest ice lens reaches a critical value, the permeability is so low that no water is able to flow to the warm side of the previously growing ice lens. Thus a new ice lens forms at the location with a temperature identical to the segregation temperature.

All the ice lens initiation criteria discussed above have in common that they require the determination of the segregation temperature (i.e., ice lens initiation temperature). However, presently, there is no specified method, other than direct determination from one dimensional frost heave test (Akagawa, 1988; Konrad, 1980), for determining the segregation temperature. However, direct determination of the segregation temperature using frost heave test is very complex and a simplified method is presented in this paper.

Experimental observations by Arenson et al. (2008) and Azmatch et al. (2008) have shown that cracking precedes the formation of ice lenses. Therefore, it is postulated that the segregation temperature can be determined using the following assumption: the ice lens initiation condition is related to the crack initiation within the frozen fringe.

## CRACK INITIATION CONDITION IN NONFROZEN SOILS

Crack initiation conditions for non-frozen drying soils can be categorized into three groups; 1) stress criterion (Ajaz and Parry, 1975; Snyder and Miller, 1985; Abu-hejleh and Znidarcic, 1995; Konrad and Ayad, 1997; Zeh and Witt 2006), 2) strain criterion (Meakin 1987; Kitsunozaki 1999; Vogel et al., 2005), and 3) empirical criteria using the soil-water characteristics curve (Peron et al., 2009).

Peron et al. (2009) carried out experimental investigation of desiccation cracking for homogeneous, cohesive soils with a focus on the mechanism of shrinkage associated with drying and crack initiation. Based on their experimental results, they concluded that cracks initiate close to the onset of desaturation and hence close to the air entry value from the soil water characteristics curve (SWCC). This observation is used in this paper to propose crack initiation condition, and hence ice lens initiation condition, for freezing soils.

Frozen soils are assumed to behave in a similar manner to unfrozen, unsaturated soils with the ice phase in frozen soils replacing the air phase in non-frozen soils. This assumption has been proposed by Spaans and Baker (1996), Koopmans and Miller (1966), Black and Tice (1989), and Williams (1964). The soil freezing characteristics curve (SFCC) for frozen soils, which is the plot of the unfrozen water content versus temperature or suction, is an analogue to the SWCC and it is essential for modeling the transport of water, heat and solutes in frozen soils (Spaans and Baker, 1996). The SFCC for frozen soils carries similar information as the SWCC for non-frozen soils. In fact, the SWCC has been used to determine the hydraulic conductivity function of frozen soils in a similar manner as the SWCC is used to determine the hydraulic conductivity function of non-frozen soils (e.g., Newman and Wilson, 1997). Hence the observation made by Peron et al. (2009), that cracks initiate close to air-entry value from the SWCC for non-frozen soils, will be postulated to hold true for frozen soils. Hence, it is assumed

that the crack initiation point on the SFCC for frozen soils is close to the ice-entry value (IEV). Since the frozen fringe has to crack before an ice lens forms (Azmatch et al., 2011), it is then hypothesized that the ice lens initiation point corresponds to the crack initiation point.

To evaluate this hypothesis, laboratory tests were conducted using Devon Silt. Laboratory tests were conducted to obtain the SFCCs under different boundary conditions. The temperature corresponding to the IEV on the SFCC was then considered to be the ice-lens initiation temperature (segregation temperature). One-dimensional frost heave tests were also conducted to observe the development of ice lenses, and to measure the ice lens initiation temperature. The ice lens initiation temperature predicted from the SFCC and that measured in the one-dimensional frost heave tests could then be compared to determine the effectiveness of the SFCC prediction.

## **EXPERIMENTAL PROGRAM**

### **Soil Properties and Sample Preparation**

The Devon Silt with a specific gravity of 2.65, a clay fraction of 25% and a silt fraction of 75% was used in the test program. It has a liquid limit of 32% and plastic limit of 20%. Soil slurry was prepared at a moisture content of 60% and then de-aired prior to being consolidated under a specific vertical stress. Different samples were prepared by initially consolidating them to 100 kPa, 200 kPa and 400 kPa.

### **Soil Freezing Characteristics Curve**

Within a frozen soil, a certain amount of water remains unfrozen at subzero temperatures because of a decrease in the free energy of soil water due to surface forces associated with soil particles and the pore geometry among these soil

particles (Dash et al., 1995). The unfrozen water content of Devon Silt was measured using the time domain reflectometry (TDR) technique. The soil sample prepared as previously described is placed in a freezing cell and then consolidated under different vertical stresses. The temperature of the actual freezing cell is separately controlled using a cooling bath. The temperature of the freezing cell is monitored using two RTDs placed at two corners within the cell. The sample are frozen isotropically once placed in the cell. An RTD and a TDR are placed inside the sample to monitor the temperature and unfrozen water content, respectively, as the soil freezes. These test results were then used to create the SFCC for Devon Silt.

The isotropic freezing allows us to control ice lenses from forming and hence in getting a representative SFCC. In addition, visual observation of the samples after the test is made to check whether the samples cracked during the SFCC test. In addition, to avoid the influence of hysteresis, the SFCCs are measured during first freezing cycle and the corresponding IEV from the frost heave tests are determined again for the first freezing cycle.

The SFCC curve for Devon Silt was determined for samples prepared under different consolidation pressures. The suction at the IEV was determined from the SFCC and the corresponding temperature was determined assuming that the general Clausius-Clapeyron equation is valid and that the ice phase is under atmospheric pressure. This temperature value is then considered to be the ice lens initiation temperature (segregation temperature) from the SFCC.

### **One-dimensional Frost Heave Tests**

One-dimensional, open system step-freezing frost heave tests were carried out using Devon Silt samples that had been previously consolidated under a particular vertical stress. The sketch showing the one-dimensional frost heave test set-up is

shown in Figure 2. The samples were frozen from the top down. RTDs, placed at 21 mm interval along the length of the sample, monitored the temperature variation with time. Time-lapse photography provided digital photo records to visually observe and document the freezing process as it advanced downward, and as ice lenses were initiated and grew. The experimental values of the segregation temperature were determined using the digital images to establish when the cracks initiated, and the temperature data from the RTDs permitted determination of what the temperature was at that location.

The temperature within the frozen fringe decreases from the water freezing point at the frost front to the segregation temperature at the warm side of the ice lens being formed. The segregation temperature is influenced by the cooling rate (Konrad, 1989), the external applied stress (Konrad and Morgenstern, 1982), and the soil type (Konrad, 2005).

To take into account the influence of the cooling rate, tests for the SFCC were carried out using the same cooling rate ( $-0.28\text{ }^{\circ}\text{C}/\text{day}$ ) as the ones recorded during the onset of the final ice lens in the frost heave tests.

The one-dimensional frost heave tests were initially conducted under zero external pressure (unconfined) to mimic the conditions from the SFCC test. Subsequent tests were conducted under different external pressure values to investigate the influence of external pressure on ice lens initiation condition. For example, for the sample consolidated to 100 kPa, the test was initially conducted at zero external pressure. Once the final ice lens formed under zero external pressure, the external pressure was then increased to 50 kPa and the final ice lens formation under this pressure condition was observed. The external pressure was then increased to 100 kPa and final ice lens formation condition under this pressure was observed.

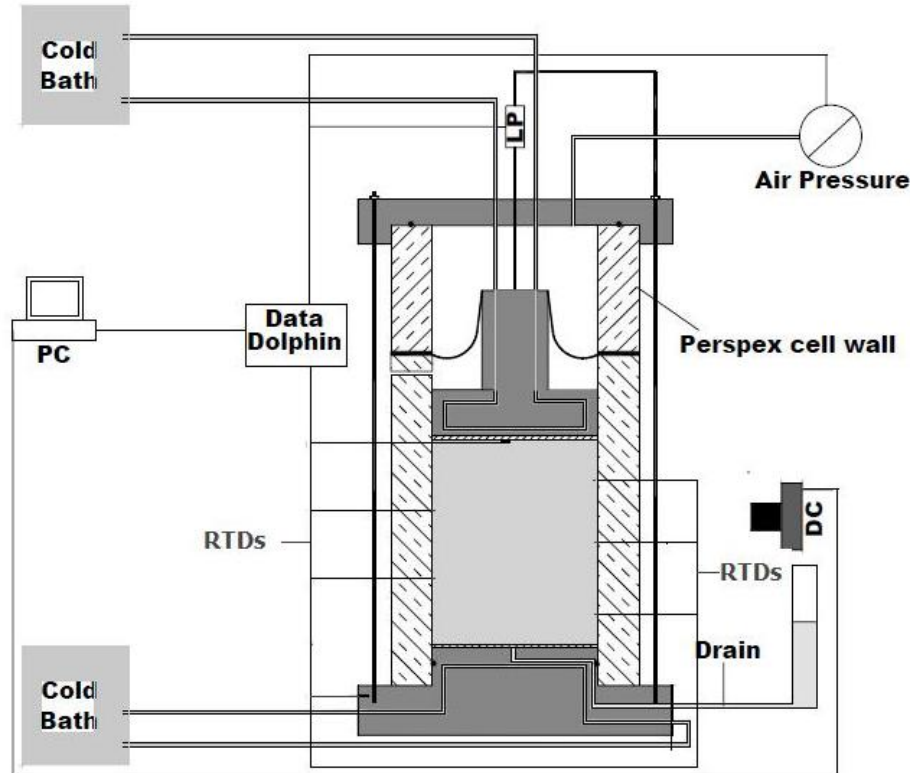


Figure 2. Sketch showing the one-dimensional frost heave test set-up, modified from Xia, (2006). DC = Digital Camera, LP = displacement transducer, PC = Personal Computer. Sketch not drawn to scale.

## EXPERIMENTAL RESULTS AND DISCUSSION

The results from the laboratory tests for the SFCCs are shown in Figure 3. In this figure the SFCC is presented as a plot of unfrozen water content versus temperature. In order to determine IEV from SFCC, the SFCC has to be plotted as unfrozen water content versus suction. For this, it is assumed that the general Clausius-Clapeyron equation is applicable and it is used to relate suction and temperature by assuming the ice phase to be under atmospheric pressure. The same assumption has been used by different authors (Spaans and Baker, 1996; Koopmans and Miller, 1966; Williams, 1964; Konrad, 1994). Therefore, the relation provided by Konrad (1994), which states that the suction increases

linearly with decreasing temperature at a rate of 1250 kPa/°C, is used to relate suction and temperature. This relation was used in plotting the SFCCs (unfrozen water content versus suction) shown in Figure 4.

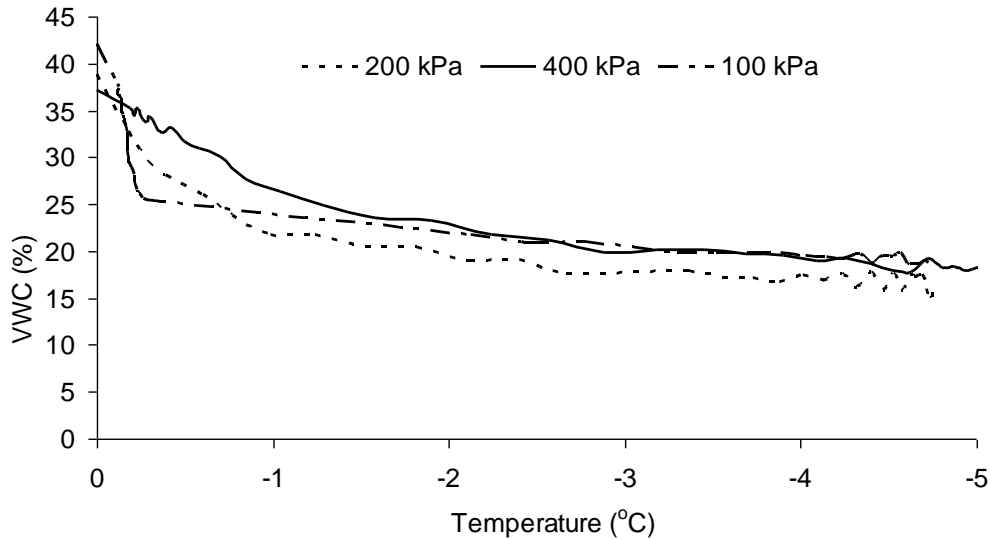


Figure 3. SFCC, unfrozen water content versus temperature, for Devon silt consolidated to different consolidation pressures

The SFCC of the samples prepared at different consolidation pressures is shown in Figure 4. The IEV is determined using the procedure shown in Figure 5. The initial straight portion of the SFCC is extended to intersect a linear extension of the middle zone (where there is a sharp drop in the unfrozen water content) of the SFCC. The intersection of the two straight lines (the solid lines in Figure 5) gives the IEV. The IEVs determined from the SFCCs for the different samples are summarized in Table 1.

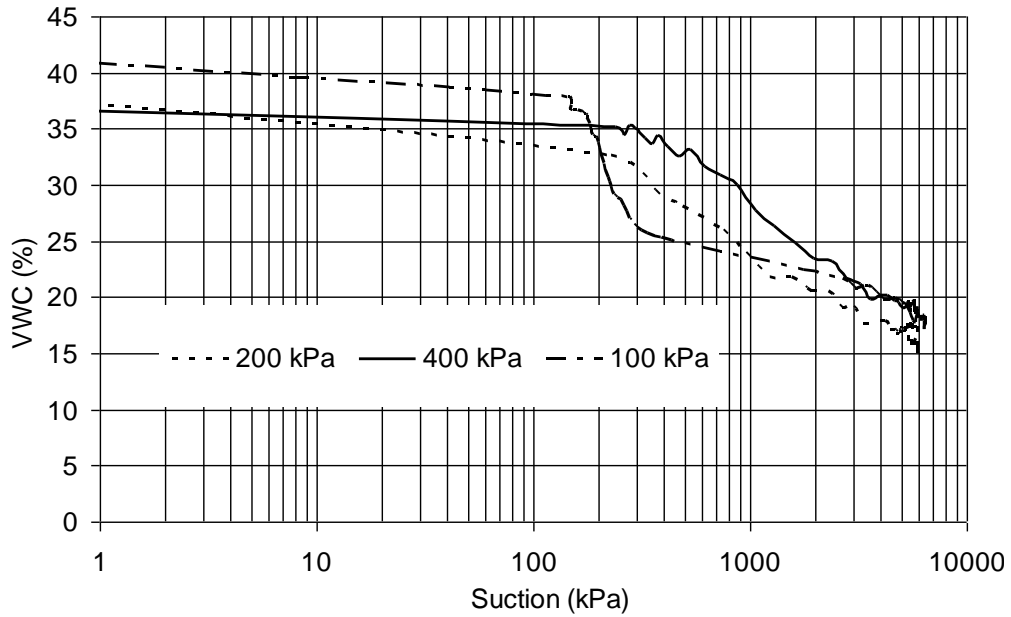


Figure 4. SFCC, unfrozen water content versus suction, for Devon silt consolidated to different consolidation pressures

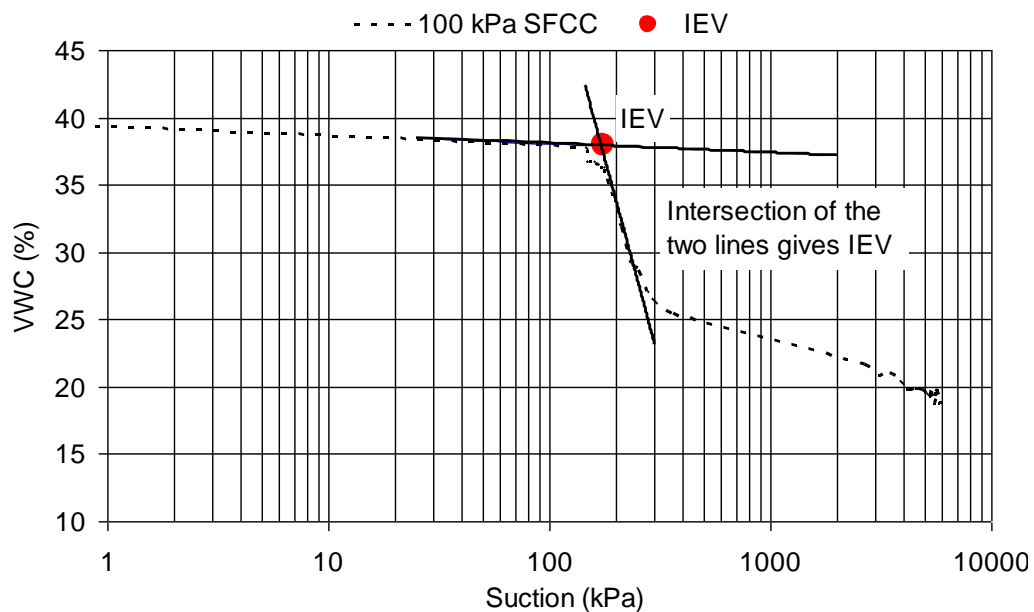


Figure 5. Procedure to determine the IEV. The solid lines are linear extensions of the initial linear portion and the middle zone.

Table 1: Ice entry values and Ice lens initiation temperatures of Devon Silt from SFCC.

Consolidation Stress, (kPa)	100	200	400
Ice Entry Value (kPa)	175	250	450
Ice Lens Initiation Temperature ( $^{\circ}\text{C}$ )	-0.14	-0.20	-0.36

The one-dimensional frost heave tests were conducted on samples initially consolidated at 100 kPa, 200 kPa, and 400 kPa. The samples were then frozen under zero external pressure. The segregation temperatures at the onset of cracking preceding formation of the final ice lens were determined using the digital images and the temperature readings from the RTDs placed inside the sample at different depths of the sample. Results from this analysis are shown in Figure 6.

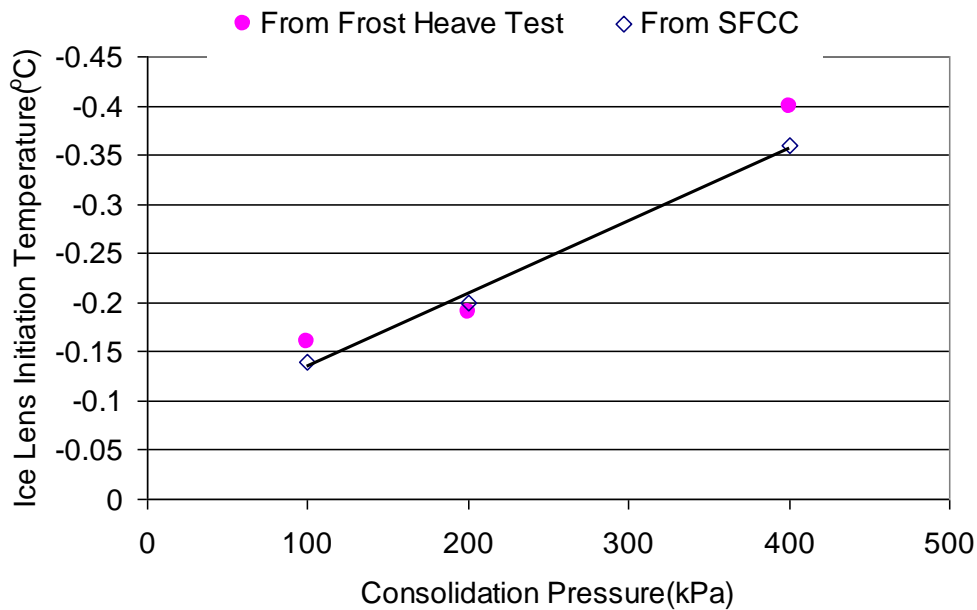


Figure 6. Ice lens initiation temperature as a function of consolidation pressure at 0 kPa external pressure.

The solid line in Figure 6 shows the trend of the ice lens initiation temperatures determined from the SFCC as the temperatures corresponding to IEVs. The experimental values determined from the frost heave tests are shown as solid data points in the figure. Excellent agreement between the experimental values from the freezing tests and the values determined from the SFCC is found.

### **Influence of External Pressure**

Using the SFCC to determine the ice lens initiation condition/segregation temperature can also guide evaluation of the influence of external pressure on the segregation temperature. This requires an additional assumption, that the influence of external pressure of magnitude  $P_e$  would be to shift the IEV (i.e., the suction at the IEV) horizontally to the right on the SFCC by this magnitude (i.e., by  $P_e$ ); and hence, to decrease the ice lens initiation temperature by a magnitude of  $(P_e/1250 \text{ kPa}/^\circ\text{C})$  from the ice lens initiation temperature at zero external pressure. This assumption is used to plot the variation in ice lens initiation temperature under external pressure as shown in Figure 8 for a sample consolidated to 100 kPa and in Figure 9 for the sample consolidated to 200 kPa. To check the validity of this assumption, one-dimensional frost heave tests were conducted under different external pressures on the samples consolidated to 100 kPa and 200 kPa. The final ice lenses at different external pressure values are shown in Figure 7 for the sample consolidated to 100 kPa. The difference in the ice lens thickness, in Figures 7 (a) – 7 (c), is not due to difference in vertical pressure. It is because we did not allow enough time for the ice lenses to grow fully when the sample was under 0 kPa and 50 kPa freezing conditions since we are interested in the ice lens initiation condition. The segregation temperatures for each case are determined using the temperature readings and the digital images. Figure 8 and Figure 9 show that there is a good agreement between the ice lens initiation temperatures determined from the SFCC and from the one-dimensional frost heave tests.

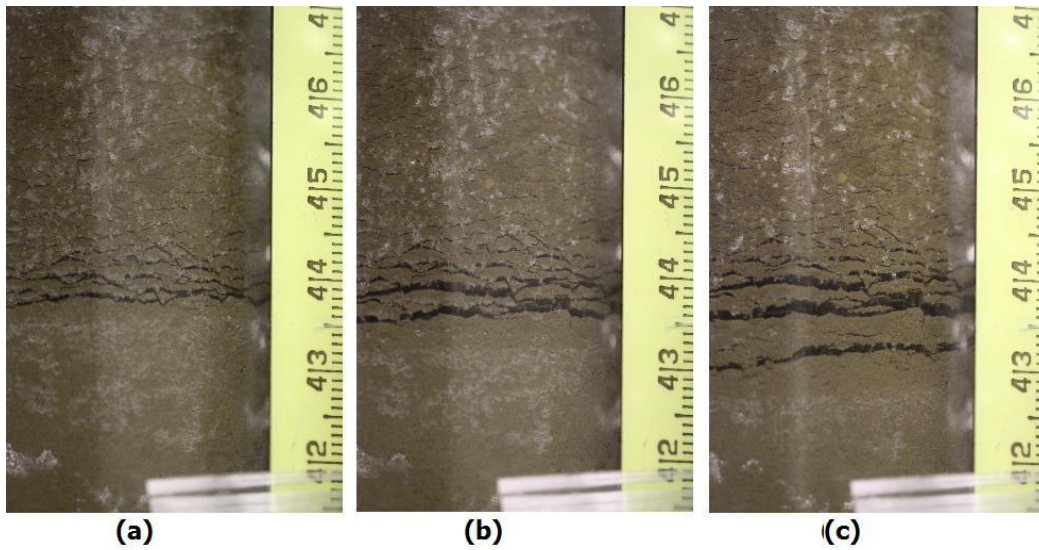


Figure 7. Final ice lenses in a soil consolidated at 100 kPa and frozen under different external pressures: (a) 0 kPa, (b) 50 kPa, (c) 100 kPa.

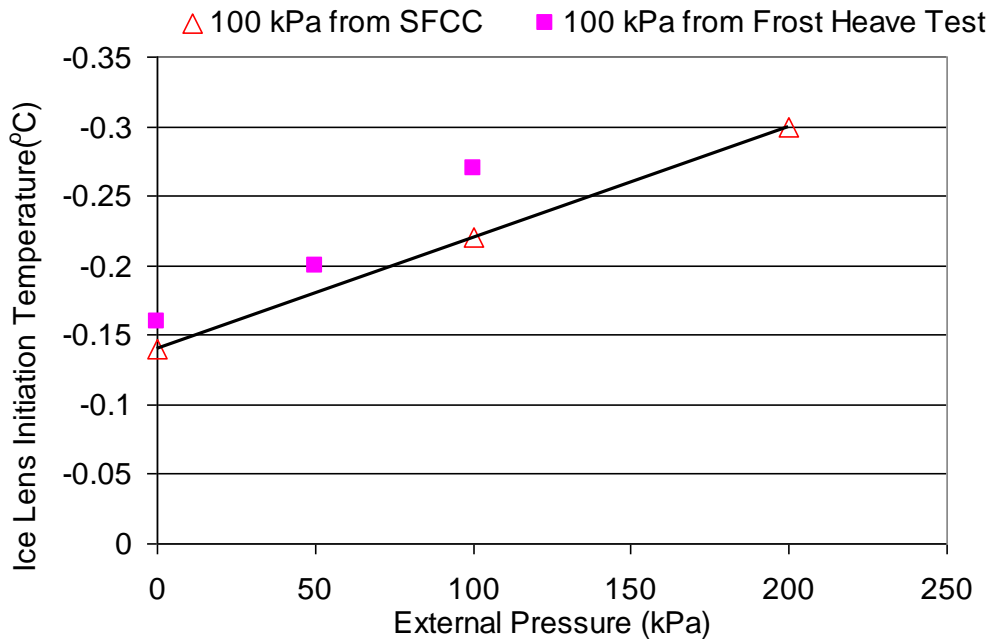


Figure 8. Ice lens initiation temperature as a function of external pressure for a sample consolidated to 100 kPa. The solid line represents the trend of the segregation temperatures determined using the SFCC.

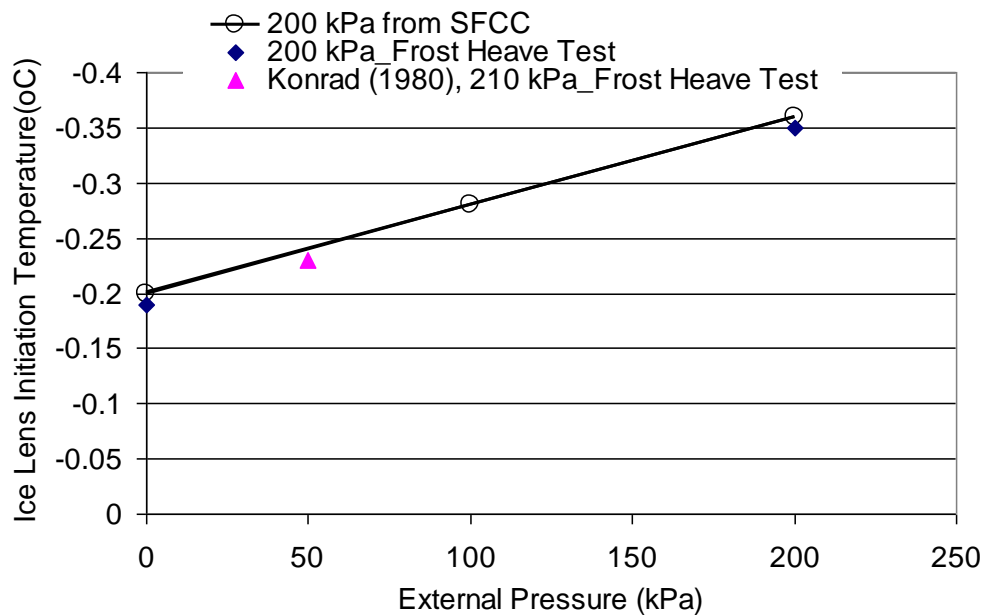


Figure 9. Ice lens initiation temperature as a function of external pressure for a sample consolidated to 200 kPa. The solid line represents the trend of the segregation temperatures determined using the SFCC.

### Comparison of results from Current Study with results from Previous Studies

Ice lens initiation temperature (segregation temperature) values for Devon Silt have previously been presented by Konrad (1980). Figure 10 shows the influence of external/overburden pressure on segregation temperature from this study compared to the results presented by Konrad (1980). The difference between the results is thought to be due to the different rates of cooling. Konrad (1980) indicates that the segregation temperature for Devon Silt was -0.26, -0.23, -0.20 °C for cooling rates of -0.54, -0.24, and -0.11 °C/day, respectively. For tests conducted under nearly identical cooling rates (-0.28 in this study and -0.24 °C/day reported in Konrad (1980)), the segregation temperature values are very similar (Figure 11).

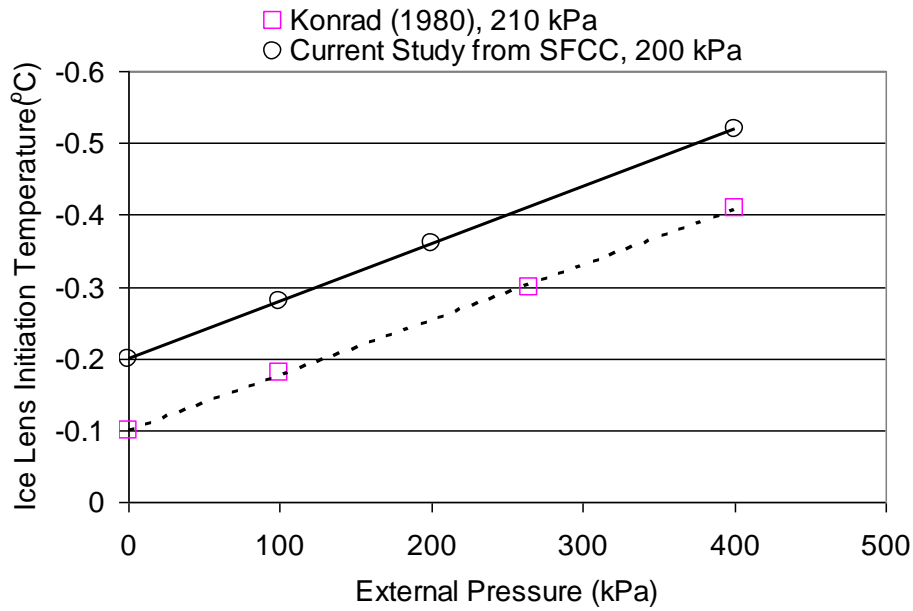


Figure 10. Ice lens initiation temperature as a function of external pressure.

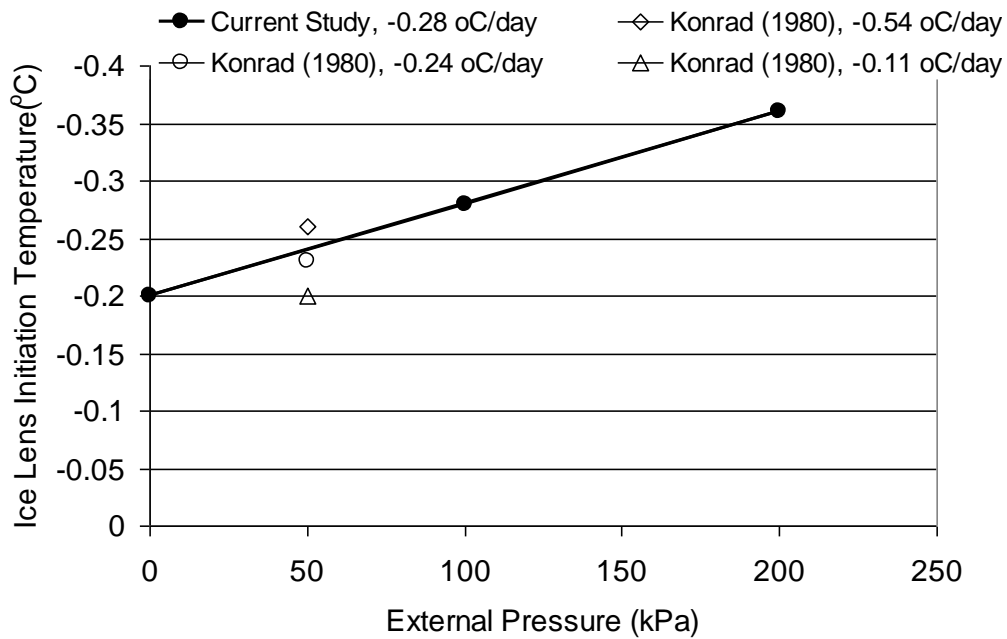


Figure 11. Influence of cooling rate on ice lens initiation temperature versus applied external pressure

One additional observation of interest illustrated in Figure 10 is that the slopes of the two trend lines are similar, which justifies the assumption used to include the influence of external applied pressure on the segregation temperature.

## CONCLUSIONS

Ice lens formation is initiated with cracking of the soil in the frozen fringe. Therefore, it is proposed that ice lens initiation conditions are related to crack initiation in the frozen fringe. A new ice lens initiation condition is presented and verified experimentally. Based on the experimental observations reported by Peron et al. (2009), that cracking in non-frozen soils starts close to the air-entry value on the SWCC, and based on similarity between SFCC and SWCC, it is postulated that an ice lens initiates close to the ice-entry value as determined from the SFCC. To verify this assumption, ice lens initiation conditions (in terms of segregation temperature) from one-dimensional frost heave tests under different boundary conditions were determined and compared with the predicted results from the SFCC tests. The two independently determined results for ice lens initiation condition showed good agreement.

The SFCC can be used to determine the ice lens initiation conditions during frost heave. The findings from this study indicate that ice lenses initiate close to the ice-entry value found using the SFCC. Once the SFCC corresponding to a particular cooling rate and zero external pressure is determined, the suction and the corresponding temperature (related by the general Clausius-Clapeyron equation, with the ice phase assumed to be at atmospheric pressure) at the ice-entry value corresponded to the ice lens initiation conditions.

The influence of an external pressure with a magnitude  $P_e$  (in kPa) was shown to result in a shift in the ice-entry value (i.e., the suction at the ice entry value) on the SFCC by the same magnitude (i.e., by  $P_e$ ); and hence, to decrease the ice lens

initiation temperature by a magnitude of  $((P/1250) ^\circ\text{C})$  from the ice lens initiation temperature at zero external pressure. Experimental data corroborated this process.

Existing frost heave models require the segregation temperature as an input parameter. This study provides a new and novel practical method to determine this temperature. The segregation temperature can be determined as the temperature corresponding to the ice-entry value on the SFCC. Therefore, the SFCC could be used as input to existing frost heave models for determining the segregation temperature.

In a situation where the exact nature of the formation of the freezing-induced cracks is unknown (whether they are desiccation cracks or thermal cracks, as indicated by Azmatch et al., 2011), the use of the SFCC to define a crack initiation condition, and hence ice lens initiation condition is a simple and repeatable approach.

### **Acknowledgement**

The research was funded from a Discovery Grants provided by the Natural Science and Engineering Research Council of Canada.

### **REFERENCES**

- Abu-Hejleh, A.N., Znidarcic, D., 1995. Desiccation theory for soft cohesive soils. *Journal of Geotechnical Engineering*, 121(6), 493–502.
- Ajaz, A., Parry, R.H.G., 1975. Stress-strain behavior of two compacted clays in tension and compression. *Geotechnique*, 25(3), 495-512.

- Akagawa, S., 1988. Experimental study of frozen fringe characteristics. *Cold Regions Science and Technology*. 15, 209–223.
- Akagawa, S., Satoh, M., Kanie, S., Mikami, T., 2007. Effects of tensile strength on ice lens initiation temperature. *Proceedings of the international conference on cold region engineering*. 23-26 July, 2007, Page 43.
- Arenson, L.U., Azmatch, T.F., Segó, D.C., Biggar, K.W., 2008. A new hypothesis on ice lens formation in frost-susceptible soils. *Proceedings of the Ninth International Conference on Permafrost, Fairbanks, Alaska 1*, 59-64.
- Azmatch, T.F., Arenson, L.U., Segó, D.C., Biggar, K.W., 2011. Tensile strength and stress–strain behaviour of Devon silt under frozen fringe conditions. *Cold Regions Science and Technology* 68, 85–90.
- Azmatch, T.F., Arenson, L.U., Segó, D.C., Biggar, K.W., 2008. Measuring ice lens growth and development of soil strains during frost penetration using particle image velocimetry (GeoPIV). *Proceedings of the Ninth International Conference on Permafrost, Fairbanks, Alaska 1*, 89-93.
- Beskow, G., 1935. Soil Freezing and frost heaving with special application to roads and railroads. *Swed. Geol. Soc., Ser.C, No.375, 26th year book No. 3* (translated by J.O. Osterberg, Northwestern Univ., 1947).
- Black, P.B., Tice, A.R., 1989. Comparison of Soil Freezing Curve and Soil Water Curve Data for Windsor Sandy Loam. *Water Resources Research* 25, 2205-2210.
- Bronfenbrener, L., Bornfenbrener, R., 2010. Modeling frost heave in freezing soils. *Cold Regions Science and Technology* 61, 43-64.

- Dash, J.G., Fu, H., Wettlaufer, J.S., 1995. The premelting of ice and its environmental consequences. *Rep. Prog. Phys.* 58, 115-167.
- Gilpin, R.R., 1980. A model for the prediction of ice lensing and frost heave in soils. *Water Resources Research* 16 (5), 918–930.
- Harlan, R.L., 1973. Analysis of coupled heat and mass transfer in partial frozen soil. *Water Resources Research* 9 (5), 1314–1323.
- Kitsunozaki, S., 1999. Fracture patterns induced by desiccation in a thin layer. *Physical Review E.* 60, 6449–6464.
- Konrad, J.M., 2005. Estimation of the segregation potential of finegrained soils using the frost heave response of two reference soils. *Canadian Geotechnical Journal* 42, 38-50.
- Konrad, J.M., 1994. 16<sup>th</sup> Canadian Geotechnical Colloquium-Frost Heave in Soils-Concepts and Engineering. *Canadian Geotechnical Journal* 31(2), 223-245.
- Konrad, J.M., 1989. Influence of cooling rate on the temperature of ice lens formation. *Cold regions science and technology.* 16, 25-36.
- Konrad, J.M., 1980. Frost heave mechanics. Ph.D. thesis, Department of Civil Engineering, University of Alberta, Edmonton, AB, Canada, 472 pp.
- Konrad, J.M., Ayad, R. 1997. An idealized framework for the analysis of cohesive soils undergoing desiccation. *Canadian Geotechnical Journal*, 34(4), 477–488.
- Konrad, J.M., Duquennoi, C., 1993. A model for water transport and ice lensing in freezing soils. *Water Resources Research* 29 (9), 3109–3124

- Konrad, J. M., Morgenstern, N. R., 1982. Effect of applied pressure on freezing soils, *Canadian Geotechnical Journal* 19, 494-505.
- Konrad, J.M., Morgenstern, N.R., 1980. A mechanistic theory of ice lens formation in fine-grained soils. *Canadian Geotechnical Journal* 17, 473–486.
- Koopmans, R.W.R. Miller, R.D., 1966. Soil Freezing and Soil Water Characteristic Curves. *Soil Sci. Soc. Am Proc.* 30, 680-685.
- Meakin, P., 1987. A simple model for elastic fracture in thin films. *Thin Solid Films* 15, 165-190.
- Miller, R.D., 1978. Frost heaving in non-colloidal soils. *Proceedings of the Third International Conference on Permafrost, Edmonton, Alberta, Canada* 1, 708-713.
- Miller, R.D., 1972. Freezing and heaving of saturated and unsaturated soils. *Highway Research Rec.* 393, 1-11.
- Newman, G.P., Wilson, W.G., 1997. Heat and mass transfer in unsaturated soils. *Canadian Geotechnical Journal* 34, 63-70.
- O'Neill, K., Miller, R. D., 1980. Numerical solutions for rigid-ice model of secondary frost heave, *Proc. 2nd Int. Symp. Ground Freezing, Trondheim, the Norwegian Institute of Technology* 1, 656-669.
- Peron, H., Hueckel, T., Laloui, L., Hu, L.B., 2009, Fundamentals of desiccation cracking of fine-grained soils: experimental characterisation and mechanisms identification, *Canadian Geotechnical Journal* 46, 1177 – 1201.

- Sheng, D., Axelsson, K., Knutsson, S., 1995. Frost Heave due to Ice Lens Formation in Freezing soils, 1: Theory and Verification, *Nordic Hydrology* 26 (2), 125-146.
- Snyder, V.A., Miller, R.D., 1985. Tensile strength of unsaturated soils. *Soil Science Society of America Journal* 49, 58–65.
- Spaans, E.J.A., Baker, J.M., 1996, The Soil Freezing Characteristic: Its Measurement and Similarity to the Soil Moisture Characteristic, *Soil Sci. Soc. Am. J* 60, 13-19.
- Taber, S., 1929. Frost heaving. *Journal of Geology* 37, 428–461.
- Vogel, H.J., Hoffmann, H., Leopold, A., Roth, K., 2005. Studies of crack dynamics in clay soil: A physically based model for crack formation. *Geoderma* 125, 213-223.
- Williams, P.J., 1964. Unfrozen water content of frozen soils and soil moisture suction. *Geotechnique* 14, 231-246.
- Xia, D., 2006. Frost heave studies using digital photographic technique. MSc Thesis, University of Alberta, Edmonton, AB, Canada, 165 pp.
- Zeh, R.M., Witt, K.J., 2006. Tensile strength of compacted clays as part of the crack prediction of clay liner in landfills. *International Congress on Environmental Geotechnics, Cardiff* 5, 816-823.

## **CHAPTER 6. USING SOIL FREEZING CHARACTERISTIC CURVE TO ESTIMATE THE HYDRAULIC CONDUCTIVITY FUNCTION OF PARTIALLY FROZEN SOILS**

This paper was previously reviewed, accepted and published in the Cold Regions Science and Technology journal. It is modified (formatting only) and presented as published as part of this Ph.D. thesis as Chapter 6.

Reference: Azmatch, T.F., Segó, D.C., Arenson, L.U., and Biggar, K.W., 2012. Using soil freezing characteristic curve to estimate the hydraulic conductivity function of partially frozen soils. Cold Regions Science and Technology, 83-84, 103-109.

## **CHAPTER 6. USING SOIL FREEZING CHARACTERISTIC CURVE TO ESTIMATE THE HYDRAULIC CONDUCTIVITY FUNCTION OF PARTIALLY FROZEN SOILS**

### **ABSTRACT**

We propose using the soil freezing characteristic curve (SFCC), instead of the soil water characteristic curve (SWCC), to estimate the hydraulic conductivity of partially frozen soils. Shortcomings associated with the use of the SWCC to estimate the hydraulic conductivity function of partially frozen soils are discussed. The hydraulic conductivity function for partially frozen Devon Silt is derived using the SFCC and the empirical relationships for hydraulic conductivity estimation method developed by Fredlund et al (1994). The SFCC for Devon Silt is determined from unfrozen water content measurement using time domain reflectometry and temperature measurements inside the soil sample. The results using this novel approach compare well with results presented by others that use different methods to determine the hydraulic conductivity function of partially frozen soils.

*Key words: hydraulic conductivity, soil freezing characteristic curve, soil water characteristic curve, partially frozen soil*

### **INTRODUCTION**

Moisture migration in partially frozen soils plays a significant role in the construction of engineering structures in cold regions. It is very important in predicting frost heave (Konrad and Morgenstern, 1980), in investigating water and solute transport and redistributions in soil during winter (Baker & Spaans

1997), and in waste disposal using artificial ground freezing (McCauley et al., 2002). Proper evaluation of the moisture migration in partially frozen soils requires determining the hydraulic conductivity of these soils. Liquid water and pore ice coexist in a partially frozen soil. The pore ice reduces the hydraulic conductivity of partially frozen soil compared to the unfrozen soil. Since the pore ice content and the unfrozen water content change with temperature, the hydraulic conductivity of the partially frozen soil also changes with temperature.

A major challenge in characterizing flow through partially frozen soils is how to formulate changes in soil hydraulic conductivity as a function of temperature and water content under freezing and thawing conditions.

Two approaches have been proposed in literature to determine the hydraulic conductivity of partially frozen soils. The first one involves direct measurement of the hydraulic conductivity and the second approach is based on indirect measurements, assuming that the transport of water in partially frozen soils is controlled by the same process as in unsaturated unfrozen soils (Harlan, 1973).

Due to major challenges of measuring the hydraulic conductivity of partially frozen soils, only a limited number of papers report results from direct measurement of hydraulic conductivity of partially frozen soils. Direct measurement of hydraulic conductivity of partially frozen soil was first conducted by Burt and Williams (1974). They developed a permeameter for the direct measurement of water movement through frozen soils under isothermal conditions. Their test set-up involves the use of reservoirs containing low concentration of lactose. Nakano et al. (1982) pointed out that the use of lactose would introduce an error in the system of unknown magnitude.

Horiguchi and Miller (1983) measured the hydraulic conductivity of frozen soils using a different experimental technique. They measured hydraulic conductivity

of frozen soils as a function of temperature in the range of 0 °C to -0.35 °C. The measured values of the hydraulic conductivities by Horiguchi and Miller (1983) decreased from values of the order of  $10^{-8}$  m/s before freezing to values in the range of  $10^{-12} - 10^{-13}$  m/s at temperatures near -0.35°C. They concluded that the direct measurements of hydraulic conductivity for partially frozen soils was at the developing stage and required extremely precise and stable control of temperature and long equilibrium periods.

The difficulties faced in making direct measurement limit the credibility of the direct measurement methods. Therefore, indirect measurement of the hydraulic conductivity of partially frozen soils has become the general approach.

## **INDIRECT METHODS TO ESTIMATE THE HYDRAULIC CONDUCTIVITY OF PARTIALLY FROZEN SOILS**

Indirect measurement methods assume that the transport of water within partially frozen soils is controlled by the same process as in unsaturated unfrozen soils. This use is based on the similarity between the drying and wetting phenomena in unfrozen soil to the freezing and thawing phenomena in frozen soil (e.g., Spaans and Baker, 1996). In drying soils, water is removed and replaced by air leaving the remaining water at an increasingly lower matric potential. The same occurs in freezing soils, except that liquid water changes phase and becomes ice. The same forces that prevent soil water from draining also prevent it from freezing (Spaans and Baker, 1996). Hence, frozen soils have been assumed to behave in a similar fashion as unfrozen, unsaturated soils with the air phase in unfrozen soil replaced by the ice phase in a freezing soil (e.g., Black and Tice, 1989).

The relation between freezing soil temperatures (or suction) and unfrozen water content, referred to as the soil freezing characteristic curve (SFCC) of partially frozen soil, is assumed to be similar to the soil water characteristic curve

(SWCC), which is a relation between suction and water content, for unfrozen soil. This assumption has been used by different authors such as Williams (1964), Koopmans and Miller(1966), Black and Tice (1989), and Spaans and Baker (1996). It is also assumed that the hydraulic conductivity of frozen soils is a function of the unfrozen water content and equals the hydraulic conductivity of unfrozen soils at the same water content. Hence, the SWCC of the soil together with hydraulic conductivity estimation methods from the SWCC is used to get the hydraulic conductivity of partially frozen soils. This approach has been used by many researchers (e.g., Cary and Maryland, 1972; Harlan, 1973; Tao and Gray, 1994; Tarnawski and Wagner, 1996; Newman and Wilson, 1997).

Some authors believed that this approach led to overprediction of water flow (Harlan, 1973; Taylor and Luthin, 1978; Jame and Norum, 1980) and hence suggested applying an impedance factor to the calculated permeability values (Jame and Norum, 1980). However, other researchers suggest that there is no need to apply an impedance factor (e.g., Newman and Wilson, 1997). Some researchers have determined the permeability without applying an impedance factor (Guymon and Luthin, 1974; Flerchinger, 1987). The problem with methods applying an impedance factor is that there is no systematic approach to determine the impedance factor and it is difficult to find a simple relation between this factors and soil type (Berg, 1983; Lundin, 1990). Black and Hardenberg (1991) stated that the use of an impedance factor is an arbitrary correction function. Newman and Wilson (1997) also concluded that an impedance factor is unnecessary when an accurate soil water characteristic curve and relationship between hydraulic conductivity and soil water pressure are defined.

A different approach was proposed by Konrad and Morgenstern (1980). They presented equations for determining the coefficient of permeability in the frozen zone that require parameters based on complex laboratory testing. They base their

calculated coefficient of permeability on the segregation temperature of the soil (i.e., the temperature at which an ice lens starts to form).

Of the different methods presented above, the most commonly used approach to determine the hydraulic conductivity of partially frozen soils is the indirect method that makes use of SWCC in combination with different hydraulic conductivity estimation methods (e.g., van Genuchten, 1980; Fredlund et al., 1994). We believe that this approach was mainly used due to (1) The development of unsaturated soil mechanics theories and the subsequent availability of different methods to estimate the hydraulic conductivity functions from the SWCCs (Fredlund et al., 1994; Mualem, 1976; Van Genuchten, 1980); and (2) lack of a well established laboratory method to determine the SFCC in combination with the availability of the Tempe cell for measuring the SWCC.

However, recent studies show that the SWCC is difficult and time consuming to measure and it is actually easier to measure the SFCC than the SWCC (Flerchinger et al, 2006). With the widespread use of the time-domain reflectometry (TDR) and with it becoming a well established method to measure unfrozen water content in partially frozen soils, it is now easier to measure the SFCC than the SWCC. Authors are even advocating the use of SFCC to get the SWCC especially for fine grained soils (Liu et al 2012).

The use of SWCC to model flow through partially frozen soils also has other problems. One of its shortcomings is that the use of SWCC to estimate the hydraulic conductivity of partially frozen soils is based on an analogy between SWCC and SFCC and this requires soil-dependent constant for which there is no established method available to determine this constant. This constant is supposed account for the surface energy difference between the ice-water and air-water interface (i.e.,  $\sigma_{iw}$ ,  $\sigma_{aw}$ ). Koopmans and Miller (1966) showed that for soils in which adsorption space is much greater than the capillary space (SS soil types)  $\sigma_{aw}$

$\sigma_{iw} = 1.0$ ; for soils in which capillary space is much greater than the adsorption space (SLS soil types)  $\sigma_{aw} / \sigma_{iw} = 2.2$ . However, for intermediate soil types, the value of this constant is between 1.0 and 2.2 and there is no way of knowing the value of this constant (other than determining both the SFCC and the SWCC of the soils and measuring the ratio, which is time consuming and complex).

Another shortcoming of using the SWCC as an analogue to the SFCC in modeling the hydraulic conductivity of partially frozen soils is that the SWCC does not take into account the influence of solutes on unfrozen water content. Most soils have dissolved solutes or impurities and these solutes are known to decrease the freezing point of water in the soils and hence to increase the unfrozen water content at a particular temperature (Watanabe and Mizoguchi, 2002).

Assuming analogy between SWCC and SFCC also does not address the influence of the freezing rate and freezing temperature to which the sample is subjected to. Azmatch et al. (2012b), for example, showed that the subzero temperature to which the sample is subjected to for freezing and hence the rate of freezing affects the SFCC of Devon Silt. However, the test method using Tempe Cell for SWCC does not provide a means to simulate influence of rate of freezing.

Considering all the limitations discussed above of using the SWCC to estimate the hydraulic conductivity function of partially frozen soils, we propose the use of the SFCC to determine the hydraulic conductivity function of partially frozen soils. This paper presents the theoretical basis for this, and shows the use of the SFCC to determine the hydraulic conductivity of partially frozen soils using examples.

## **EXPERIMENTAL PROGRAM**

### **Soil Properties and Sample Preparation**

The soil tested is Devon Silt with a specific gravity of 2.65, a clay fraction of 25% and a silt fraction of 75%. It has a liquid limit of 32% and plastic limit of 20%. Slurry of the soil is prepared at a moisture content of 60% and then consolidated under a specific consolidation pressure (50 kPa, 100 kPa and 400 kPa).

Slurry of the soil was also prepared by mixing Devon silt with water at a salinity of 5gm/L (by mixing 1 litre of distilled water with 5 gm of pure sodium chloride). This slurry was consolidated to 50 kPa. SWCC test and SFCC tests were conducted on samples prepared from this slurry. The results from these tests would enable comparison of SWCC and SFCC under the presence of solutes.

### **Test for Soil Freezing Characteristics Curve**

There are a number of methods to determine the unfrozen water content (Anderson and Morgenstern, 1973), such as time domain reflectometry (TDR), calorimeters, and nuclear magnetic resonance (NMR). For this study, unfrozen water content is measured using TDR. The TDR method measures the dielectric property, which is then converted to volumetric water content using the empirical equation provided by Topp et al. (1980). The TDR was first used for unfrozen soils and later extended to frozen soils (e.g. Patterson and Smith, 1980).

The soil sample was placed in a freezing cell, whose temperature was controlled using a temperature control bath. The temperature of the freezing cell is monitored using two resistance temperature detectors (RTDs) placed at two corners within the cell. The sample was frozen isotropically once placed in the cell. The isotropic freezing allows us to control ice lenses from forming and hence

in getting a representative SFCC. In addition, visual observation of the samples after the test is made to check whether ice lenses formed or not.

An RTD and a TDR were placed inside the sample to monitor the temperature and the unfrozen water content, respectively, during freezing. The RTD was placed outside the zone of influence of the TDR, which is 1.4 times the spacing between the TDR rods (Topp and Davis, 1985), so that it does not influence the reading of the TDR. The TDR test was carried out on samples prepared from slurry and consolidated to different pressures (50 kPa, 100 kPa, 400 kPa). The test is conducted with the samples unloaded to zero pressure.

### **Test for Soil Water Characteristics Curve**

To compare the SFCC and the SWCC of Devon Silt, the SWCC of Devon Silt prepared by consolidating to 100 kPa pressure was determined using Tempe Cell. The same procedure was used in preparing the samples for the SWCC test and the SFCC test.

## **EXPERIMENTAL RESULTS AND DISCUSSION**

The SFCC can be plotted as unfrozen water content versus temperature or as unfrozen water content versus suction. The results from the laboratory tests for the SFCCs are shown in Figure 1. In Figure 1 the SFCC is presented as a plot of unfrozen water content versus temperature. The Clausius-Clapeyron equation, Equation 1, is used to correlate suction,  $\psi$ , with temperature,  $T$ , assuming the ice pressure to be atmospheric. A similar approach has been used to get the SWCC from the SFCC by Spaans and Baker (1996). This enables us plotting the SFCC as unfrozen water content versus suction, as shown in Figure 2.

$$\Psi = \frac{L_f}{g} \ln \frac{T_m - T}{T_m} \quad (1)$$

where  $\psi$  is suction in (m),  $L_f$  is the latent heat of freezing water,  $g$  is acceleration due to gravity,  $T_m$  is the freezing temperature of bulk water, and  $T$  is temperature in degree Kelvin.

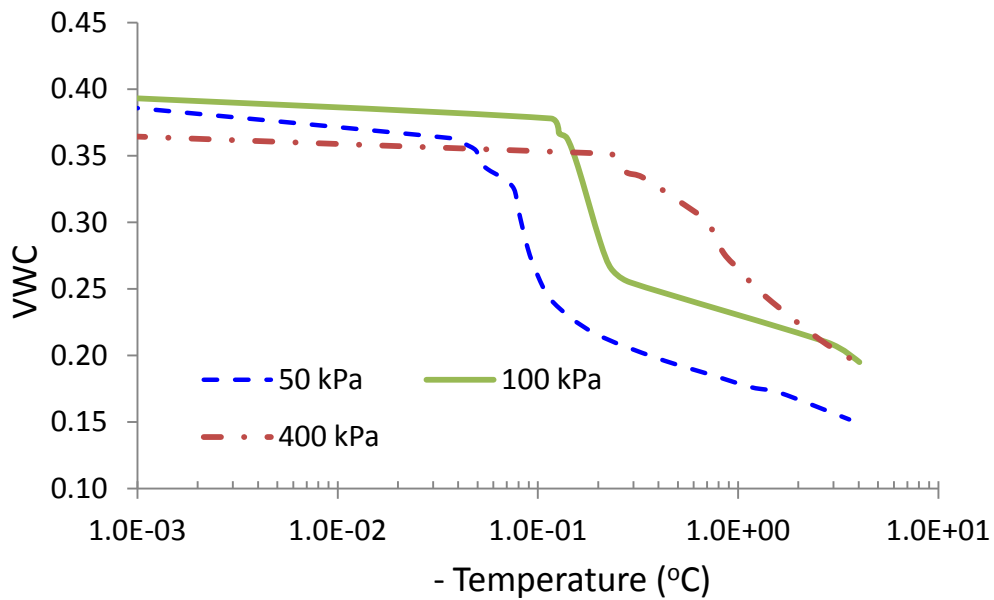


Figure 1. SFCC of Devon silt consolidated to different pressure, plotted as volumetric water content versus temperature.

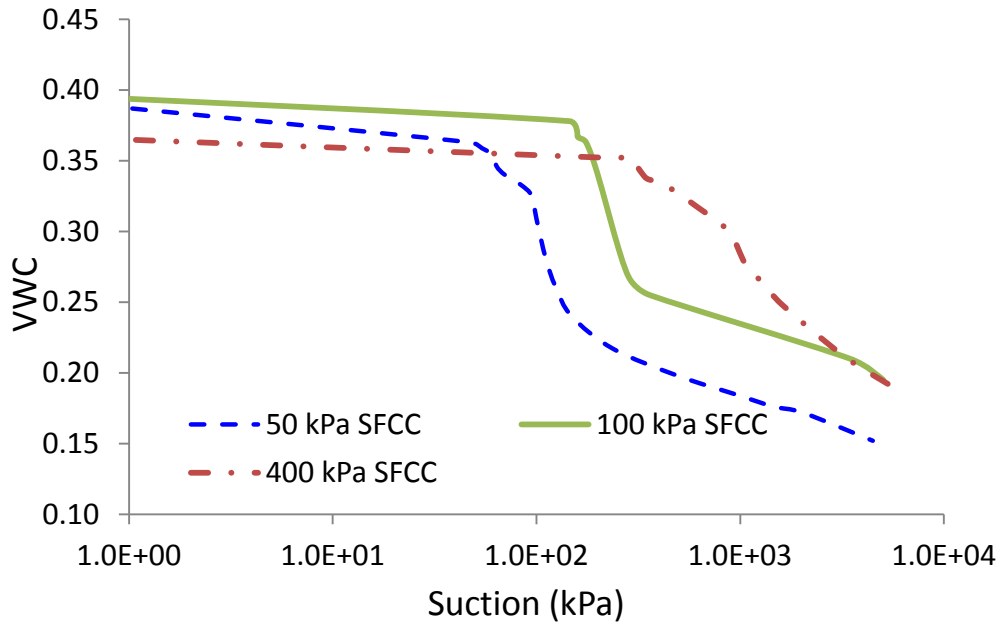


Figure 2. Experimental result of the SFCC plotted as volumetric water content versus suction.

### Influence of Solutes

The results from the SWCC test and the SFCC test for solute effects are presented in Figure 3. Figure 3 indicates that the SWCC for a sample prepared at zero salinity is almost the same as the SWCC of the sample prepared at a salinity of 5 gm/L. However, the SFCC for the sample prepared at zero salinity is much different from the SFCC of the sample prepared at a salinity of 5 gm/L. It can, therefore, be stated that the use of the SWCC to represent the SFCC of soils with salinity is wrong. Hence, estimating the hydraulic conductivity function of partially frozen soils with solutes from the corresponding SWCC would lead to wrong results.

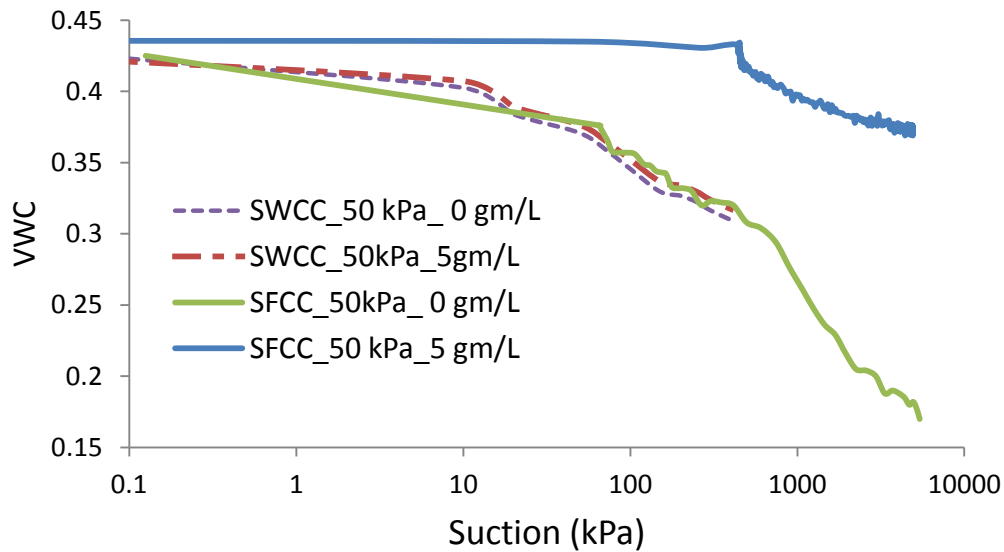


Figure 3. Comparison of SWCC and SFCC for Devon silt with salinity. Curves with broken lines show the SWCC and curves with solid lines show the SFCC

### Hydraulic Conductivity of Partially Frozen Soils

Various empirical models have been proposed to predict the hydraulic conductivity function of an unsaturated soil (e.g., Brooks and Corey 1964; Mualem 1980; van Genuchten 1980; Fredlund et al. 1994). These models use the SWCC and the saturated hydraulic conductivity of a particular soil to compute the unsaturated hydraulic conductivity function.

Previous studies (e.g., Leong and Rahardjo, 1997; Benson and Gribb, 1997) have shown that the integration procedures by Fredlund et al. (1994) involving the use of the Fredlund and Xing (1994) SWCC equation (Equation (2)), provide a good estimate of the permeability function. Therefore, in this study, the permeability function of the partially frozen Devon Silt is predicted using the saturated coefficient of permeability and the SFCC together with Fredlund et al. (1994) empirical functions for predicting the permeability function.

$$\theta = \left\{ 1 - \left[ \frac{\ln\left(1 + \frac{\Psi}{C_r}\right)}{\ln(1 + 1000000/C_r)} \right] \right\} \left[ \frac{\theta_{sat}}{\left\{ \ln\left[e + (\Psi/a_f)^{n_f}\right] \right\}^{m_f}} \right] \quad (2)$$

Where  $\theta$  is volumetric water content,  $\theta_{sat}$  is saturated volumetric water content,  $\psi$  is suction,  $C_r$  is suction corresponding to residual water content,  $e$  is the natural number 2.71828, and  $a_f$ ,  $n_f$ , and  $m_f$  are Fredlund and Xing (1994) curve fit parameters.

The estimation of the hydraulic conductivity function using the Fredlund et al. (1994) requires that the laboratory SFCC data points be fit with Equation (2).

The SFCC data points determined from the laboratory testing are fit with Equation (2) using SoilVision (Fredlund, 1996). The results are presented in Figure 4 (together with the lab data points for comparison) and in Figure 5 (Fredlund and Xing (1994) fit curves only). The Fredlund and Xing (1994) curve fit parameters ( $a_f$ ,  $n_f$ ,  $m_f$ ) determined for the SFCCs are presented in Table 1.

The Fredlund and Xing (1994) curve fit were then used together with a saturated hydraulic conductivity value of  $10^{-9}$  m/s to estimate the hydraulic conductivity function using the Fredlund et al. (1994) method in SoilVision (Fredlund, 1996). The results from these analyses are as shown in Figure 6.

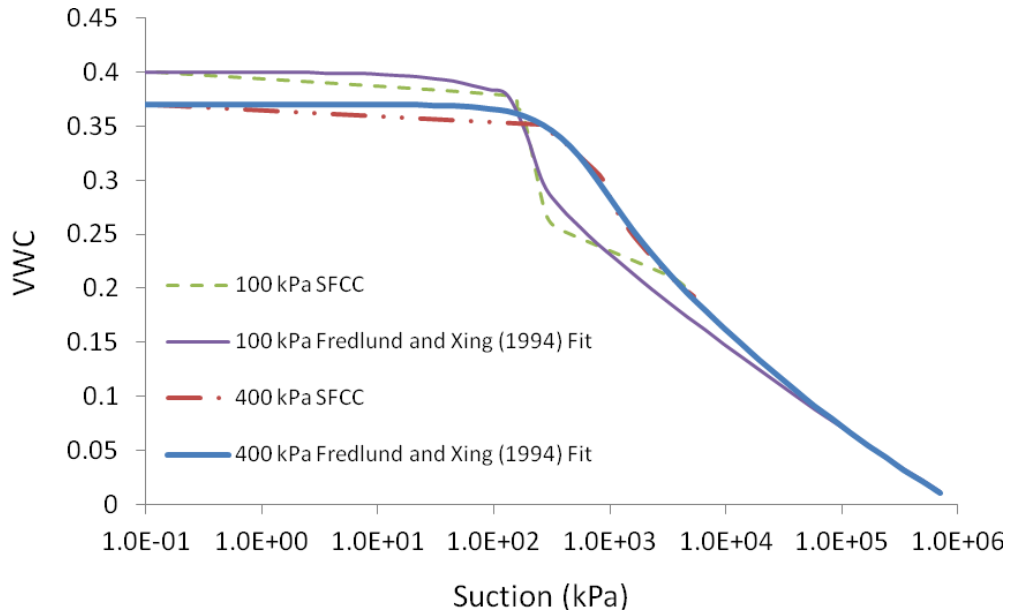


Figure 4. Comparison of the SFCC from laboratory experiments with the SFCC fit using the Fredlund and Xing (1994) method

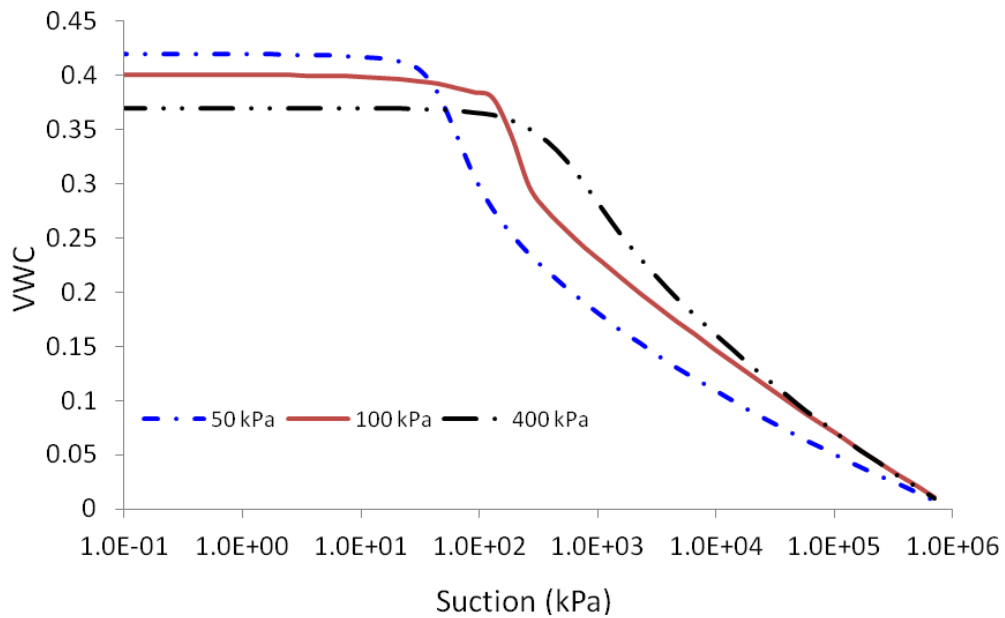


Figure 5. Fredlund and Xing (1994) fit for the SFCC of Devon silt consolidated to different pressures.

Figure 6 shows that, at the same temperature, the hydraulic conductivity values for the sample consolidated to 400 kPa are greater than the hydraulic conductivity values of the sample consolidated to 100 kPa. This is explained by the unfrozen water content at the corresponding temperatures. The unfrozen water content in the 400 kPa sample is more than that in the 100 kPa sample (Figure 1). This results in higher hydraulic conductivity value in the 400 kPa sample. The 400 kPa sample has higher unfrozen water content than the 100 kPa sample due to its lower initial void ratio which results in a lower freezing temperature.

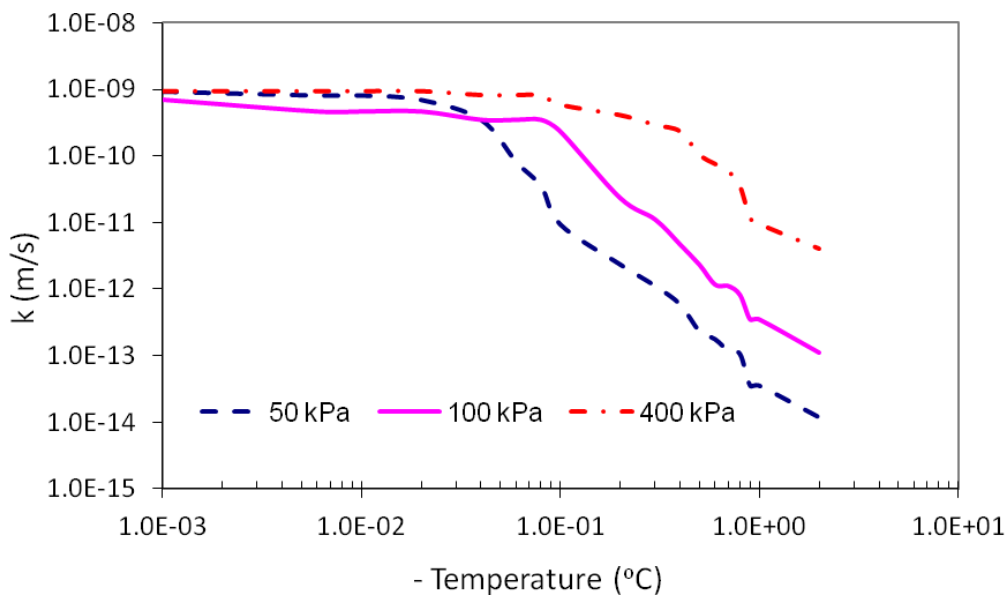


Figure 6. Hydraulic conductivity functions of partially frozen Devon silt estimated using the SFCC and Fredlund et al. (1994) method. The hydraulic conductivity functions shown are for samples consolidated to different pressures.

Table 1: Fredlund and Xing (1994) curve fit parameters for the SFCCs

Soil Sample	$a_f$	$n_f$	$m_f$
50 kPa Sample	44.45	4.27	0.23
100 kPa Sample	167.76	20.00	0.09
400 kPa Sample	448.66	1.86	0.35

The results (Figure 6) show that there is less than one order of magnitude decrease in the hydraulic conductivity before the temperature drops to the temperature corresponding to the Ice Entry Value (IEV). The IEV is defined as the suction/temperature at which ice first begins to enter the largest soil pores. The IEV on the SFCC is determined as the intersection point of the linear extension of the initial straight portion of the SFCC and the linear extension of the middle zone (where there is a sharp drop in the unfrozen water content) of the SFCC (Azmatch et al., 2012a).

Once the temperature drops below the IEV temperature, there is a sharp decrease in hydraulic conductivity with further decrease in temperature. Therefore, we have replotted the hydraulic conductivity functions to show the variation of hydraulic conductivity with temperature after the temperature has dropped below the IEV temperature (Figure 7). The results suggest a linear relationship in a log-log space of hydraulic conductivity versus the negative of the subzero temperature.

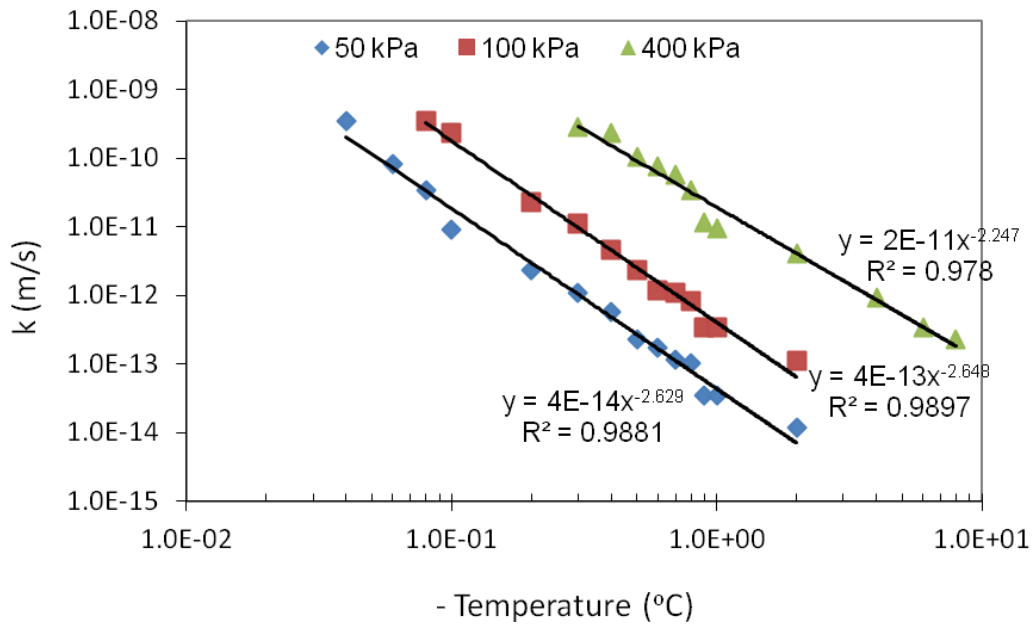


Figure 7. Hydraulic conductivity functions of partially frozen Devon silt estimated using the SFCC and Fredlund et al. (1994) method. The hydraulic conductivity functions shown are for samples consolidated to different pressures and below the ice-entry values for each sample. The solid lines indicate trend lines fitted to the data.

### Comparison of Hydraulic Conductivity Estimation using SFCC with Hydraulic Conductivity Estimation using SWCC for Devon Silt

In this section, the hydraulic conductivity function of partially frozen Devon Silt is estimated using its SWCC and the Fredlund et al (1994) hydraulic conductivity estimation method. This requires that the data points obtained from laboratory test, consisting of a series of disconnected data points, be best-fitted using the Fredlund and Xing (1994) SWCC equation. SoilVision was used for this purpose. The results from this are shown in Figure 8. The SFCC are also shown in the same plot for comparison. Figure 8 shows that the SWCC and the SFCC are almost identical. This, according to Koopmans and Miller (1966), indicates that Devon

Silt falls under the SS soil type for which  $\sigma_{aw} / \sigma_{iw} = 1.0$ . Such behaviour might be due to the presence of only 25% clay in Devon Silt.

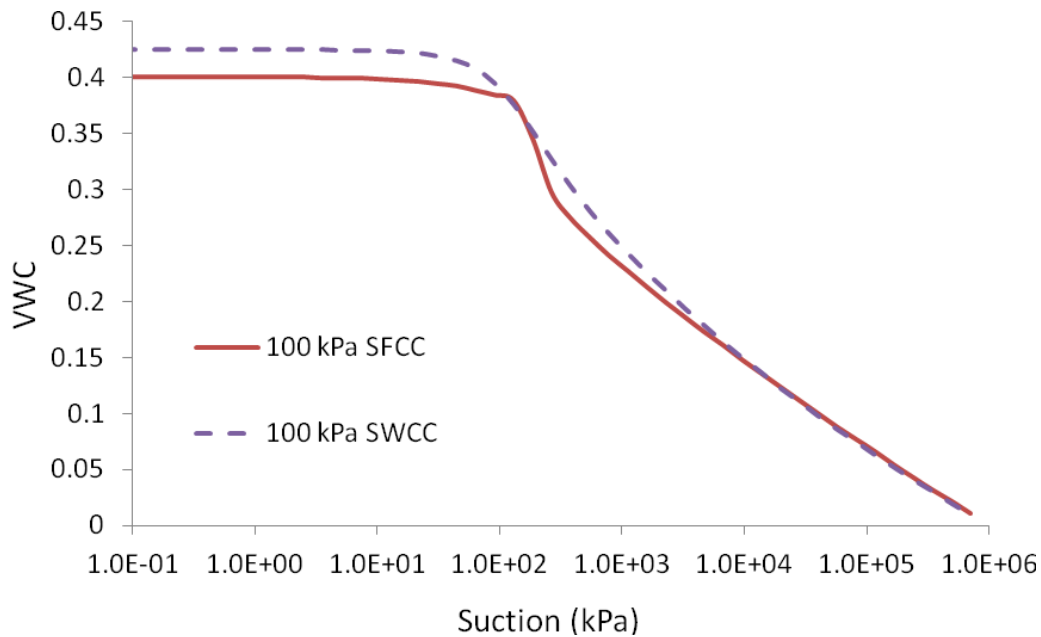


Figure 8. Comparison of the SWCC and SFCC of Devon silt consolidated to 100 kPa pressure.

The hydraulic conductivity function of partially frozen Devon Silt determined using the SWCC curve and Fredlund et al. (1994) estimation method is shown in Figure 9. The hydraulic conductivity function determined by using the SFCC and Fredlund et al. (1994) estimation method is also included in Figure 9, for comparison. The results show that the hydraulic conductivity estimation from the SFCC and the SWCC are in agreement. However, this may not be always the case; especially in situations where solutes are present and freezing rates are different, since the SWCC does not account for the influence of these parameters as noted in Figure 3 (for the case with solutes).

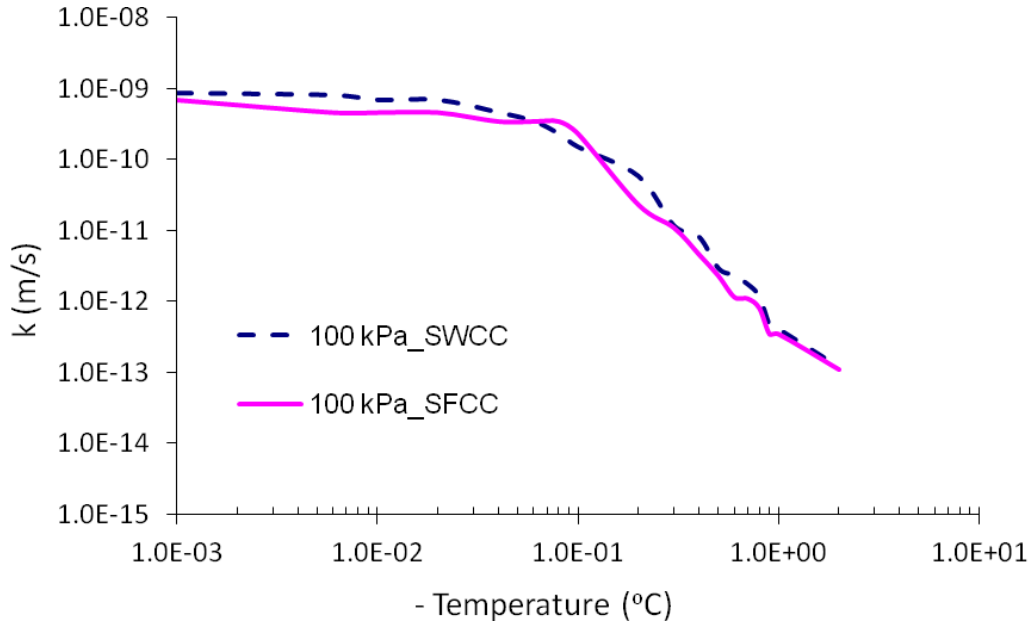


Figure 9. Comparison of hydraulic conductivity functions of partially frozen Devon silt estimated using the SFCC and the SWCC. Fredlund et al. (1994) method is used in both cases. The hydraulic conductivity functions are for a sample consolidated to 100 kPa pressure

### Comparison of predicted hydraulic conductivity with direct measurements

Horiguchi and Miller (1983) conducted direct measurement of hydraulic conductivity of partially frozen Chena Silt at different subzero temperatures and they reported hydraulic conductivity values as a function of temperature in the temperature range of 0 to -0.35 °C. They provided the following relationship between hydraulic conductivity and temperature for Chena Silt.

$$k = CT^D \quad (3)$$

Where  $k$  is the hydraulic conductivity in m/s,  $T$  is the temperature in °C, and  $C$  and  $D$  are constants with values  $C = 8.8 \times 10^{-12}$ , and  $D = 3.9$

This relationship is plotted in Figure 10 together with the hydraulic conductivity function of a Devon Silt sample consolidated to 100 kPa for which the hydraulic conductivity function was estimated using the method proposed in this study.

The difference in hydraulic conductivity values could be a result of difference in soil composition and due to the presence of lactose in the soil tested by Horiguchi and Miller (1983), which increases the unfrozen water content and hence the hydraulic conductivity.

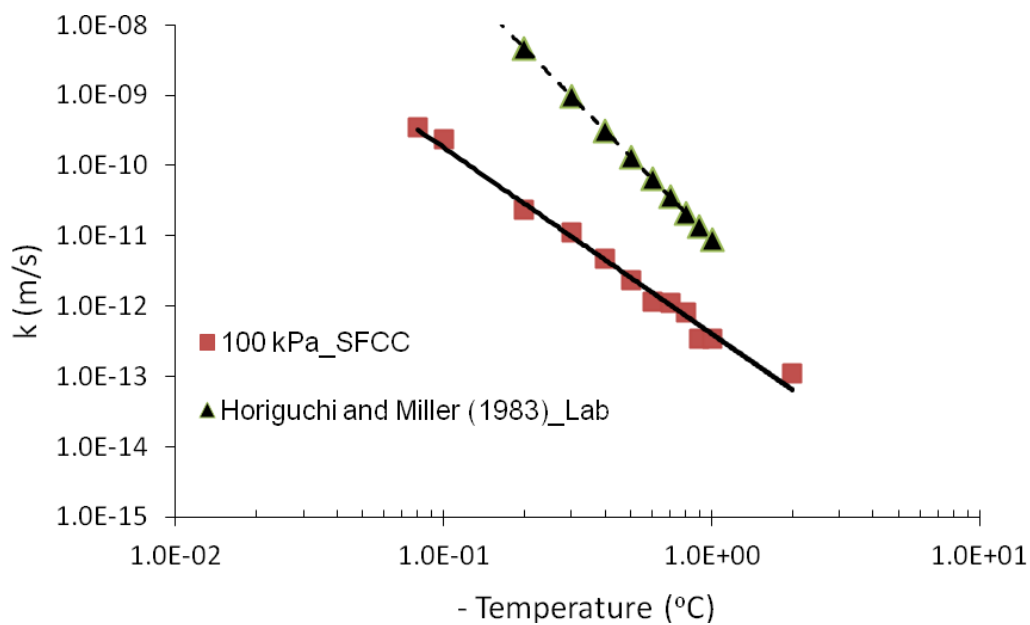


Figure 10. Comparison of hydraulic conductivity function from this study with hydraulic conductivity function reported by Horiguchi and Miller (1983) from direct laboratory test on Chena silt.

## Comparison of results from this study with results from other indirect methods

Tarnawski and Wagner (1996) present a mathematical model for predicting the hydraulic conductivity of partially frozen soils. They provided the following equation for the hydraulic conductivity of partially frozen soils.

$$k = k_{sat} \left( \frac{\theta_{un}}{\theta_{sat}} \right)^{2b+3} \quad (4)$$

Where  $k_{sat}$  is the saturated hydraulic conductivity,  $\theta_{un}$  is the volumetric unfrozen water content,  $\theta_{sat}$  is the saturated volumetric water content, and  $b$  is an empirical parameter based on soil particle size distribution.

$$b = d_g^{-0.5} + 0.2\sigma_g \quad (5)$$

Where  $d_g$  is the geometric mean particle diameter; and  $\sigma_g$  is geometric standard deviation to be determined as:

$$d_g = \exp(m_{cl} \ln(d_{cl}) + m_{si} \ln(d_{si}) + m_{sa} \ln(d_{sa})) \quad (6)$$

$$\sigma_g = \exp \left[ \sum_1^3 m_i (\ln(d_i))^2 - \left( \sum_1^3 m_i \ln(d_i) \right)^2 \right]^{-0.5} \quad (7)$$

Where  $m_{cl}$ ,  $m_{si}$ ,  $m_{sa}$  are clay, silt, and sand mass fractions respectively; and  $d_{cl}$ ,  $d_{si}$ ,  $d_{sa}$  are the particle size limits separating clay, silt and sand, respectively ( $d_{cl} = 0.001 \text{ mm}$ ,  $d_{si} = 0.026 \text{ mm}$ ,  $d_{sa} = 1.025 \text{ mm}$ ).

A different relationship was proposed by Fowler and Krantz (1994), who provided the following equation for estimating the hydraulic conductivity,  $k$

$$k = k_{sat} \left( \frac{\theta}{\phi} \right)^\gamma \quad (8)$$

Where  $k_{sat}$  is the saturated hydraulic conductivity,  $\theta$  is the volumetric water content,  $\phi$  is porosity, and  $\gamma$  is hydraulic conductivity exponent (ranging from 7-9).

Both these methods require the volumetric water content as input to determine the hydraulic conductivity function. Therefore, the SFCC of Devon Silt was used to get the hydraulic conductivity function. The following values were used as input parameters  $m_{cl}=0.25$ ,  $m_{si}=0.75$ ,  $m_{sa}=0$ ,  $\theta_{sat}=0.40$ ,  $\phi=0.40$ ,  $\gamma=8$ ,  $k_{sat}=10^{-9}$  m/s.

The results from the two approaches are presented in Figure 11 together with the hydraulic conductivity function estimated using the method proposed in this study. There is reasonable agreement of the hydraulic conductivity functions estimated using the different methods.

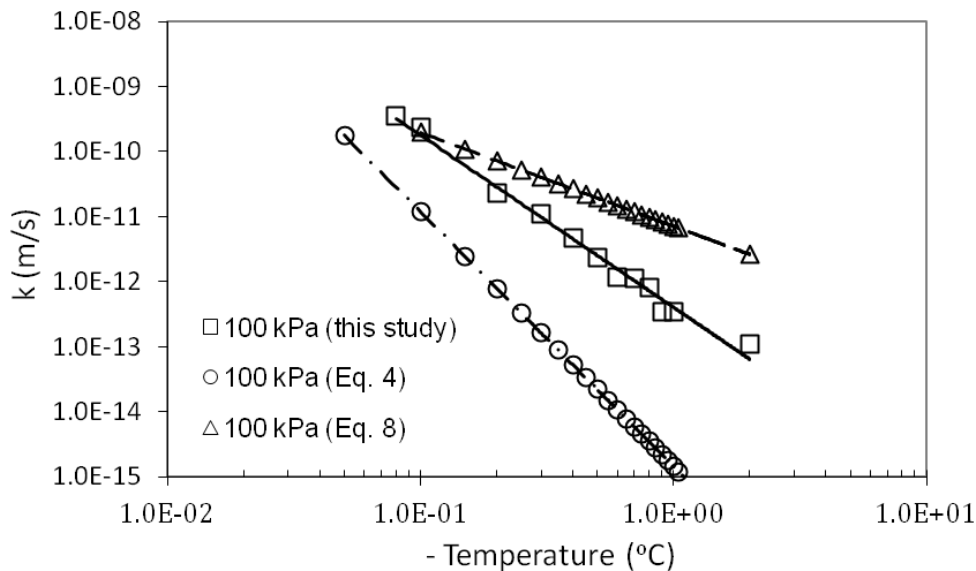


Figure 11. Comparison of hydraulic conductivity functions from this study with other indirect methods of hydraulic conductivity function estimation,

## **CONCLUSIONS**

This paper proposes using the soil freezing characteristic curve (SFCC), instead of the soil water characteristic curve (SWCC), for estimating the hydraulic conductivity of partially frozen soils. This approach uses the SFCC together with hydraulic conductivity estimation methods known from unsaturated soil mechanics (Fredlund et al. (1994) is used in this study).

The permeability function of partially frozen Devon Silt is predicted using the saturated coefficient of permeability and the SFCC. The results from this study compared well with results from other methods for estimating the hydraulic conductivity function of partially frozen soils as well as with direct measurements of a partially frozen silt.

Further study is required to address the robustness of the approach presented in this study compared with other methods; especially when solutes are present and also when the influence of rate of freezing is considered, since the SWCC test procedure does not account for their influences.

## **Acknowledgement**

The research was funded from a Discovery Grants provided by the Natural Science and Engineering Research Council of Canada.

## **REFERENCES**

Anderson, D.M., Morgenstern, N.R. 1973. Physics, chemistry and mechanics of frozen ground. 2nd International Conference on Permafrost, Yakutsk, USSR, 257-288.

- Azmatch, T.F., Segó, D.C., Arenson, L.U., Biggar, K.W., 2012a. New ice lens initiation condition for frost heave in fine-grained soils, *Cold Regions Science and Technology* 82, 8–13
- Azmatch, T.F., Arenson, L.U., Segó, D.C., Biggar, K.W., 2012b. Soil freezing characteristic curve of Devon Silt. Published in *Proceedings of the David C. Segó Symposium*, University of Alberta, Edmonton, Alberta, Canada, April 26-27.
- Baker, J. M., Spaans, E. J. A., 1997. Mechanics of meltwater movement above and within frozen soil, in *International Symposium on Physics, Chemistry, and Ecology of Seasonally Frozen Soils*, Fairbanks, Alaska, June 10– 12, Spec. Rep. 97(10), 31–36, U.S. Army Cold Reg. Res. and Eng. Lab., Hanover, N. H.
- Benson, C. H., Gribb, M. M., 1997. Measuring Unsaturated Hydraulic Conductivity in the Laboratory and Field. *Geotech. Spec. Publ.* 68, 113–168.
- Berg, R.L., 1983. Status of numerical models of heat and mass transfer in frost-susceptible soils. *Proceedings of the Fourth International Conference on Permafrost*, Fairbanks, Alaska, 67-71
- Black , P.B., Hardenberg, M.J., 1991. Historical perspectives in frost heave research, the early works of S. Taber and G. Beskow. *CRREL Special Report*, Publication 91 -23
- Black, P. B., Tice, A.R., 1989. Comparison of soil freezing and soil water curve data for Windsor sandy loam, *Water Resour. Res.*, 25, 2205– 2210.
- Brooks, R.H., Corey, A.T., 1964. Hydraulic properties of porous media. *Colorado State Univ. Hydrol. Paper*, No. 3: 27.

- Burt, T. P., Williams, P. J., 1974. Measurement of hydraulic conductivity of frozen soils. *Canadian Geotechnical Journal* 11, 647-650.
- Cary, J.W., Maryland, H.F., 1972. Salt and water movement in unsaturated frozen soil. *Soil Science Society of America Journal* 36, 549-555
- Flerchinger, G.N. 1987. Simultaneous heat and water model of a snow-residue-soil system. Ph.D. thesis, Washington State University, Pullman, Wash.
- Flerchinger, G. N., Seyfried, M. S., Hardegree, S. P., 2006. Using Soil Freezing Characteristics to Model Multi-Season Soil Water Dynamics. *Vadose Zone Journal* 5:1143–1153.
- Fowler, A.C., Krantz, W.B., 1994. A generalized secondary frost heave model. *SIAM Journal on Applied Mathematics* 54 (6), 1650–1675.
- Fredlund, M.D., 1996. Soil Vision users guide, Version 2.0, Edition 1.0. Soil Vision Systems Ltd, Saskatoon
- Fredlund, D.G., Xing, A., 1994. Equations for the soil-water characteristic curve. *Canadian Geotechnical Journal*, 31: 521-532.
- Fredlund, D.G., Xing, A., Huang, S., 1994. Predicting the permeability function for unsaturated soils using the soil-water characteristic curve. *Canadian Geotechnical Journal*, 31: 533-546.
- Guymon, G.L., Luthin, J.N. 1974. A coupled heat and moisture transport model for arctic soils. *Water Resources Research*, 10(5), 995-1001.
- Harlan, R. L., 1973. Analysis of coupled heat and mass transfer in partial frozen soil, *Water Resour. Res.* 9(5), 1314-1323.

- Horiguchi, K., and Miller, R. D. 1983. Hydraulic conductivity functions of frozen materials, Proc. 4th Int. Conf. Permafrost, National Academy Press, Washington, D.C., 504-508.
- Jame, Y. W., Norum, D. I., 1980. Heat and mass transfer in freezing unsaturated porous media, Water Resour. Res., 16, 811 – 819.
- Konrad, J. M., Morgenstern, N. R., 1980. A mechanistic theory of ice lens formation in fine-grained foils, Canadian Geotechnical Journal 17, 473-486.
- Koopmans, R.W.R., Miller, R.D., 1966. Soil freezing and soil water characteristic curves, Soil Sci. Soc. Am. Proc., 30, 680-685
- Leong, E.C., Rahardjo, H., 1997. Review of soil-water characteristic curve equations. J Geotech Eng Div ASCE 123(12), 1106–1117
- Liu, Z., Zhang, B., Yu, X., Tao, J., 2012. A New Method for Soil Water Characteristic Curve Measurement Based on Similarities Between Soil Freezing and Drying. Geotechnical Testing Journal, 35, 1
- Lundin, L.Ch., 1990. Hydraulic properties in an operational model of frozen soil. Journal of Hydrology 118, 289-310
- McCauley, C. A., D. M. White, M. R. Lilly, D. M. Nyman, 2002. A comparison of hydraulic conductivities, permeabilities and infiltration rates in frozen and unfrozen soils, Cold Reg. Sci. Technol. 34, 117– 125
- Mualem, Y., 1976. A new model for predicting the hydraulic conductivity of unsaturated porous media, Water Resour. Res. 12, 513–522.

- Nakano, Y., Tice, A., Oliphant, J., Jenkins, T., 1982. Transport of water in frozen soil: experimental determination of soil-water diffusivity under isothermal conditions. *Advances in Water Resources* 5, 221-226
- Newman, G.P., Wilson, G.W., 1997. Heat and mass transfer in unsaturated soils during freezing, *Canadian Geotechnical Journal* 34, 63-70
- Patterson, D.E., Smith, M.W., 1980. The use of time domain reflectometry for the measurement of unfrozen water content in frozen soils. *Cold Regions Science and Technology*, 3:205-210
- Spaans, E. J. A., Baker, J. M., 1996. The soil freezing characteristic: Its measurement and similarity to the soil moisture characteristic, *Soil Sci. Soc. Am. J.* 60, 13– 19.
- Tao, Y.X., Gray, D.M. 1994. Prediction of snowmelt infiltration into frozen soils. *Numerical Heat Transfer. Part A: Applications* 26:643-665
- Tarnawski, V.R., Wagner, B., 1996. On the prediction of hydraulic conductivity of frozen soils. *Canadian technical Journal* 33, 176 -180
- Taylor, G.S., Luthin, J.N., 1978. A model for coupled heat and moisture transfer during soil freezing. *Canadian Geotechnical Journal* 15, 548-555
- Topp, G.C., Davis, J.L., 1985. Time domain reflectometry (TDR) and its application to irrigation scheduling, *Advances in Irrigation*, Academic Press, 3:107-127
- Topp, G.C., Davis, J.L., and Annan, A.P., 1980. Electromagnetic determination of soil water content: measurements in coaxial transmission lines. *Water Resources Research*, 16(3), 574-582

van Genuchten M.Th., 1980. A closed form equation for predicting the hydraulic conductivity of unsaturated soils. *Soil Sci Soc Am J* 44:892–898

Watanabe, K., Mizoguchi, M., 2002. Amount of unfrozen water in frozen porous media saturated with solution. *Cold Regions Science and Technology* 34, 103–110.

Williams, P., 1964. Unfrozen water content of frozen soil and soil moisture suction, *Geotechnique*, 14, 231–246.

## **CHAPTER 7. HYDRAULIC CONDUCTIVITY ESTIMATION OF THE FROZEN FRINGE TAKING INTO ACCOUNT THE PRESENCE OF CRACKS IN THE FROZEN FRINGE**

### **ABSTRACT**

Results from previous studies on frost heave indicate the presence of freezing - induced cracks in the frozen fringe (e.g., Arenson et al., 2008). These cracks affect the hydraulic conductivity of the frozen fringe and hence the moisture transfer process during frost heave. The presence of the cracks necessitates the use of a dual porosity model for estimating the hydraulic conductivity function within the frozen fringe. Hence, the hydraulic conductivity of the frozen fringe will have two components: hydraulic conductivity of the soil matrix and hydraulic conductivity of the ice-filled cracks. A dual porosity model is proposed and methods are discussed to estimate the two components. The hydraulic conductivity of the cracked frozen fringe is then estimated as the weighted average of the two components based on the respective porosity ratio. The dual porosity hydraulic conductivity model is then used to carry out parametric study of the influence of the cracks on the hydraulic conductivity. The results indicated that the cracks have considerable influence on the hydraulic conductivity of the frozen fringe while occupying a small percent of the pore space.

### **INTRODUCTION**

Studies to understand the frost heave process have been carried out by many researchers for nearly a century (e.g. Taber, 1929; Beskow, 1935; Harlan, 1973; Konrad and Morgenstern, 1980; Gilpin, 1980; Sheng et al., 1995; Bronfenbrener and Bronfenbrener, 2010). The results from these studies indicated that significant frost heave observed in the field or laboratory is due to ice lens formation and moisture transport leading to the growth of these ice lenses. Horizontal ice lenses

and vertical ice veins are formed during freezing forming a reticulate ice lens structure as observed in Figure 1. Three distinct zones exist in a freezing soil during frost heave: the frozen zone, the unfrozen zone and the frozen fringe. These zones are as shown in Figure 1. The frozen fringe is the zone between the growing (warmest) horizontal ice lens and the frost front (zero degree isotherm), i.e., it is the zone where the warmest pore ice exists. Since, the concept of the frozen fringe was first presented by Miller (1972), it has been recognized that the characteristics of this zone play a very important role in the frost heave process. One of the most important properties of the frozen fringe is its hydraulic conductivity. The magnitude and rate of heave is influenced by the hydraulic conductivity of the frozen fringe since it has primary control on the rate of moisture movement that feeds the ice lens growth.

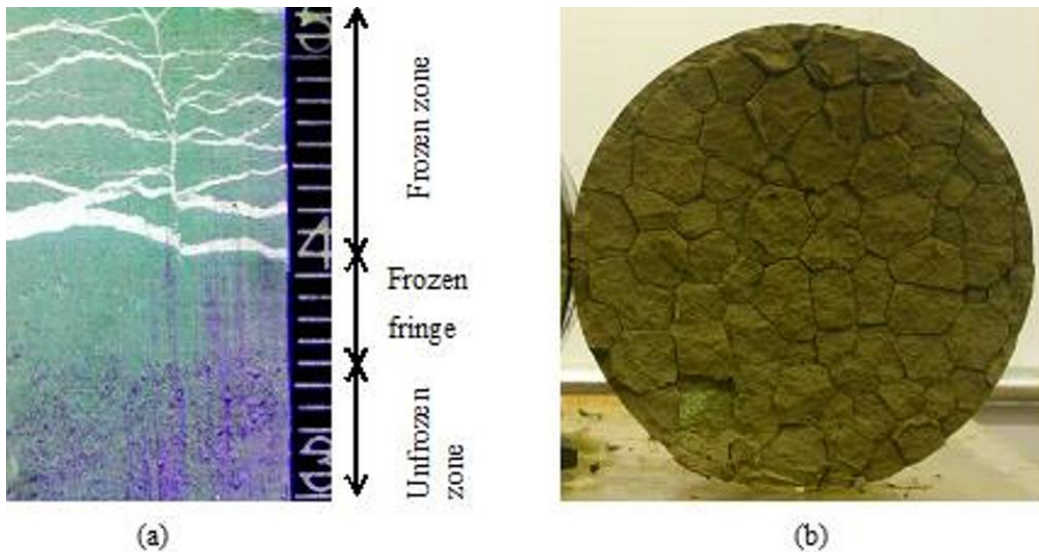


Figure 1: Frost heave features: (a) Reticulate ice structure viewed in vertical sample section and, (b) freezing-induced cracks within the frozen fringe viewed on a horizontal sample cross section at the base of the final ice lens (Xia, 2006). Sample diameter = 10.0 cm.

The hydraulic conductivity of the frozen fringe is affected by the structure of the soil in the frozen fringe. Studies by researchers such as Chamberlain and Gow

(1979) and Arenson et al. (2008) have shown the presence of freezing-induced cracks in the frozen fringe. One-dimensional freezing tests using Devon Silt and carried out by Xia (2006) showed the existence of these cracks in and/or through the frozen fringe from tests carried out under various boundary conditions (Figure 1). These cracks that precede the formation of horizontal ice lenses and vertical ice veins are important features associated with the frost heave process as they are believed to influence both the magnitude of frost heave and the moisture transfer rate or the hydraulic conductivity within the frozen fringe (Azmatch et al., 2008; Arenson et al., 2008). Therefore, the influence of the freezing-induced cracks on the moisture migration process has to be taken into account for proper evaluation of frost heave since the cracks form a secondary pore system within the frozen fringe.

Studies in nonfrozen soils show that secondary pore systems have considerable influence on hydraulic conductivity of cracked soils while taking only a few percent of pore space (Durner, 1994). The cracks provide a preferential flow pathway and the hydraulic conductivity of the soil is significantly increased (e.g., Novak et al., 2000). Keller et al. (1985) studied the hydraulic conductivity of a fractured glacial till and found that the saturated hydraulic conductivity was approximately two orders of magnitude higher than its intact matrix hydraulic conductivity.

Neglecting this secondary pore system may lead to large errors in the prediction of the hydraulic conductivity of cracked soils. Hence, dual porosity models should be used to predict the hydraulic conductivity. However, none of the existing frost heave models take into account the influence of freezing induced cracks on the moisture migration process. Existing hydraulic conductivity estimation methods for the frozen fringe consider the frozen fringe as a uniform single porosity material. But the presence of these cracks in the frozen fringe necessitates the use of dual porosity models for a better estimation of the hydraulic conductivity of the frozen fringe.

This paper proposes a dual porosity model for estimating the hydraulic conductivity of the frozen fringe. The model is then used to address the influence of the freezing-induced cracks in the moisture migration process, through the frozen fringe, during frost heave.

## DUAL POROSITY MODEL FOR THE HYDRAULIC CONDUCTIVITY OF THE FROZEN FRINGE

Figure 2 shows the model for the frozen fringe. Evaluation of the flow through the frozen fringe requires estimation of the flow through both the soil matrix and the cracks adjacent to the vertical ice veins that penetrate the frozen fringe. Therefore, the hydraulic conductivity of the frozen fringe will have two components:

1. hydraulic conductivity of the frozen soil matrix,  $k_m$
2. hydraulic conductivity of the cracks in the frozen fringe,  $k_{cr}$

The average hydraulic conductivity of the frozen fringe,  $k_{ff}$ , will then be computed based on the porosity ratio of the cracks and the soil matrix, weighted according to the respective porosities, as:

$$k_{ff} = \left[ \frac{n_{cr}}{n_{tot}} \right] k_{cr} + \left[ \frac{n_m}{n_{tot}} \right] k_m \quad (1)$$

Where  $n_{cr}$  is the crack porosity calculated as the area of cracks divided by the total cross-sectional area of the soil sample,  $n_{tot}$  is the total porosity calculated as the porosity of the soil before the soil cracked (using  $wG_s = eS$ ),  $n_m$  is the matrix porosity calculated as  $(n_{tot} - n_{cr})$ .

It is assumed that the combined matrix and crack medium qualify as a continuum with the same suction value applying for the two overlapping porous continua. Similar assumption has been used by Zhang and Fredlund (2004).

The following assumptions, regarding the cracks, are also made to establish the crack geometry:

- The spacing between the cracks is assumed to be equal to the depth of cracks (Lachenbruch, 1962).
- The depth of the cracks is assumed to be equal to the thickness of the frozen fringe.
- The cracks are assumed to have a constant width/thickness with depth and are rectangular in cross-section, although the actual cracks have a triangular cross-section with the tip of the triangle at the frost front.

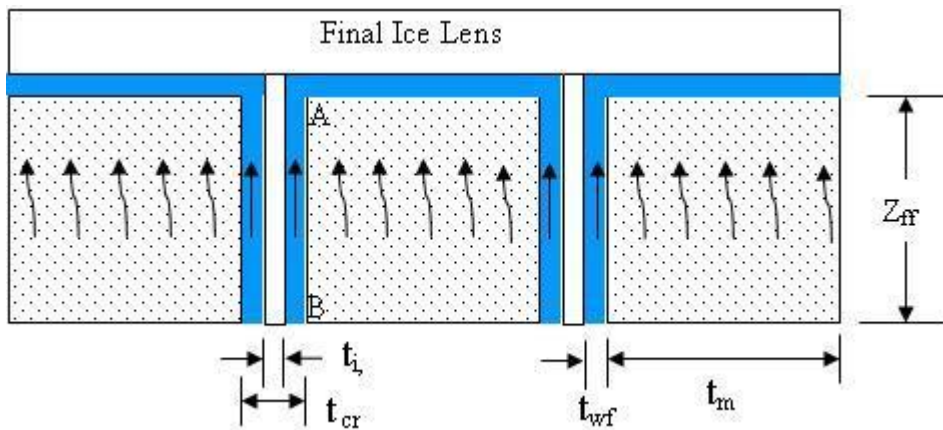


Figure 2. Frozen fringe model for hydraulic conductivity estimation.

### Hydraulic conductivity estimation of the frozen soil matrix

Hydraulic conductivity estimation methods developed for partially frozen soils can be used to estimate the matrix hydraulic conductivity component of the frozen fringe. Different approaches have been used to predict the hydraulic conductivity of partially frozen soils. The first approach involves the use of direct methods to determine the hydraulic conductivity. Such an approach has been used by Burt and Williams (1974) and Horiguchi and Miller (1983). However, measuring the

hydraulic conductivity of partially frozen soils remains very difficult. Hence, the difficulties faced in making direct measurement (especially when the soil is cracked) limit the credibility of the direct measurement methods. Therefore, indirect measurement methods have become the general approach to estimate the hydraulic conductivity of the frozen fringe.

Indirect measurement methods assume that the transport of water within partially frozen soils is controlled by the same process as in unsaturated unfrozen soils (Harlan, 1973). The relation between freezing soil temperatures (or suction) and unfrozen water content, referred to as the soil freezing characteristic curve (SFCC) of partially frozen soil, is assumed to be similar to the soil water characteristic curve (SWCC), which is a relation between suction and water content, for unfrozen soil. This assumption has been used by different authors such as Williams (1964), Koopmans and Miller (1966), Black and Tice (1989), and Spaans and Baker (1996). It is also assumed that the hydraulic conductivity of frozen soils is a function of the unfrozen water content and equals the hydraulic conductivity of unfrozen soils at the same water content. Hence, the SWCC of the soil together with hydraulic conductivity estimation method from the SWCC (e.g., Mualem, 1976; van Genuchten, 1980; Fredlund and Xing, 1994) is used to determine the hydraulic conductivity of partially frozen soils. This approach has been used by many researchers (e.g., Cary and Maryland, 1972; Harlan, 1973; Tao and Gray, 1994; Tarnawski and Wagner, 1996; Newman and Wilson, 1997).

Recently, Azmatch et al. (2012), indicated that the use of the SWCC for estimating the hydraulic conductivity of partially frozen soils has major drawbacks. They indicated that the influence of solutes and the influence of rate of freezing are not properly addressed when using the SWCC to estimate the hydraulic conductivity of partially frozen soils. They also indicated that the use of SWCC requires soil-dependent constant for which there is no established method to determine this constant. Hence, they suggested the use of SFCC, instead of the SWCC, to estimate the hydraulic conductivity of partially frozen soils.

Therefore, in this study, the method proposed by Azmatch et al. (2012) will be used to estimate the hydraulic conductivity of the partially frozen soil matrix. According to Azmatch et al. (2012), the SFCC together with hydraulic conductivity estimation methods known from unsaturated soil mechanics (e.g., Fredlund et al., 1994) are used to estimate the hydraulic conductivity of the frozen soil matrix.

### **Hydraulic Conductivity of the Cracks /Secondary Pore System in the frozen Fringe**

All the indirect methods used to determine the hydraulic conductivity of partially frozen soils do not take into account the existence of the secondary pore systems in the frozen fringe due to the cracks observed in the frozen fringe. This results in incorrect prediction of the hydraulic conductivity of the frozen fringe and hence the rate of frost heave.

The measurement of the hydraulic conductivity for cracked soil is extremely difficult, even for nonfrozen soils. Consequently, estimation procedures become attractive for determining the hydraulic conductivity of a cracked soil.

Different conceptual models and modeling approaches for the flow of water through saturated fractured porous media have been developed by researchers (Berkowitz 2002). According to Fredlund et al. (2010), Wu and Pruess (2005) categorized the models for fractured and cracked media into three categories: (1) an explicit discrete-fracture and matrix model (2) a dual-continuum model, and (3) an effective-continuum model.

The application of these models is currently limited because of the computational intensity involved, as well as an inability to obtain a detailed understanding of the fractures and the matrix geometric properties as well as the associated spatial distributions of fractures at a given site (Fredlund et al., 2010).

A different, but simpler, approach involves the use of methods that superimpose the SWCC for the intact portion of the soil with another independent analysis for the fractured portion. The resulting SWCC is used to estimate the hydraulic conductivity of a cracked medium (e.g., Zhang and Fredlund 2004). Zhang and Fredlund explained that a fractured rock will produce a bimodal material with a matrix phase and a fracture phase. The overall soil–water characteristic curve will be the sum of the effects of the two material phases weighted according to the respective porosities.

In this study, a more simplified approach is used to determine the component of flow through the cracks since the main objective of the paper is to show the influence of the cracks in the water transport process during frost heave (and not to present a rigorous approach for the computation of the flow through the cracks).

### **Flow through Cracks**

The flow through the cracks can be estimated by using the parallel plate theory. The cracks are assumed to be planar. If laminar flow in the planar crack is assumed, the saturated flow law through the crack with an aperture  $t$  is (where  $t$  is the unfrozen water film thickness in the cracks),

$$q = \frac{\gamma_w t^3}{12\eta} J \quad (3)$$

Where  $q$  is the flow rate,  $\gamma_w$  is the unit weight of water,  $\eta$  is the dynamic viscosity, and  $J$  is the hydraulic gradient between two points (A and B) across the depth of the crack.

$$J = \frac{h_A - h_B}{L_{AB}} \quad (4)$$

In this case  $L_{AB}$  is the depth of the cracks assumed to be equal to the thickness of the frozen fringe.

Comparing this to Darcy's law, the hydraulic conductivity component from the cracks/the flow through the cracks / can be determined using the following equation.

$$k = \frac{\gamma_w t^2}{12\eta} \quad (5)$$

Application of this equation requires that the unfrozen film thickness be determined. The unfrozen water film thickness varies with subzero temperature and is influenced by interparticle van der Waals force, solutes, curvature and pressure.

#### **Unfrozen water film thickness in the cracks of the frozen fringe**

When the temperature  $T$  is lowered below the freezing temperature of bulk water,  $T_m$ , ice is assumed to grow from the centre of the parallel plates, but water in the vicinity of the parallel plate walls (in contact with frozen soils) remains in the liquid state (owing to the surface forces effect, pressure effect, and solutes or impurities effect).

The unfrozen water film thickness,  $t$ , can be determined using the relationship provided by Wettlaufer (1999), as presented in Watanabe and Mizoguchi (2002):

$$T_m - T = \frac{T_m}{\rho_l q} \left[ \frac{RT_m N_i}{t} - \frac{\Delta\gamma\sigma^2}{t^3} - \frac{\Delta\gamma c}{2} \sqrt{\frac{N_i}{t}} \times \left( 1 + \frac{\sigma}{t} \right) \exp\left( -c \sqrt{\frac{N_i}{t}} (t - \sigma) \right) \right] \quad (6)$$

Where  $\rho_l$  is the molar density of the solvent,  $R$  is the gas constant,  $N_i$  is the number of moles per unit area of the electrolyte,  $\Delta\gamma$  is the difference in free

energy between the dry and wet surfaces,  $\sigma$  is a short range cutoff of the order of molecular diameter, and  $c$  is a constant.

This expression cannot be solved analytically in the general case (Hansen-Goos and Wettlaufer, 2010). However, when the effect of pressure and solutes is neglected and only the effect of the van der Waals forces on the unfrozen water thickness is considered, the unfrozen water film thickness,  $t$ , can be estimated using the following equation provided by Dash et al. (2005):

$$t = \left[ -\frac{A}{6\pi\rho_i L_f} \left( \frac{T_m}{T_m - T} \right) \right]^{1/3} \quad (7)$$

Where  $A$  is the Hamaker constant (J, Joule),  $\rho_i$  is the density of ice ( $\text{kg/m}^3$ ),  $L_f$  is the latent heat of fusion (J/kg), and the temperature is given in Kelvin.

In the absence of interfacial forces, the above general equation reduces to the following form, which shows the influence of impurities or solutes on unfrozen water film thickness.

$$\rho_l q_m \frac{T_m - T}{T_m} = \frac{RT_m N_i}{t} \quad (8)$$

where  $R$  is the gas constant,  $q_m$  is the latent heat of melting per mole,  $\rho_l$  is the molar density of the liquid,  $\rho_i = N_i/t$  is the molar density of the impurities,  $T_m$  is bulk melting temperature of ice.

Extremely small concentrations of impurities in the parent liquid can exert major impact during surface melting and hence increase the unfrozen water film thickness. Benatov and Wettlaufer (2004) indicate that the unfrozen water film thickness could be a few micrometers for small concentration of impurities (See Figure 1 of Benatov and Wettlaufer, 2004).

The influence of solutes on unfrozen water film is more pronounced in the frozen fringe, since the freezing front is known to push away the water soluble ions as well as the water-nonsoluble compounds (e.g., Corte, 1962; Halde, 1980; Ostrumov et al., 2001). This results in an increased concentration of solutes in the pore fluid within the frozen fringe below the final ice lens. Zones of high concentration are formed at the interface of segregation ice lens and mineral layers in freezing ground ( Ostrumov et al, 2001). Therefore, extremely small background concentrations of impurities in the soil can exert major changes on the unfrozen water films (Dash et al., 2006) of the frozen fringe.

### **INFLUENCE OF THE FREEZING-INDUCED CRACKS ON THE HYDRAULIC CONDUCTIVITY OF THE FROZEN FRINGE**

The hydraulic conductivity of the frozen fringe can be estimated using Equation (1), once the hydraulic conductivity component from the freezing-induced cracks and from the soil matrix are determined using the methods presented above.

Results from laboratory tests carried out on Devon silt will be used to establish the influence of the freezing-induced cracks on the hydraulic conductivity of the frozen fringe. The laboratory tests conducted include one-dimensional frost heave tests and tests for the soil-freezing characteristic curve (SFCC). Details of the test procedures are presented in Azmatch et al. (2012). The tests were conducted on Devon silt sample consolidated from slurry to a pressure of 100 kPa. The result from the test for the soil freezing characteristic curve is presented in Figure 3.

After the one-dimensional frost heave test was completed, a horizontal section was taken immediately below the final ice lens. The crack structure was similar to the one shown in Figure 1(b). Digital images of the sample were taken and used to measure the length of the cracks in horizontal cross-section. The length was measured using ImageJ and it was determined to be 1.96 m.

The width of the cracks was measured using Scanning Electron Microscope (SEM). The SEM picture shows the width of the cracks (Figure 4).

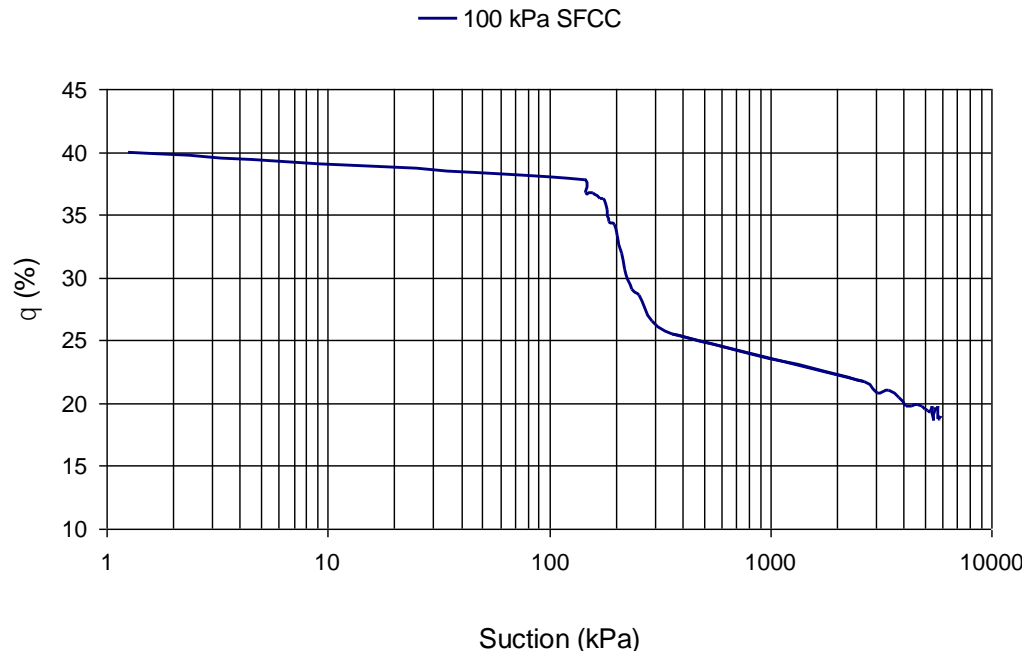


Figure 3. Soil freezing characteristic curve of Devon silt consolidated at 100 kPa

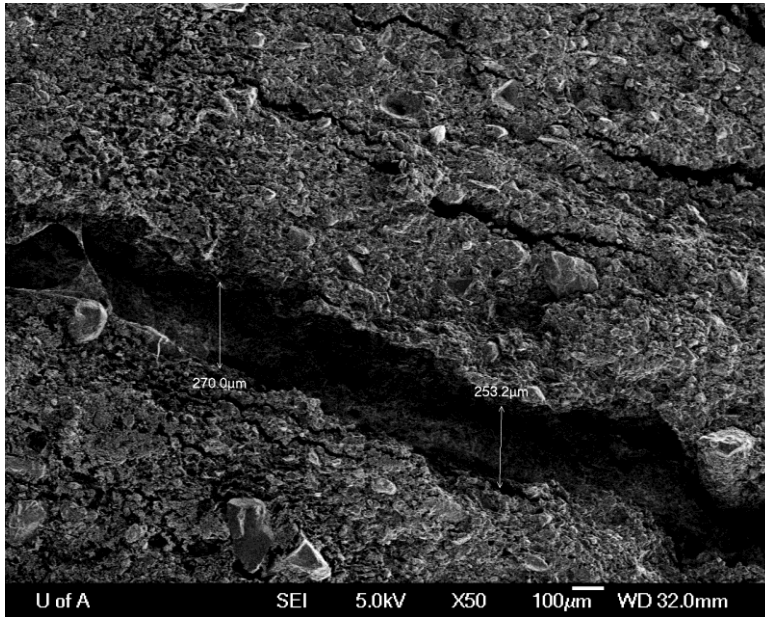


Figure 4: Scanning Electron Microscope (SEM) measurement of the width of the cracks in Devon silt.

## Matrix Component of the Hydraulic Conductivity of the Frozen Fringe

The SFCC together with the hydraulic conductivity estimation method proposed by Fredlund et al. (1994) is used to estimate the matrix hydraulic conductivity,  $k_m$ , using Soil Vision software. The result from this analysis is plotted in Figure 5.

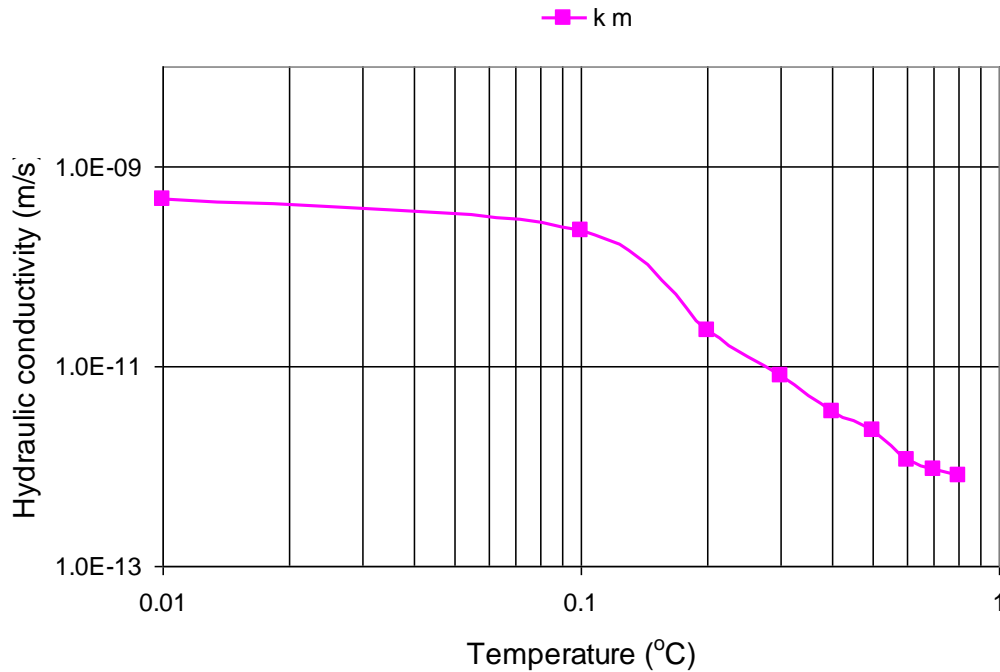


Figure 5: Hydraulic conductivity function,  $k_m$ , of the soil matrix of Devon silt.

## Hydraulic conductivity of the cracks

The estimation of the hydraulic conductivity variation of the cracks with temperature requires data on the variation of the unfrozen water film thickness with temperature. Since the analytical solution of the equation for the unfrozen water film thickness is difficult, the influence of the cracks would be investigated for a range of assumed but reasonable values of the unfrozen water film thickness under the conditions within frozen fringe. These unfrozen water film thickness values are then used to estimate the hydraulic conductivity of the cracks using Equation (4).

The unfrozen water film thickness will be assumed to vary from the thickness of a crack at 0 °C to an assumed value of the thickness of the unfrozen water films at -1.0°C.

One dimensional frost heave test was carried out using Devon silt sample consolidated at 100 kPa. The cracks in the frozen fringe of this test sample are similar to the ones shown in Figure 1. The thickness of the cracks was measured using SEM (Figure 4) and the average value was determined to be 100 µm (half the total thickness).

To establish the range of values for the unfrozen water film thickness at -1.0°C, simplifying assumptions and experimental observations by other researchers are used. Equation (6), which takes into account the influence of van der Waals forces but ignores the influence of solutes and pressure, establishes the lower limit of the unfrozen water film thickness value at -1.0°C. The following parameters are used to determine the variation of unfrozen water film thickness with temperature using Equation (6):  $L_f = 3.34 \cdot 10^5 \text{ J/kg}$   $A = -10^{-18} \text{ J}$   $\rho_i = 917 \text{ kg/m}^3$   
 $T_m = 273.15 \text{ K}$

The results suggest that a conservative value of 1 nm is a realistic lower limit of the unfrozen water film thickness at -1.0°C.

The influence of solutes is taken into account to set an upper limit for the range of unfrozen water film thickness values (at -1.0°C) to be investigated for determining the hydraulic conductivity of the cracks. The influence of solutes will be to increase the unfrozen water film thickness. Benatov and Wettlaufer (2004) investigated the influence of solutes on unfrozen water film thickness and computed unfrozen water film thickness values greater than 1µm in the temperature range of -0.1°C to -1.0°C . Hence, the upper limit value of the range of unfrozen water film thickness to be investigated would be set as 1µm. This assumption of micrometer thick unfrozen water film thickness is reasonable for the condition that we are investigating since Devon silt has a background total

dissolved solids concentration of just over 0.5 gm/L (Konrad and McCmmon, 1990).

Therefore, the variation of the hydraulic conductivity of the cracks with temperature is determined by assuming that the unfrozen water film thickness value varies linearly from 125  $\mu\text{m}$  at unfrozen state ( $0\text{ }^{\circ}\text{C}$ ) to: Case 1: 10 nm at -1.0  $^{\circ}\text{C}$ , Case 2: 50 nm at -1.0  $^{\circ}\text{C}$ , Case 3: 100 nm at -1.0  $^{\circ}\text{C}$ , Case 4: 1000 nm (or  $1\mu\text{m}$ ) at -1.0  $^{\circ}\text{C}$ . The assumed linear variation of unfrozen water film thickness with temperature is presented on log-log scale (Figure 6) and is based on observation of results presented by Benatov and Wettlaufer (2004).

The assumed unfrozen water film thickness variation with temperature is presented in Figure 6. The hydraulic conductivity function (variation with temperature) of the cracks for these cases of unfrozen water film thicknesses are plotted in Figure 7.

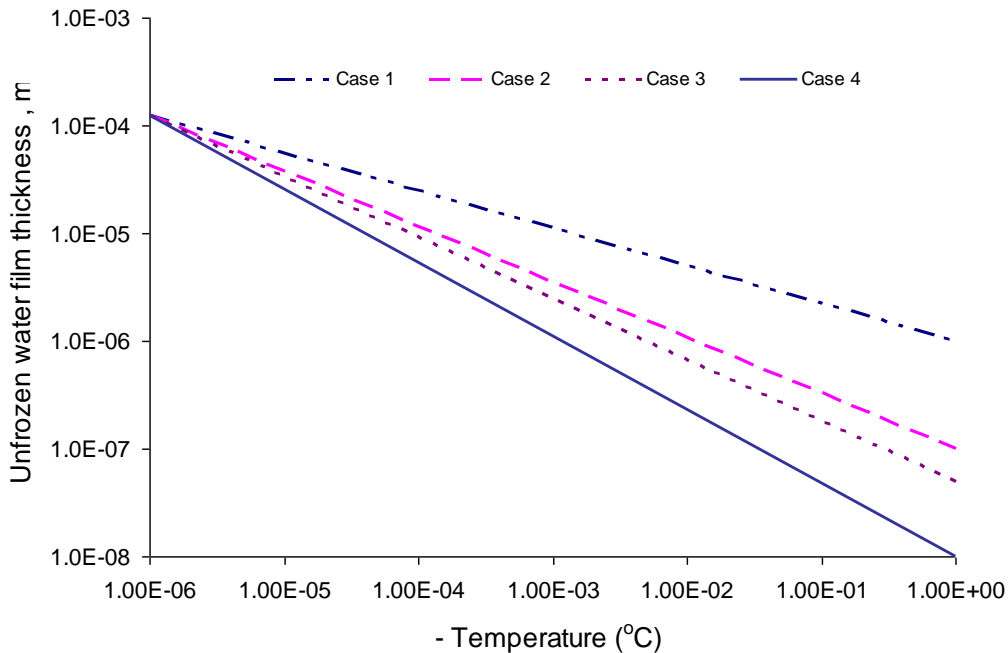


Figure 6. The assumed unfrozen water film thickness variation with temperature.

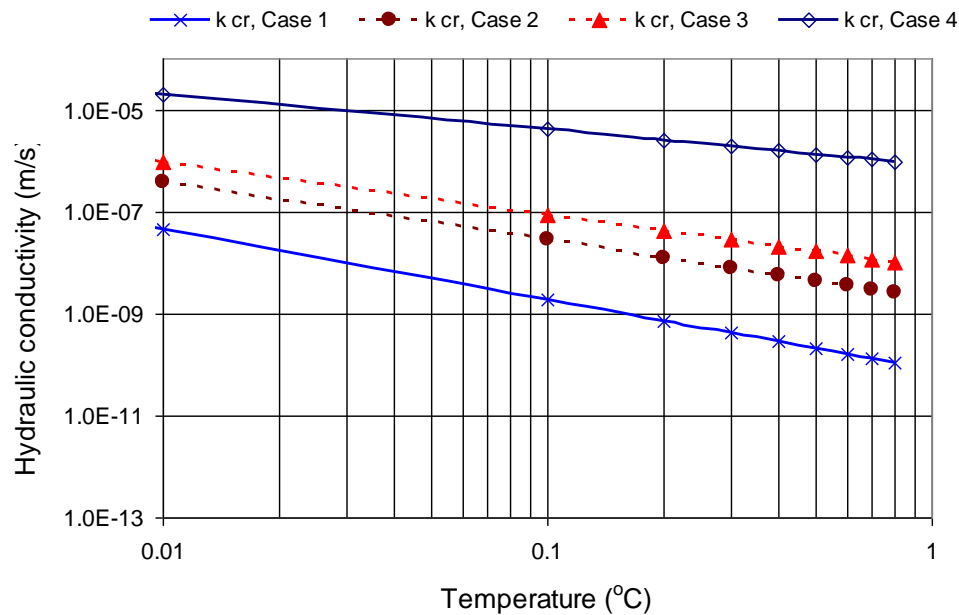


Figure 7. Hydraulic conductivity function,  $k_{cr}$ , of the cracks in the frozen fringe.

### Hydraulic conductivity of the frozen fringe with the influence of the Cracks

Equation (1), together with the computed hydraulic conductivity components, is used to compute the hydraulic conductivity of the frozen fringe with cracks. This requires computation of the porosity ratios.

Results from one-dimensional frost heave tests (Figure 1 (b)) are used to establish the geometry of the cracks.

The length of the cracks is measured using ImageJ. The measured value of the length of the cracks in plan cross-section varies from 2.42 m to 3.92 m. An average value of 3.0 m is set as the length of the cracks.

The width of the cracks is measured using SEM (Figure 4). The average measured value of the width of the cracks is 250  $\mu\text{m}$ . Since, half the width of the cracks is

used to compute the flow through the films, a conservative average value of 125  $\mu\text{m}$  is used as the thickness of the cracks.

The void ratio of Devon silt consolidated at 100 kPa is 0.792. Hence, the porosity (called the total porosity,  $n_{tot}$ ) is 0.42.

The crack porosity,  $n_{cr}$ , is calculated as:

$$n_{cr} = \frac{A_{cr}}{A_{tot}} = \frac{L_{cr} \times b_{cr}}{(\pi d^2 / 4)}$$

With  $L_{cr}$  is the length of the cracks (= 3.0 m),  $b_{cr}$  is the width of the cracks (= 125  $\mu\text{m}$ ), and  $d$  is the diameter of the soil sample tested (0.10 m). This would give  $n_{cr}$  value of 0.048. The porosity ratio of the cracks ( $n_{cr} / n_{tot}$ ) would then be about 0.10. This means that the cracks contribute to about 10 % of the porosity of the soil. Hence, the matrix porosity ratio ( $n_m / n_{tot}$ ) would be 0.90, which implies the matrix porosity would contribute to 90 % of the total porosity.

The hydraulic conductivity function of the frozen fringe is therefore computed using the following equation:

$$k_{ff} = \left[ \frac{n_{cr}}{n_{tot}} \right] k_{cr} + \left[ \frac{n_m}{n_{tot}} \right] k_m = 0.10k_{cr} + 0.90k_m$$

The resulting hydraulic conductivity functions of the frozen fringe, corresponding to different thicknesses of the unfrozen water film associated with each ice-filled crack are presented in Figure 8 – Figure 11.

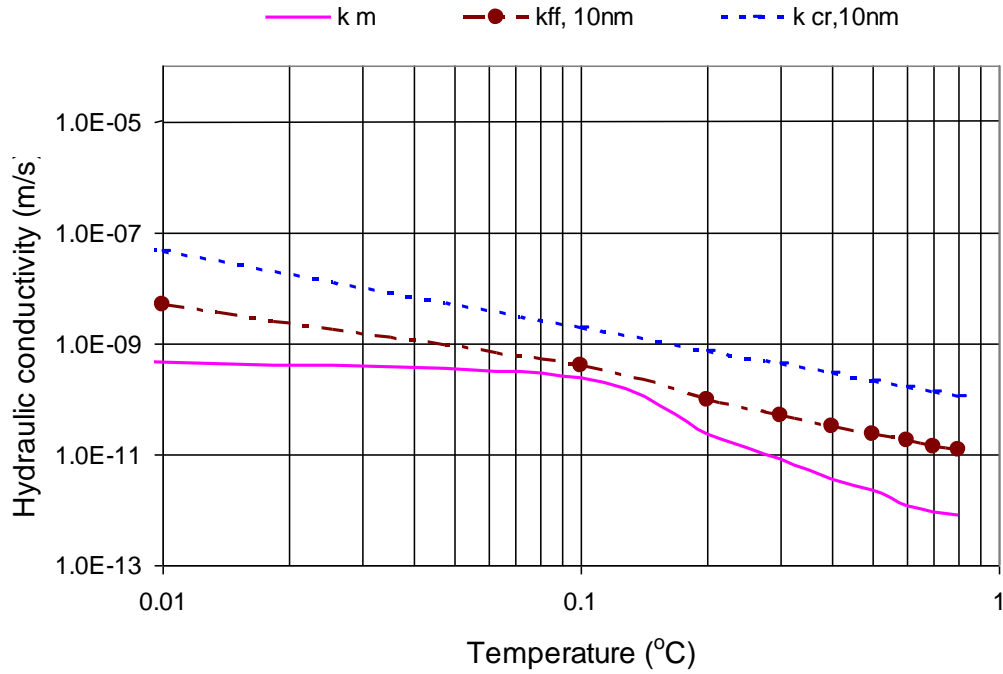


Figure 8. Hydraulic conductivity of the frozen fringe,  $k_{ff}$ . Unfrozen water film thickness variation from  $125\mu\text{m}$  (at  $0^\circ\text{C}$ ) to  $10\text{nm}$  (at  $-1.0^\circ\text{C}$ ) in the cracks.

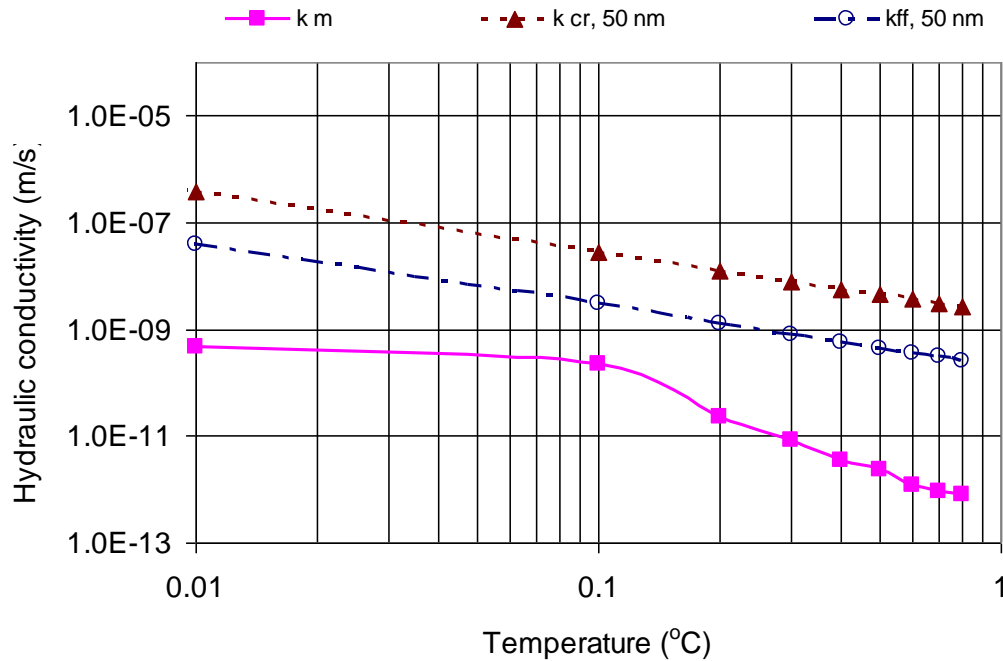


Figure 9. Hydraulic conductivity of the frozen fringe,  $k_{ff}$ . Unfrozen water film thickness variation from  $125\mu\text{m}$  (at  $0^\circ\text{C}$ ) to  $50\text{nm}$  (at  $-1.0^\circ\text{C}$ ) in the cracks.

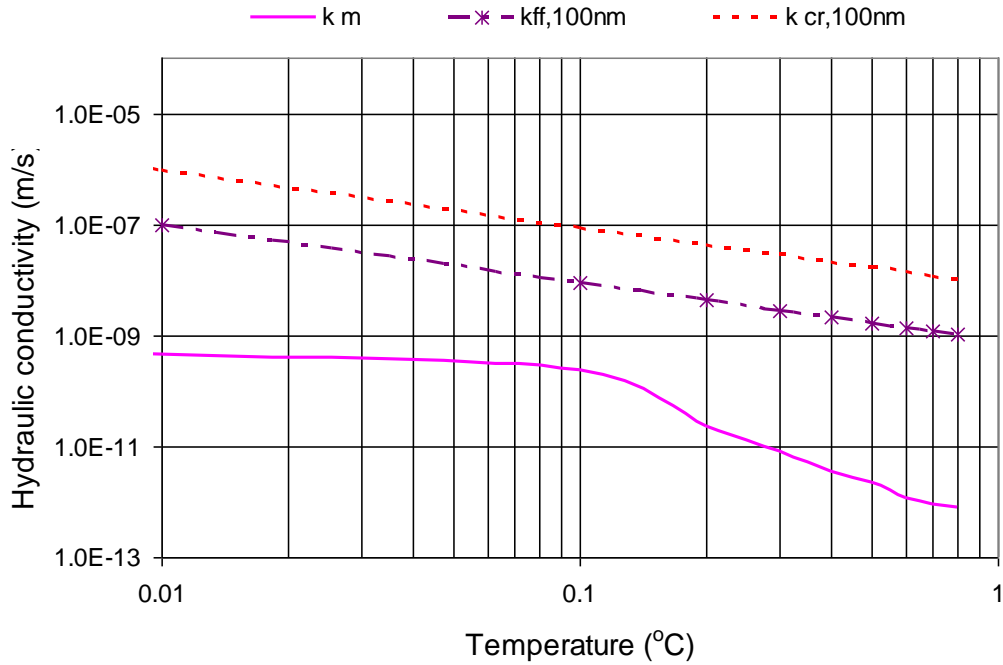


Figure 10. Hydraulic conductivity of the frozen fringe,  $k_{ff}$ . Unfrozen water film thickness variation from 125 $\mu$ m (at 0°C) to 100nm (at -1.0°C) in the cracks.

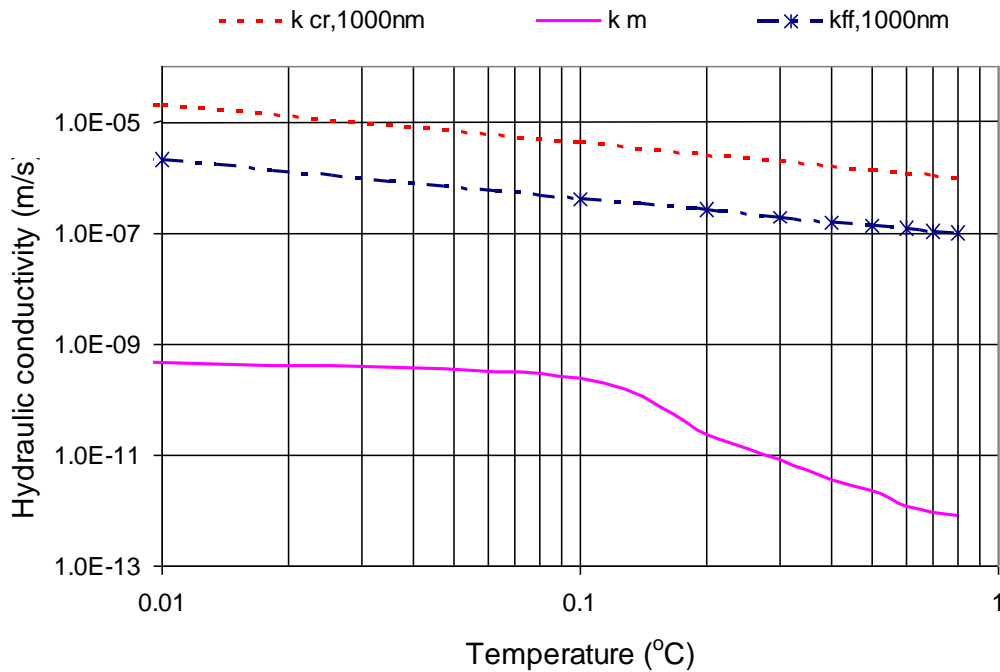


Figure 11. Hydraulic conductivity of the frozen fringe,  $k_{ff}$ . Unfrozen water film thickness variation from 125 $\mu$ m (at 0°C) to 1000nm (at -1.0°C) in the cracks.

The results indicate that the cracks have considerable influence on the hydraulic conductivity of the frozen fringe while taking only a few percent of the pore space. One- to three-orders of magnitude increase in the hydraulic conductivity of the frozen fringe is estimated, depending on the thickness of the unfrozen water films.

Figure 8, which corresponds to 10 nm thick unfrozen water film thickness, shows that the cracks influence the hydraulic conductivity of the frozen fringe, especially when the temperature drops below  $-0.30\text{ }^{\circ}\text{C}$ .

A significant increase in hydraulic conductivity is observed when the unfrozen water film thickness varies from  $125\text{ }\mu\text{m}$  (at  $0\text{ }^{\circ}\text{C}$ ) to  $50\text{ nm}$  (at  $-1.0\text{ }^{\circ}\text{C}$ ) in the cracks. The authors believe that unfrozen water film thickness values of such magnitude would be more representative of the real situation expected to occur under natural conditions since many soils on-site would have background concentration of solutes which influences the frozen fringe in a pronounced way.

## **DISCUSSION**

When the soil within the frozen fringe is not cracked, it can be assumed to be homogeneous and its hydraulic conductivity function can be estimated using a single porosity hydraulic conductivity models. Under such conditions the hydraulic conductivity of the soil within the frozen fringe can be estimated using the SFCC together with hydraulic conductivity estimation method by Fredlund et al. (1994). Hence, the hydraulic conductivity of the soil within the frozen fringe would have only one component, which is the matrix hydraulic conductivity.

When cracks are present in the soil within the frozen fringe, its hydraulic conductivity function will have two components: the matrix component and the crack component. The dual porosity model presented in this study can be used under these conditions.

Another factor that needs to be taken into account when investigating the hydraulic conductivity of the soil within the frozen fringe is the effect of the consolidation process during frost heave. Azmatch et al. (2008) have used particle image velocimetry (GeoPIV) to study the processes during frost heave. Their study has indicated that ice lens formation or frost heave is preceded by consolidation of the soil matrix in the frozen fringe. This consolidation would change the matrix component of the hydraulic conductivity function. The hydraulic conductivity function presented in the previous sections does not account for this issue since the SFCC used to estimate the hydraulic conductivity is determined from isotropic freezing under zero pressure. Proper estimation of the hydraulic conductivity, however, requires that the influence of the consolidation be taken into account. The influence of the consolidation would be to decrease the saturated hydraulic conductivity of the soil matrix in the frozen fringe before it starts to freeze. The magnitude of the consolidation pressure can be approximated to be equal to the suction value at the corresponding temperature of the frozen fringe. For the conditions under investigation, the ice lens initiation temperature is  $-0.15\text{ }^{\circ}\text{C}$ . The suction corresponding to this would be 187.5 kPa. Hence, the soil matrix in the frozen fringe would have been consolidated under a pressure of 187.5 kPa before the final ice lens initiates. This means that the initial hydraulic conductivity of the soil matrix would be reduced by one- to two-orders of magnitude before it starts to freeze. In here we assume that the shape of the hydraulic conductivity function as determined from the SFCC would remain the same but the magnitude of the hydraulic conductivity of the soil matrix would be reduced by two-orders of magnitude. This gives the modified hydraulic conductivity function,  $k_{m,consol}$ , which takes into account the influence of consolidation (Figure 12). Further study is required to understand the influence of the consolidation on the hydraulic conductivity of the soil within the frozen fringe.

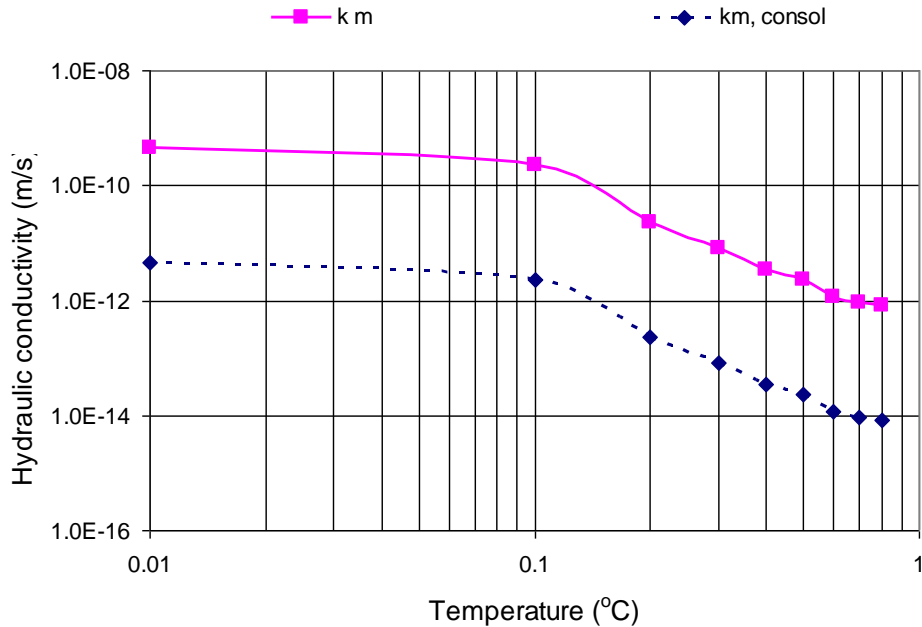


Figure 12. Modified matrix hydraulic conductivity function taking into account the influence of the consolidation process that precedes freezing.

## CONCLUSION

The presence of cracks in the frozen fringe makes it behave as a combination of two materials: the partially frozen soil matrix and the partly-ice-filled cracks. Hence, it was proposed to use a dual porosity hydraulic conductivity model to estimate the hydraulic conductivity of the frozen fringe.

The hydraulic conductivity of the frozen fringe was estimated using the proposed dual porosity model; and, assumed unfrozen water film thicknesses values for the temperature condition of the frozen fringe to investigate the influence of the cracks on the hydraulic conductivity of the frozen fringe.

The results indicated that the cracks have considerable influence on the hydraulic conductivity of the frozen fringe while only occupying a few percent of the pore space.

## REFERENCES

- Arenson, L.U., Azmatch, T.F., Segó, D.C., and Biggar, K.W. 2008. A new hypothesis on ice lens formation in frost-susceptible soils. Proceedings of the Ninth International Conference on Permafrost, Fairbanks, Alaska 1: 59-64.
- Azmatch, T.F., Segó, D.C., Arenson, L.U., Biggar, K.W., 2012. Using soil freezing characteristic curve to estimate the hydraulic conductivity of partially frozen soils. *Cold Regions Science and Technology* 83/84, 103-109
- Azmatch, T.F., Arenson, L.U., Segó, D.C., and Biggar, K.W. 2008. Measuring ice lens growth and development of soil strains during frost penetration using particle image velocimetry (GeoPIV). Proceedings of the Ninth International Conference on Permafrost, Fairbanks, Alaska 1: 89-93
- Benatov, L., Wettlaufer, J.S., Abrupt grain boundary melting in ice, *Phys. Rev. E* 70 (2004) 061606-1–061606-7.
- Berkowitz, B., 2002. Characterizing flow and transport in fractured geological media: a review. *Advances in Water Resources* 25, 861-884
- Beskow, G. 1935. Soil Freezing and frost heaving with special application to roads and railroads. *Swed. Geol. Soc., Ser.C, No.375*, 26th year book No. 3 (translated by J.O. Osterberg, Northwestern Univ., 1947)
- Black, P. B., Tice, A.R., 1989. Comparison of soil freezing and soil water curve data for Windsor sandy loam, *Water Resour. Res.*, 25, 2205– 2210.
- Bronfenbrener, L., Bornfenbrener, R., 2010. Modeling frost heave in freezing soils. *Cold Regions Science and Technology* 61, 43-64.

- Burt, T. P., Williams, P. J., 1974. Measurement of hydraulic conductivity of frozen soils. *Canadian Geotechnical Journal* 11, 647-650.
- Cary, J.W., Maryland, H.F., 1972. Salt and water movement in unsaturated frozen soil. *Soil Science Society of America Journal* 36, 549-555
- Chamberlain EJ, Gow AJ. 1979. Effect of freezing and thawing on the permeability and structure of soils. *Engineering Geology* 13: 73–92.
- Corte, A.E., 1962. Vertical migration of particles in front of moving freezing plane. *Journal of Geophysical Research* 67, 1085 -1090
- Dash, J.G., Fu, H., Wettlaufer, J.S., 1995. The premelting of ice and its environmental consequences. *Rep. Prog. Phys.*, 58, 115-167
- Dash, J.G., Rempel, A.W., Wettlaufer, J.S., 2006. The physics of premelted ice and its geophysical consequence. *Reviews of Modern Physics* 78, 695-741
- Durner, W., 1994. Hydraulic conductivity estimation for soil with heterogeneous pore structure. *Water Resources Research* 30(2), 211-223
- Fredlund, D.G., Houston, S.L., Nguyen, Q., Fredlund, M.D., 2010. Moisture movement through cracked soil profiles. *Geotechnical and Geological Engineering* 28 (6), 865-888
- Fredlund, D.G., Xing, A., 1994. Equations for the soil-water characteristic curve. *Canadian Geotechnical Journal*, 31: 521-532.
- Fredlund, D.G., Xing, A., Huang, S., 1994. Predicting the permeability function for unsaturated soils using the soil-water characteristic curve. *Canadian Geotechnical Journal*, 31: 533-546.

- Gilpin, R. R. 1980 A model for the prediction of ice lensing and frost heave in soils, *Water Resour. Res.*, 16(5): 918-930.
- Halde, R. 1980. Concentration of impurities by progressive freezing. *Water Research* 14(6), 575-580
- Hansen-Goos, H., Wettlaufer, J.S., 2010, Theory of ice premelting in porous media, *Physical Review E* 81, 031604, 031604-1-031604-13.
- Harlan, R. L. 1973. Analysis of coupled heat and mass transfer in partial frozen soil, *Water Resour. Res.*, 9(5): 1314-1323.
- Horiguchi, K., and Miller, R. D. 1983. Hydraulic conductivity functions of frozen materials, *Proc. 4th Int. Conf. Permafrost*, National Academy Press, Washington, D.C., 504-508.
- Keller, C.K., van der Kamp, G., Cherry, J.A., 1985. Fracture permeability and groundwater flow in clayey till near Saskatoon, Saskatchewan. *Canadian Geotechnical Journal* 23, 229-240
- Konrad and McCmmon, 1990. Solute Partitioning in freezing soils. *Canadian Geotechnical Journal* 67, 726-736
- Konrad, J. M., and Morgenstern, N. R. 1980. A mechanistic theory of ice lens formation in fine-grained foils, *Can. Geotech. J* 17, 473-486.
- Koopmans, R.W.R., Miller, R.D., 1966. Soil freezing and soil water characteristic curves, *Soil Sci. Soc. Am. Proc.*, 30, 680-685
- Miller, R.D. 1972. Freezing and heaving of saturated and unsaturated soils. *Highway Research Rec.* 393:1-11

- Mualem, Y., 1976. A new model for predicting the hydraulic conductivity of unsaturated porous media, *Water Resour. Res.* 12, 513–522.
- Newman, G.P., Wilson, G.W., 1997. Heat and mass transfer in unsaturated soils during freezing, *Canadian Geotechnical Journal* 34, 63-70
- Novak, V., Simunek, J., van Genuchten, M.Th., 2000. Infiltration into soil with fractures, *Journal of Irrigation Drain Engineering* 126 (1), 41-47
- Ostroumov, V., Hoover, R., Ostroumova, N., Van Vliet-Lanoe, B., Siegert, Ch., Sorokovikov, V., 2001. Redistribution of soluble components during ice segregation in freezing ground. *Cold Regions science and technology* 32, 175-182
- Sheng, D., Axelsson, K., and Knutsson, S. 1995. Frost Heave due to Ice Lens Formation in Freezing soils, 1: Theory and Verification, *Nordic Hydrology*, 26 (2): 125-146.
- Spaans, E. J. A., Baker, J. M., 1996. The soil freezing characteristic: Its measurement and similarity to the soil moisture characteristic, *Soil Sci. Soc. Am. J.* 60, 13– 19.
- Taber, S. 1929. Frost Heaving. *Journal of Geology* 37: 428 – 461
- Taber, S. 1930. The mechanics of frost Heaving. *Journal of Geology* 38 (4): 303 – 317
- Tao, Y.X., Gray, D.M. 1994. Prediction of snowmelt infiltration into frozen soils. *Numerical Heat Transfer. Part A: Applications* 26:643-665
- Tarnawski, V.R., Wagner, B., 1996. On the prediction of hydraulic conductivity of frozen soils. *Canadian technical Journal* 33, 176 -180

- van Genuchten M.Th., 1980. A closed form equation for predicting the hydraulic conductivity of unsaturated soils. *Soil Sci Soc Am J* 44:892–898
- Watanabe, K., Mizoguchi, M. 2002. Amount of unfrozen water in frozen porous media saturated with solution. *Cold Regions Science and Technology* 34, 103–110
- Wettlaufer, J.S., 1999. Impurity effects in the premelting of ice. *Physical Review Letters*, 82 (12): 2516-2519
- Williams, P., 1964. Unfrozen water content of frozen soil and soil moisture suction, *Geotechnique*, 14, 231–246.
- Wu, YS, Preuss, K., 2005. A physically based numerical approach for modeling fracture-matrix interaction reservoirs. *Proceedings of the World Geothermal Congress, Antalya, Turkey*, 1-8
- Xia, D., 2006. Frost heave studies using digital photographic technique. MSc Thesis, University of Alberta, Edmonton, AB, Canada, 165 pp.
- Zhang, L., Fredlund, D.G., 2004. Characteristics of water characteristic curves for unsaturated fractured rocks. *The second Asian Conference on Unsaturated Soils, Unsat-Asia, Osaka, Japan*, 425-428

## **CHAPTER 8. SUMMARY, CONCLUSIONS AND RECOMMENDATIONS**

The results from previous studies on frost heave (e.g., Taber, 1929; Beskow, 1935; Harlan, 1973; Konrad and Morgenstern, 1980; Gilpin, 1980; Bronfenbrener and Bronfenbrener, 2010) indicate that frost heave observed in the field or laboratory is attributed to ice lens formation associated with water migration to the freezing front and the segregational ice that develops contributes significantly to the heave. Hence frost heave prediction models require an ice lens initiation criteria and the hydraulic conductivity in the frozen fringe.

Existing frost heave prediction methods do include complex procedures in estimating the hydraulic conductivity. Ice lens initiation conditions in existing methods are also not easy to evaluate and implement. In fact, some of the existing frost heave prediction methods lack inclusion of the ice lens initiation condition.

The objective of this thesis was to investigate and develop the ice lens initiation criteria and a method to estimate the hydraulic conductivity that are simple to implement. A method, involving the use of the soil freezing characteristic curve (SFCC), for predicting the ice lens initiation condition and the hydraulic conductivity of the frozen fringe has been proposed and verified in this study.

The proposed methods can be used to analyze frost heave theory. The methods can also be used to determine the input parameters for existing frost heave models. For example, the segregation potential theory requires the segregation temperature as input parameter. This parameter can be readily determined using the SFCC as the temperature corresponding to the ice-entry value on the SFCC.

The segregation potential theory also requires the hydraulic conductivity within the frozen fringe. This hydraulic conductivity within the frozen fringe can be determined using the SFCC together with empirical methods for estimating the hydraulic conductivity of soils.

This research has produced the following:

- New ice lens initiation condition
  - Using the SFCC
  - Using the tensile strength of the frozen fringe
- New hydraulic conductivity estimation method for the soil within the frozen fringe and for partially frozen soils
  - Using the SFCC alone when cracks are not present
  - Dual porosity model when cracks are present
- Influence of cracks on hydraulic conductivity of the frozen fringe is investigated
- New method to estimate the segregation temperature, which is used as an input parameter in the segregation potential theory
- Tensile strength measurement of partially frozen soils using four-point bending test
- Tensile strength and stress-strain behavior under frozen fringe conditions

## **NEW ICE LENS INITIATION CONDITION**

Ice lens formation is initiated with cracking of the soil in the frozen fringe. Therefore, it is proposed and verified that ice lens initiation conditions are related to crack initiation in the frozen fringe. A new ice lens initiation condition is presented and verified experimentally. Based on the experimental observations reported by Peron et al. (2009), that cracking in non-frozen soils starts close to the air-entry value found from the soil water characteristic curve (SWCC), and based on similarity between SFCC and SWCC, it is postulated that an ice lens initiates close to the ice-entry value as determined from the SFCC. To verify this assumption, ice lens initiation conditions (in terms of segregation temperature) from one-dimensional frost heave tests under different temperature and vertical stress boundary conditions were determined and compared with the values

measured using the SFCC tests. The two independently determined results for ice lens initiation condition showed excellent agreement.

The SFCC can be used to determine the ice lens initiation conditions during frost heave. The findings from this study indicate that ice lenses initiate close to the ice-entry value found using the SFCC. Measuring SFCC that corresponds to a particular cooling rate and zero external pressure allows the suction and the corresponding temperature (related by the general Clausius-Clapeyron equation, with the ice phase assumed to be at atmospheric pressure) at the ice-entry value for the ice lens initiation conditions to be evaluated.

The influence of an external pressure with a magnitude  $P_e$  (in kPa) was shown to result in a shift in the ice-entry value (i.e., the suction at the ice entry value) on the SFCC by the same magnitude (i.e., by  $P_e$ ); and hence, to decrease the ice lens initiation temperature by a magnitude of  $((P_e/1250) ^\circ\text{C})$  from the ice lens initiation temperature at zero external pressure. Experimental data corroborated this approach for determining the ice lens initiation temperature.

Existing frost heave models require the segregation temperature as an input parameter. This study provides a new and novel practical method to determine this temperature. The segregation temperature can be determined as the temperature corresponding to the ice-entry value from the SFCC. Therefore, the SFCC can be used as input to existing frost heave models for determining the segregation temperature for a particular soil under evaluation.

## **ESTIMATION OF THE HYDRAULIC CONDUCTIVITY WITHIN THE FROZEN FRINGE AND IN PARTIALLY FROZEN SOILS**

This study proposed and verified the use of the SFCC for estimating the hydraulic conductivity of partially frozen soils. This approach uses the SFCC together with hydraulic conductivity estimation methods used extensively in unsaturated soil mechanics (Fredlund et al., 1994).

The hydraulic conductivity function of partially frozen Devon Silt is predicted using the saturated unfrozen hydraulic conductivity and the SFCC. The results from this study compared well with results from other methods for estimating the hydraulic conductivity function of partially frozen soils as well as with direct measurements of a partially frozen silt.

The hydraulic conductivity function of the frozen fringe can be estimated using this hydraulic conductivity estimation approach (Chapter 6), if it is assumed to be homogeneous.

The hydraulic conductivity of the frozen fringe is affected by the structure of the soil in the frozen fringe. The studies by researchers such as Chamberlain and Gow (1979) and Arenson et al. (2008) have shown the presence of freezing-induced cracks in the frozen fringe. One-dimensional freezing tests using Devon Silt and carried out by Xia (2006) showed the existence of cracks in and/or through the frozen fringe observed in tests carried out under various boundary conditions. These cracks that precede the formation of horizontal ice lenses and vertical ice veins are important features associated with the frost heave process since they are believed to influence both the magnitude of frost heave and the moisture transfer mechanism and rate or the hydraulic conductivity within the frozen fringe (Azmatch et al., 2008; Arenson et al., 2008). Therefore, the influence of the freezing-induced cracks on the moisture migration process has to be taken into account for proper evaluation of frost heave since the cracks form a secondary pore system in the frozen fringe.

Ignoring of the secondary pore system may lead to significant errors in the prediction of the hydraulic conductivity of cracked partially frozen soils. The challenge is that none of the existing frost heave models take into account the influence of freezing-induced cracks in the moisture migration process. Existing hydraulic conductivity estimation methods for the frozen fringe consider the frozen fringe as a uniform material with a single porosity. But the presence of

cracks in the frozen fringe necessitates the use of dual porosity models for a better estimation of the hydraulic conductivity of the frozen fringe.

This study proposed a dual porosity model for estimating the hydraulic conductivity of the frozen fringe. Accordingly, the hydraulic conductivity of the frozen fringe will have two components: hydraulic conductivity of the soil matrix and hydraulic conductivity of the cracks. Methods are discussed to estimate the two hydraulic conductivity components. The hydraulic conductivity of the cracked frozen fringe is then estimated as the weighted average of the two components based on the respective porosity ratio.

The SFCC together with hydraulic conductivity estimation methods known from unsaturated soil mechanics (e.g., Fredlund et al., 1994) are used to estimate the hydraulic conductivity of the frozen soil matrix.

The second component of the hydraulic conductivity of the frozen fringe, which is the hydraulic conductivity of the cracks, is determined using the theory for flow between parallel plates assuming laminar flow and making use of Poiseuille's law.

The proposed dual porosity hydraulic conductivity model was then used to carry out parametric study of the influence of the cracks on the hydraulic conductivity of the frozen fringe. The results indicated that the cracks have considerable influence on the hydraulic conductivity of the frozen fringe while only occupying a few percent of the pore space.

## CONCLUSIONS

- Ice lens formation is initiated with cracking of the soil in the frozen fringe.
- The soil freezing characteristic curve (SFCC) can be used to determine the ice lens initiation conditions during frost heave.
- The results from this study indicate that ice lenses initiate close to the ice-entry value found using the SFCC.
- The influence of an external pressure with a magnitude  $P_e$  (in kPa) is to result in a shift in the ice-entry value (i.e., the suction at the ice entry value) on the SFCC by the same magnitude (i.e., by  $P_e$ ); and hence, to decrease the ice lens initiation temperature by a magnitude of  $((P_e/1250) \text{ } ^\circ\text{C})$  from the ice lens initiation temperature at zero external pressure. Experimental data corroborated this process.
- The segregation temperature can be determined as the temperature corresponding to the ice-entry value on the SFCC. Therefore, the SFCC could be used as input to existing frost heave models for determining the segregation temperature.
- The permeability function of partially frozen homogeneous soils can be estimated predicted using the saturated coefficient of permeability and the soil freezing characteristic curve.
- The hydraulic conductivity function of the partially frozen soils within the frozen fringe (when cracks are not present or when it is assumed homogeneous with a single porosity) can be estimated using the SFCC and the saturated hydraulic conductivity of the soil together with hydraulic conductivity estimation methods from unsaturated soil mechanics.
- The results from this study indicated that the cracks in the partially frozen soil within the frozen fringe have considerable influence on the hydraulic conductivity of the frozen fringe while taking occupying a small percent of the pore space.
- Dual porosity models should be used to describe the hydraulic conductivity function of partially frozen soils within the frozen fringe when cracks are

present. Under such a condition, the hydraulic conductivity of the frozen fringe will have two components: hydraulic conductivity of the soil matrix and hydraulic conductivity of the cracks. Methods are discussed to estimate the two hydraulic conductivity components. The hydraulic conductivity of the cracked frozen fringe is then estimated as the weighted average of the two components based on the respective porosity ratio.

- The shape of the SFCC is influenced by the rate of cooling, the consolidation pressure (initial void ratio) and the external pressure. The shape of the SFCC is also influenced by the number of freeze-thaw cycles.
- The ice-entry value (IEV) is dependent on the cooling rate and the void ratio. The IEV increases with a decrease in initial void ratio and it also increases with an increase in cooling rate.
- The IEV is influenced by the number of freeze-thaw cycles. The IEV was higher for the first cycle. The results show that a lower suction, hence a higher temperature, is required for ice to penetrate the soil during the second cycle of freezing than the first cycle.
- The soil within the frozen fringe possesses considerable tensile strength.
- Ice lens initiation is related to the tensile strength of the soil within the frozen fringe, since the soil's tensile strength needs to be exceeded for it to crack.
- The influence of deformation rate on tensile strength of partially frozen soils is temperature dependent. Under the frozen fringe temperature conditions, the tensile strength decreased as the deformation rate increased. A unique behavior of the frozen fringe

## **RECOMMENDATIONS**

It is recommended that further study be conducted in the following areas:

- Ice lens initiation criteria based on tensile strength of the frozen fringe: This requires that the tensile strength of the frozen fringe be investigated under varying strain rates similar to that expected under the freezing conditions.

Tests need to also be conducted on samples prepared under different consolidation pressures.

- Implementing the ice lens initiation criteria and hydraulic conductivity estimation methods presented in this thesis in a revised frost heave models to explain the frost heave processes.
- Developing frost heave prediction method using the SFCC: Since the ice lens initiation criteria and the hydraulic conductivity estimation methods proposed in this thesis are based on the SFCC, it should be possible to predict the segregation potential that controls frost heave using the SFCC.
- Using the SFCC to develop frost susceptibility criterion for soils: The SFCC of the soil can also be used in estimating the frost susceptibility of a soil. The ice-entry value (IEV) and the slope of the SFCC curve can be used as parameters indicative of the frost susceptibility of soils.

## REFERENCES

- Arenson, L.U., Azmatch, T.F., Segoo, D.C., and Biggar, K.W. 2008. A new hypothesis on ice lens formation in frost-susceptible soils. Proceedings of the Ninth International Conference on Permafrost, Fairbanks, Alaska 1: 59-64.
- Beskow, G., 1935. Soil Freezing and frost heaving with special application to roads and railroads. Swed. Geol. Soc., Ser.C, No.375, 26th year book No. 3 (translated by J.O. Osterberg, Northwestern Univ., 1947).
- Bronfenbrener, L., Bornfenbrener, R., 2010. Modeling frost heave in freezing soils. Cold Regions Science and Technology 61, 43-64.
- Chamberlain EJ, Gow AJ. 1979. Effect of freezing and thawing on the permeability and structure of soils. Engineering Geology 13: 73–92.
- Fredlund, D.G., Xing, A., 1994. Equations for the soil-water characteristic curve. Canadian Geotechnical Journal, 31: 521-532.
- Fredlund, D.G., Xing, A., Huang, S., 1994. Predicting the permeability function for unsaturated soils using the soil-water characteristic curve. Canadian Geotechnical Journal, 31: 533-546.
- Gilpin, R.R., 1980. A model for the prediction of ice lensing and frost heave in soils. Water Resources Research 16 (5), 918–930.
- Harlan, R.L., 1973. Analysis of coupled heat and mass transfer in partial frozen soil. Water Resources Research 9 (5), 1314–1323.
- Konrad, J.M., Morgenstern, N.R., 1980. A mechanistic theory of ice lens formation in fine-grained soils. Canadian Geotechnical Journal 17, 473–486.

Peron, H., Hueckel, T., Laloui, L., Hu, L.B., 2009, Fundamentals of desiccation cracking of fine-grained soils: experimental characterisation and mechanisms identification, *Canadian Geotechnical Journal* 46, 1177 – 1201.

Taber, S., 1929. Frost heaving. *Journal of Geology* 37, 428–461.

Xia, D., 2006. Frost heave studies using digital photographic technique. MSc Thesis, University of Alberta, Edmonton, AB, Canada, 165 pp.

## **APPENDIX**

## A.1 Analysis of the Tension Tests Using Four-Point Bending Test

The four-point bending test set-up is as shown in Figure A.1 below.

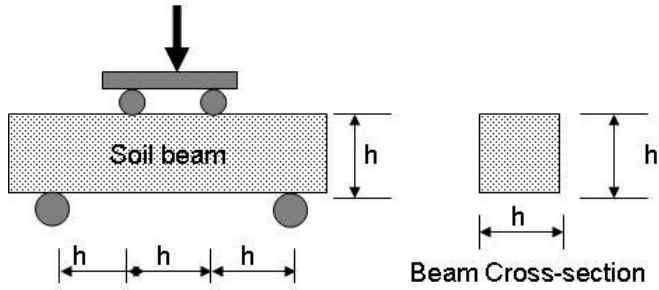


Figure A.1 Four-point bending test set-up and sample dimensions,  $h = 76.2$  mm

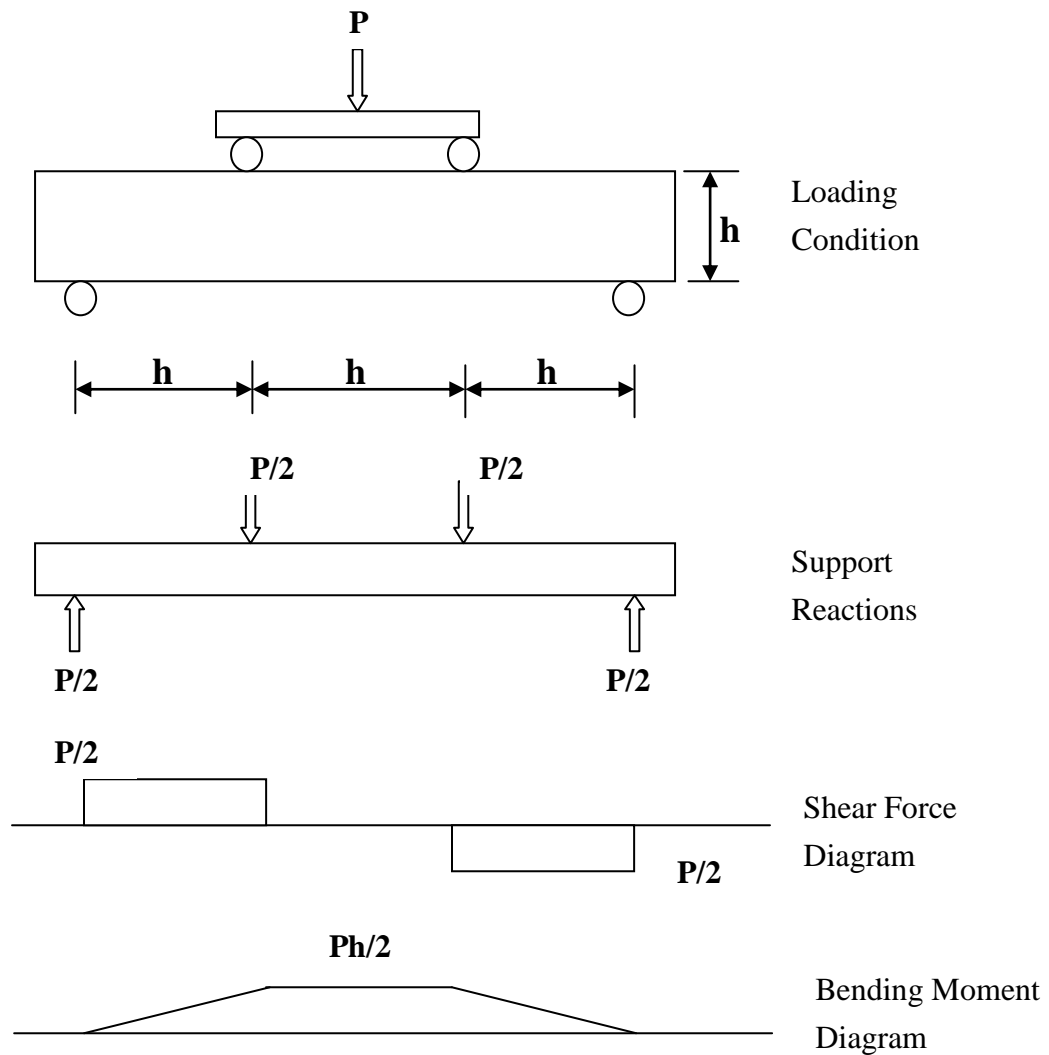


Figure A.2 Analysis of the four-point bending test

During bending the top part of the soil sample is under compression and the bottom part is under tension. The tensile strength of the soil is calculated using the following equation:

$$\sigma_t = \frac{My}{I}$$

Where  $\sigma_t$  is the tensile stress,  $M$  is the bending moment, and  $y$  is distance to the bottom from the centerline, and  $I$  is the moment of inertia of the cross-section.

$$M = \frac{Ph}{2}, y = \frac{h}{2}, I = \frac{bh^3}{12} = \frac{h^4}{12}$$

Table A.1 below presents the testing conditions under which the four –point bending tests were conducted.

Table A.1 Summary of Tension Tests

Test Number	Average Test Temperature (°C)	Deformation Rate (mm/min)
4	-1.00	0.80
6	-0.50	0.80
7	-0.30	0.80
8	-1.40	0.80
10	-0.65	0.80
11	-0.65	0.08
13	-0.65	8.00
14	-0.65	3.00
18	-5.45	8.00
16	-5.45	3.00
20	-5.45	0.80

## A.2 Temperature Conditions during the Tension Tests

The sample to be used for the FPBT is placed in a freezing cell. The temperature of the freezing cell is controlled by flowing cold fluid through brass coils (placed inside the freezing cell) from a cooling bath. The temperature of the freezing cell is monitored by two RTDs placed at two corners within the cell. The sample is let to freeze isotropically to the desired temperature once placed in the cell. The samples are first frozen at  $-4.0\text{ }^{\circ}\text{C}$  for about 16 hours and then the temperature is raised to the desired temperature and the sample is left to equilibrate at the desired test temperature for a minimum of 24 hours.

Variation of the freezing cell temperature is presented in Figure A.3. To test the sensitivity of the sample temperature to the temperature variation in the freezing cell a test was conducted by inserting an RTD in a soil sample of similar size as the ones used for the tension tests. The result is shown in Figure A.4 and Figure A.5. It can be seen that once the sample reaches the desired temperature, its temperature is not significantly affected by short duration changes in temperature of the freezing cell. The abrupt changes in the freezing cell temperature are during the defrost cycle of the cooling system.

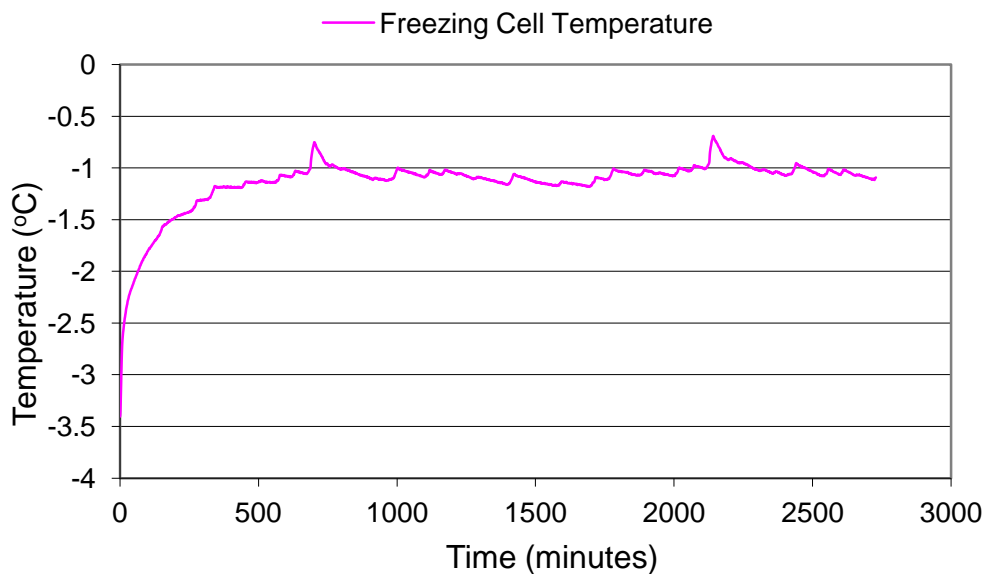


Figure A.3 Freezing cell variation with time.

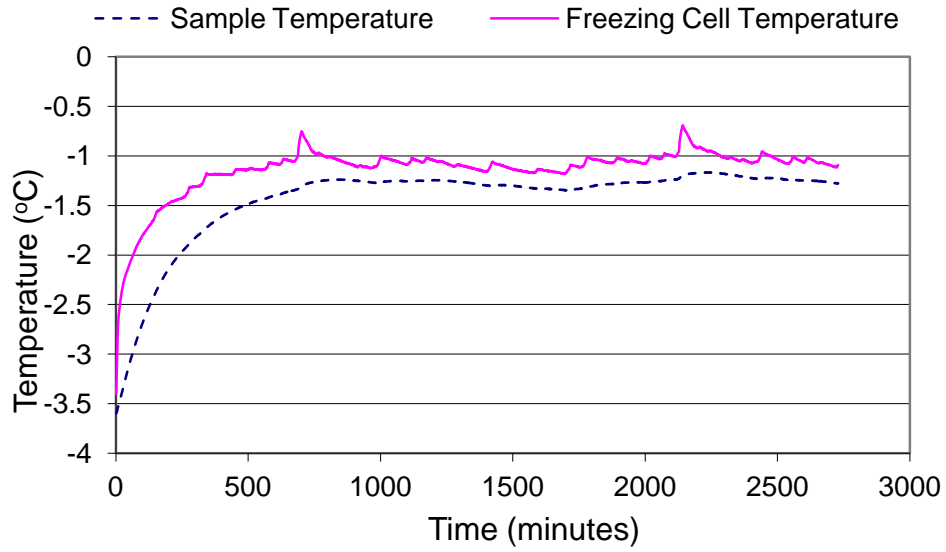


Figure A.4 Freezing cell temperature variation and sensitivity of sample temperature to the freezing cell temperature variation

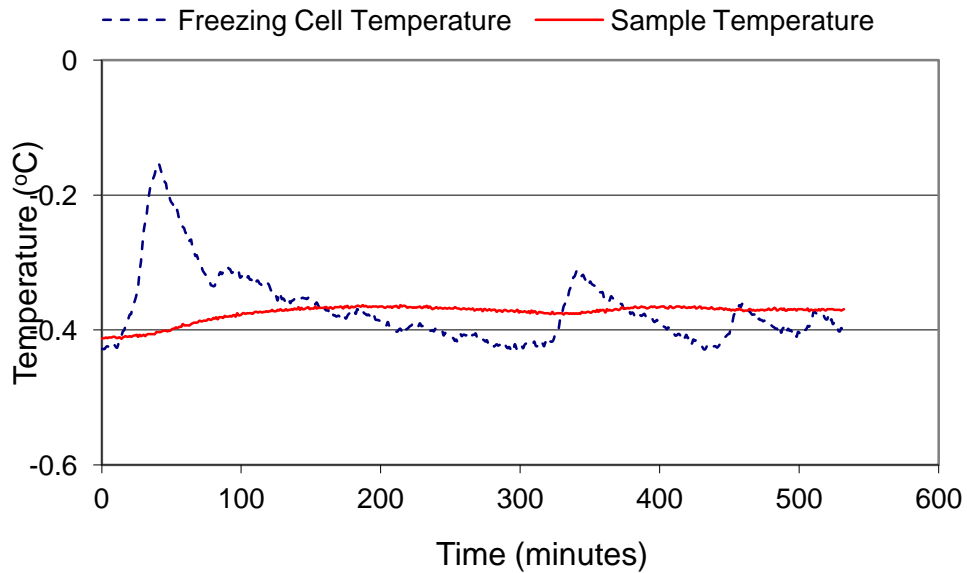


Figure A.5 Freezing cell temperature variation and sensitivity of sample temperature to the freezing cell temperature variation

Figures A.6 to A.9 show the temperature variation during the loading stage of the tensile strength tests. The duration of the loading stage of the four-point bending test is short and hence much change in temperature is no expected

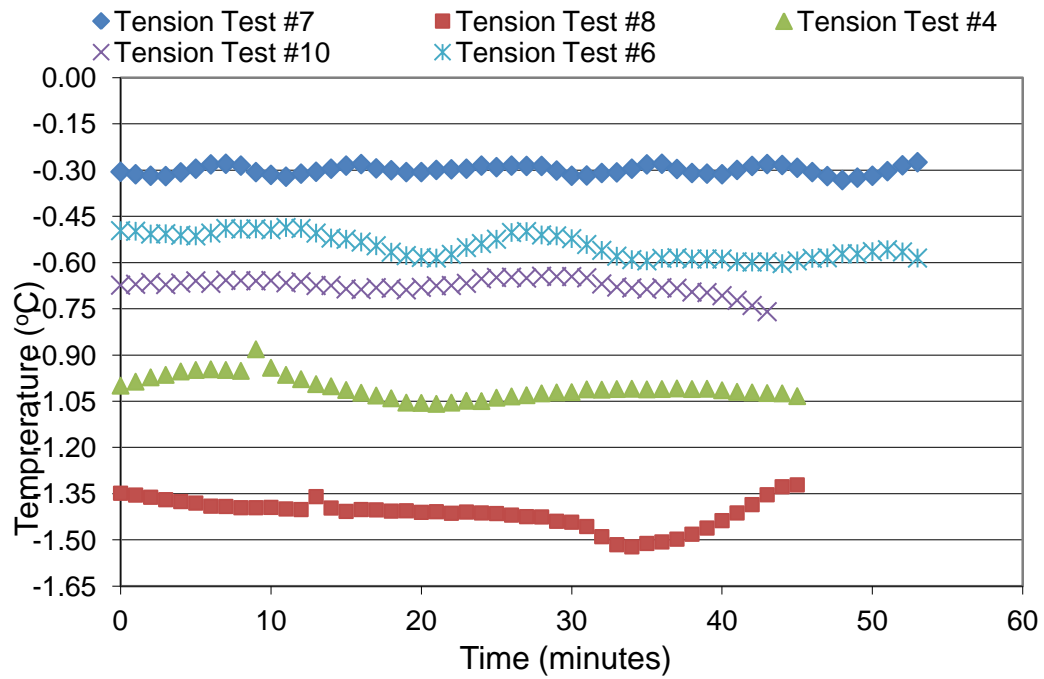


Figure A.6 Variation of Temperature during tension tests conducted at different temperatures but at the same deformation rate of 0.8 mm/min.

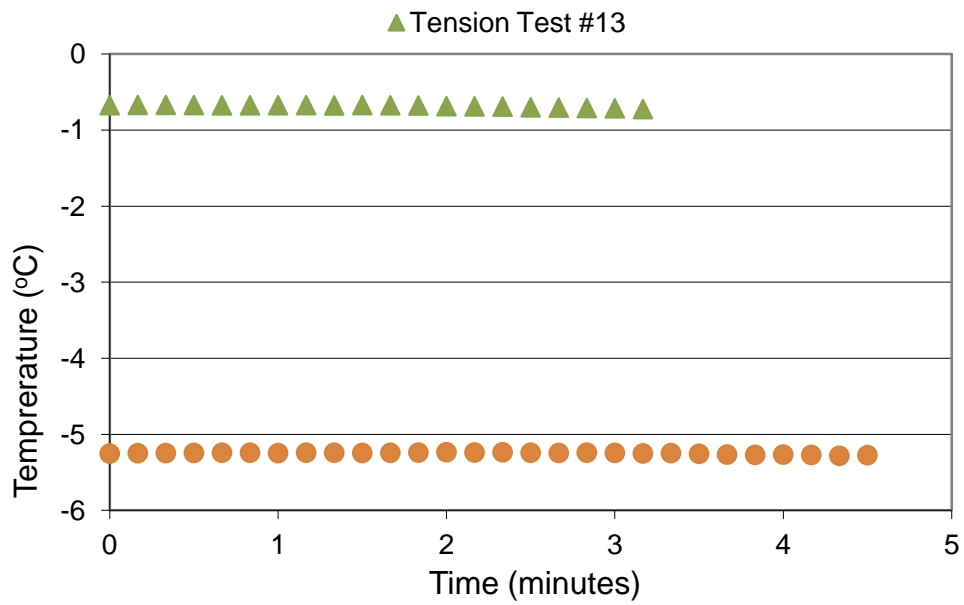


Figure A.7 Variation of temperature during tension tests conducted at different temperatures but at the same deformation rate of 8 mm/min.

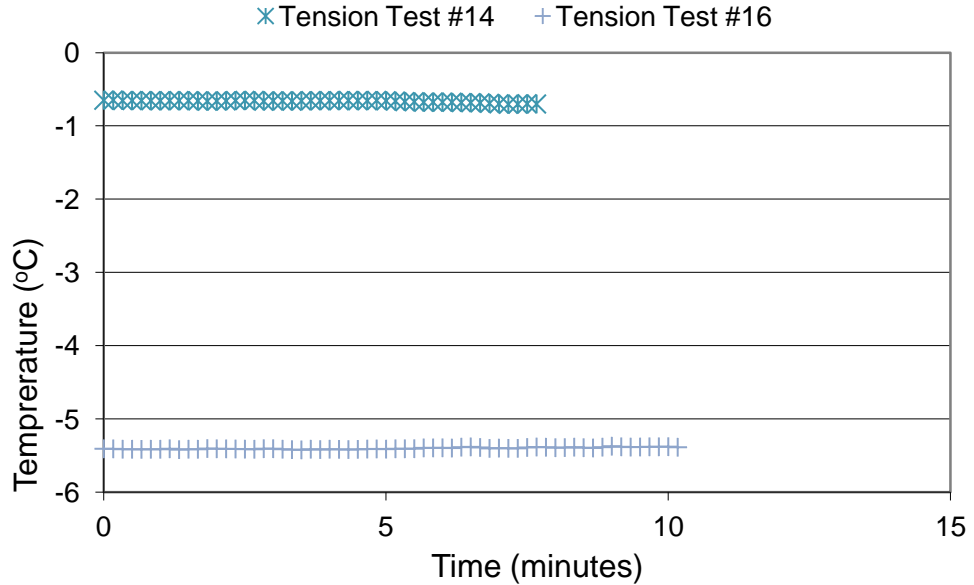


Figure A.8 Variation of temperature during tension tests conducted at different temperatures but at the same deformation rate of 3 mm/min.

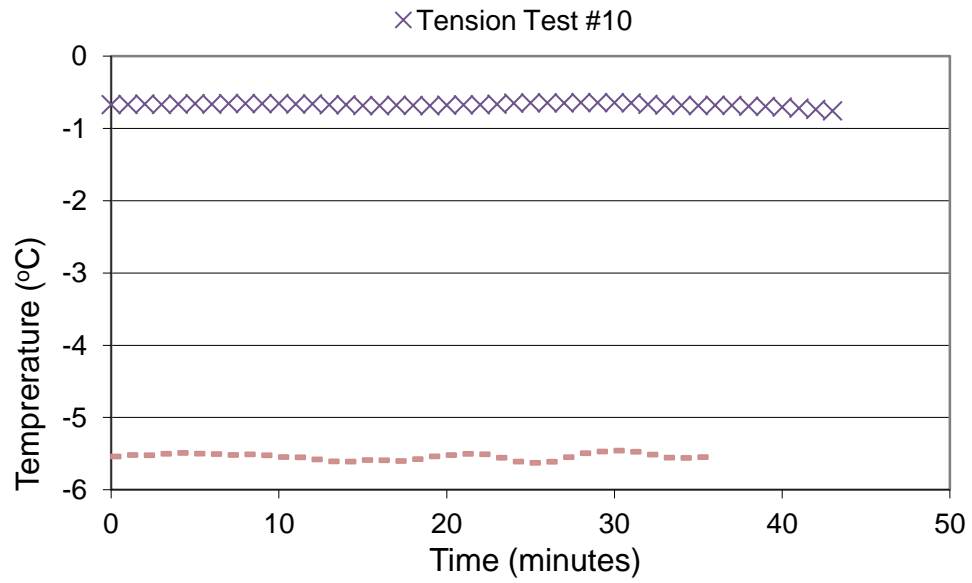


Figure A.9 Variation of temperature during tension tests conducted at different temperatures but at the same deformation rate of 0.8 mm/min.

### A.3 Temperature Conditions during the Soil Freezing Characteristic Curve (SFCC) Tests

Figures A.10 to A.13 show the temperature variation during the loading stage of the tensile strength tests. The abrupt changes in the room temperature are during the defrost cycle of the cooling system. The figures show that the sample temperatures are not affected by the abrupt changes since the changes are for short duration of time.

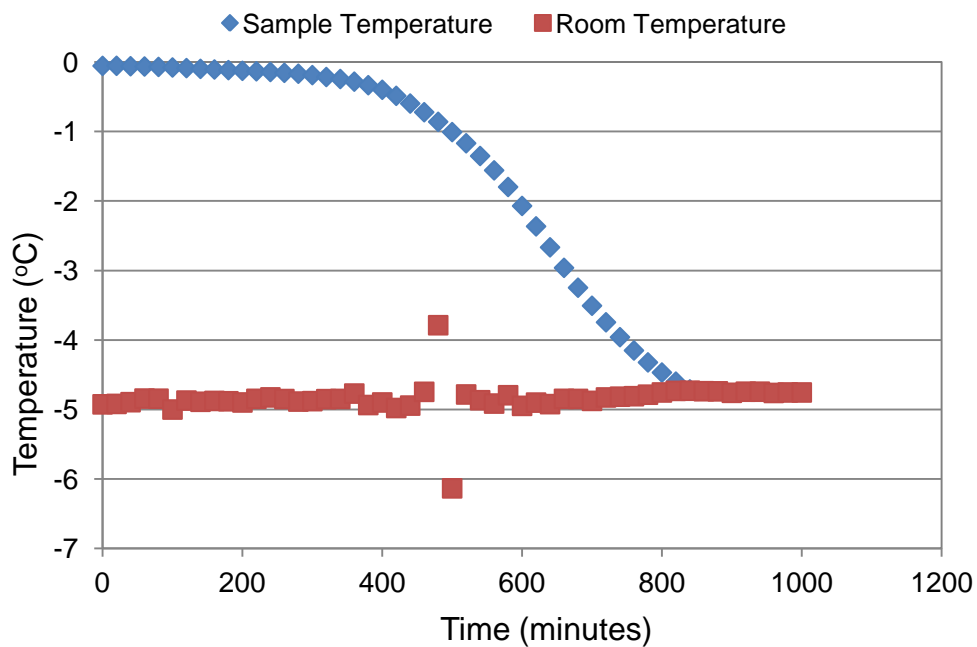


Figure A.10 Variation of temperature during SFCC test on soil sample consolidated to 50 kPa pressure.

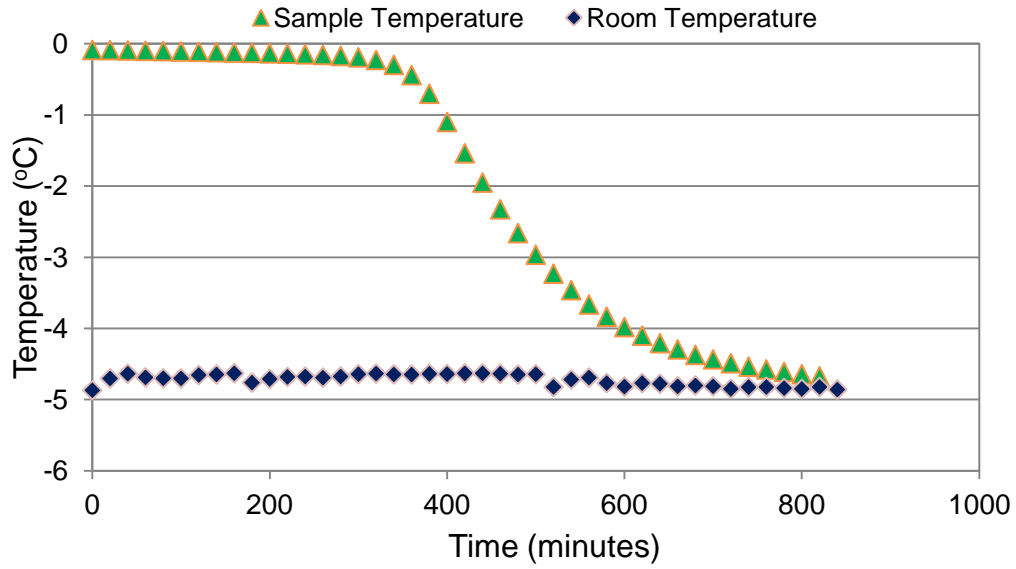


Figure A.11 Variation of temperature during SFCC test on soil sample consolidated to 100 kPa pressure.

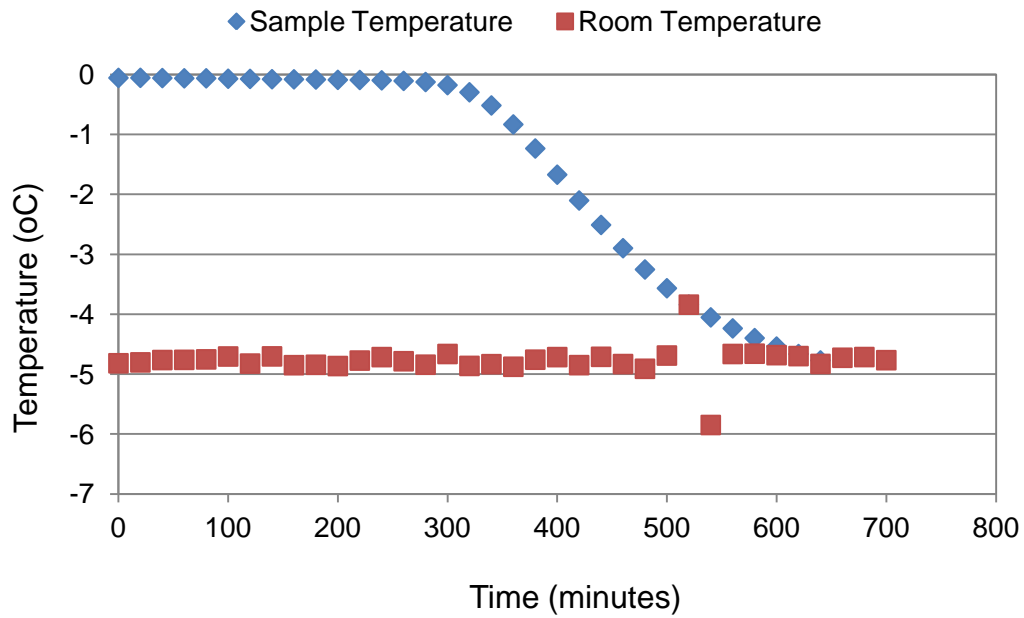


Figure A.12 Variation of temperature during SFCC test on soil sample consolidated to 200 kPa pressure.

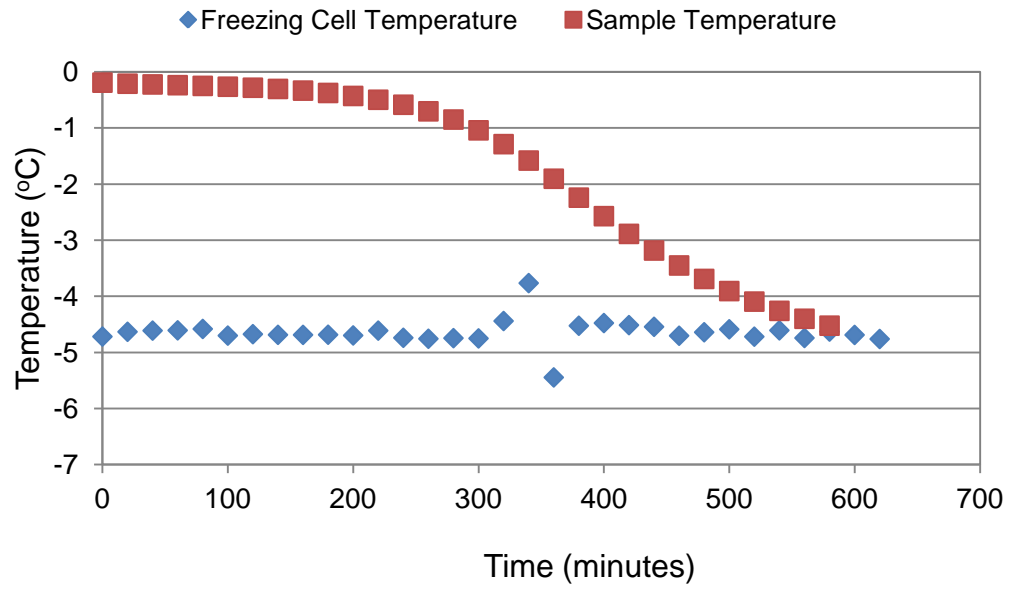


Figure A.13 Variation of temperature during SFCC test on soil sample consolidated to 400 kPa pressure.